DEVELOPMENT OF METAL MATRIX/COCONUT SHELL ASH PARTICULATE COMPOSITES FOR AUTOMOTIVE APPLICATION

BY

ADAOKOMA APASI

DEPARTMENT OF MECHANICAL ENGINEERING
AHMADU BELLO UNIVERSITY, ZARIA
NIGERIA

FEBRUARY, 2015

DEVELOPMENT OF METAL MATRIX/COCONUT SHELL ASH PARTICULATE COMPOSITES FOR AUTOMOTIVE APPLICATIONS

BY

ADAOKOMA APASI
(PGD Mech.Eng.UNI AGRIC.MAKURDI, M.Eng. FUT MINNA)
PHD/ENG/10694/2007-08

A DISSERTATION SUBMITTED TO THE SCHOOL OF POSTGRADUATE STUDIES, AHMADU BELLO UNIVERSITY, ZARIA NIGERIA

IN PARTIAL FULFILMENT OF THE REQUIREMENTS FOR THE AWARD OF DOCTOR OF PHILOSOPHY IN MECHANICAL ENGINEERING (PRODUCTION ENGINEERING)

DEPARTMENT OF MECHANICAL ENGINEERING
AHMADU BELLO UNIVERSITY, ZARIA
NIGERIA

FEBRUARY, 2015

DECLARATION

I declare that the work in the dissertation titled 'Development of Metal Matrix/Coconut Shell Ash Particulate Composites for Automotive Application' has been performed by me in the Department of Mechanical Engineering under the supervision of DR. D.S. YAWAS, PROF. S.Y. AKU and PROF. A.I. OBI.

The information derived from the literature has been duly acknowledged in the text and a list of references provided. No part of this dissertation was previously presented for another degree or diploma at any University.

Adaokoma Apasi	_____	_____
Name of Student	Signature	Date

CERTIFICATION

This dissertation titled "**Development of Metal Matrix/Coconut Shell Ash Particulate Composites for Automotive Applications"** by Adaokoma Apasi meets the regulations governing the award of the degree of Doctor of Philosophy of Ahmadu Bello University, Zaria and is approved for its contribution to knowledge and literary presentation.

Dr. D.S. Yawas	_____	_____
Chairman, Supervisory Committee	Signature	Date
Prof. S.Y Aku	_____	_____
Member, Supervisory Committee	Signature	Date
Prof. A.I. Obi	_____	_____
Member, Supervisory Committee	Signature	Date
Dr. M. Dauda	_____	_____
Head of Department	Signature	Date
Prof. A.Z. Hassan	_____	_____
Dean School of Postgraduate Studies	Signature	Date

ACKNOWLEDGEMENT

I give honour and glory to the Almighty God for making this research a reality. I am grateful to the Management of Kaduna Polytechnic for the opportunity given me to pursue this programme to its logical conclusion.

My profound gratitude goes to the Chairman supervisory committee Dr. D.S. Yawas for his thorough supervision, invaluable advice, absolute interest and understanding throughout the duration of this work. I sincerely appreciate the guidance and contribution of Professors S.Y. Aku and A.I. Obi who are members of my supervisory committee. The immense contribution of Dr. Victor Aigbodion of University of Nigeria, Nsukka is greatly appreciated.

I am grateful to all members of staff of the Department of Mechanical Engineering, Ahmadu Bello University, Zaria for their assistance in one way or the other throughout the duration of this undertaking.

My sincere appreciation goes to all members of my family for their love, prayers, understanding and encouragement. Finally, I wish to acknowledge all my friends, colleagues and all those that showed love and concern during the period but whose names can not appear for want of space, I thank them all.

ABSTRACT

This research presents the development of metal matrix composite using coconut shell ash as the reinforcement for automotive applications. Test samples were produced by stir casting method and machined into standard sizes for the purpose of determining micro structural analysis, physical, thermal, corrosion, mechanical and wear properties. The results obtained were compared with standard composite materials used in the production of connecting rod. The metal matrix composites (MMC's) were prepared by addition of 3, 6, 9, 12 and 15wt% CSAp particulates. The results of the microstructural analysis of the composites revealed the uniform distribution of the coconut shell ash particles. The increase in reinforcement volume fraction resulted in the decrease of matrix grain size in the composites. The results obtained also showed that addition of coconut shell ash particles reinforcement to Al-Si-Fe alloy increased the tensile strength and the hardness value of composites, but slightly reduced the impact energy. It is observed that, as the applied load increases, the wear rate also increases. This is because, whenever applied load increases, friction at the contact surface of the material and rotating disc obviously increases. For optimum service performance of this alloy, coconut shell ash particle addition should be between 6-9% by weight of CSAP particulates and not exceed 9% in order to develop better necessary properties. A sample of the produced MMCs connecting rod was tested using a Toyota 12 valve model E series automobile engine to determine performance and effectiveness of the device. The results obtained showed a fuel consumption saving of 0.0034 liters/min and it can be deduced that high improvement in combustion efficiency could be achieved compared to the regular connecting rod.

TABLE OF CONTENT

Title page - - - - - - - - - i

Declaration - - - - - - - - - iv

Certification - - - - - - - - - v

Acknowledgement - - - - - - - - - vi

Abstract - - - - - - - - - vii

Table of Content - - - - - - - - - viii

CHAPTER ONE

INTRODUCTION

1.1. Background to the Study - - - - - - 2

1.2 Statement of Research Problem - - - - - 3

1.3 The Present Research - - - - - - - 5

1.4 Aim and Objective of the study - - - - - 5

1.4 Significance of the Study - - - - - - 6

1.5 Scope of the Work - - - - - - - 6

CHAPTER TWO

LITERATURE REVIEW

2.1 Metal Matrix Composite (MMCS) - - - - - 7

2.2 Mechanical Properties of MMCS - - - - - 7

2.3 Properties of Aluminium Matrix Composites (AMCS) - - 11

2.4 Types of AMCS - - - - - - - 13

2.4.1 Particle Reinforced Aluminium Matrix Composites (PAMCS) - 14

2.4.2 Short Fibre and Whisker-Reinforced Aluminium Matrix Composites (Sfamcs) - - - - - - - - - 15

2.4.3 Continuous Fibre-Reinforced Aluminium Matrix Composites (CFAMCS) 16

2.4.4 Monofilament Reinforced Aluminium Matrix Composites (MFAMCS) 16

2.5 Effect of Ceramic Reinforcements on the Behaviour of Aluminium Matrix in AMCS - - - - - - - 17

2.5.1 Intrinsic Effects of Ceramic Reinforcements - - - - 17

2.5.2 Extrinsic Effects of Ceramic Reinforcement - - - - 18

2.6 Applications of AMCS - - - - - - 18

2.7 Review of Past Works- - - - - - - 19

2.8 Nigeria Coconut - - - - - - - 20

2.9 Connecting Rod - - - - - - - 22

2.9.1. Forces on Connecting Rod (I) - - - - - 25

CHAPTER THREE

MATERIALS AND METHODS

3.1 Experimental Procedure - - - - - - 29

3.2 Materials - - - - - - - - 29

3.3 Equipment - - - - - - - - 29

3.4 Method - - - - - - - - 30

3.4.1 The Processing and Chemical Analysis of the Coconut Shell Ash - 30

3.4.2 Specimen Preparation - - - - - - - 32

3.4.3 Density Measurement - - - - - - - 33

3.4.4 X-RAY Diffractometer (XRD) Analysis - - - - 34

3.4.5 Microstructural Analysis - - - - - - 35

3.4.6 Hardness Testing - - - - - - - 35

3.4.7 Tensile Test - - - - - - - - 36

3.4.8 Impact Energy Test - - - - - - - 36

3.4.9 Wear Test - - - - - - - - 36

3.4.10 Thermal Analysis - - - - - - - 37

3.4.11 Corrosion Test - - - - - - - - 37

3.4.12 Design of the Connecting Rod - - - - - 39

3.4.13 Small End of the Connecting Rod - - - - - 45

3.4.14 Big End of the Connecting rod - - - - - 46

3.4.15 Connecting rod shank - - - - - - - 46

3.4.16 Casting Process - - - - - - - 51

3.4.17 Fabrication (Casting and Machining) of the Connecting Rod - 55

3.4.18 Forces Acting on Connecting Rod (ii) - - - - 59

3.4.19 Inertia Bending Forces - - - - - - - 61

3.5 Finishing Operation (Machining) - - - - - - 69

3.5.1 Heat Treatment (solution – treatment and aging. "STA") - - 69

3.5.2 Performance Test on the Connecting Rod - - - - 70

CHAPTER FOUR

RESULTS AND DISCUSSIONS

4.1 Results - - - - - - - - - 73

4.2 Characterization of the Coconut Shell Ash - - - - 73

4.2.1 Particle Size Analysis of the Coconut Shell Ash - - - 73

4.2.2 Density of the Coconut Shell Ash Particle - - - - 73

4.2.3 Refractoriness of the Coconut Shell Ash Particles - - - 74

4.2.4 XRF Chemical Composition Analysis of the Coconut Shell Ash Particles - - - - - - - - - 74

4.2.5 Compositional Analysis and Microstructure of the Coconut Shell Ash Particles (CSAP) - - - - - - - 75

4.2.6 FTIR Analysis of the Coconut Shell Ash Particles - - - 76

4.3 Macrostructural Observations - - - - - - 78

4.4 Density of the Composites - - - - - - 79

4.5 Microstructural and the Interfacial Study of the Composites - - 81

4.5.1 X-Ray Diffraction Analysis (XRD) - - - - - 81

4.5.2 Microstructural Analysis of Composites - - - - 82

4.6 Hardness Values - - - - - - - 88

4.7 Tensile Properties - - - - - - - 89

4.8 Impact Energy- - - - - - - - 93

4.9 Wear Behaviour - - - - - - - 94

4.10 Thermal Behaviour - - - - - - - 100

4.11 Corrosion Behavior - - - - - - - 102

4.12 Test of the connecting rods produced - - - - 104

CHAPTER FIVE

5.0 **CONCLUSION AND RECOMMENDATION**

5.1 Conclusion - - - - - - - - 111

5.2 Recommendations for Further Studies - - - - 113

References - - - - - - - - 115

Appendices - - - - - - - - 120

LIST OF FIGURES

Fig. 2.1: Typical application of a connecting rod in an engine - - 24

Fig. 2.2: Piston force and inertia force acting on connecting rod - - - 25

Fig 2.3: Connecting rod sections - - - - - - 28

Fig. 3.1: Schematic drawing of Stir-Casting - - - - - 33

Fig. 3.2: Sketch for the corrosion test - - - - - - 38

Fig. 3.3 Bucking of connecting rod - - - - - - 41

Fig. 3.4 I-section of connecting rod - - - - - - 43

Fig. 3.5: Sectional view of section A-B - - - - - 47

Fig. 3.6: Design diagram of a connecting rod assembly - - - 48

Fig. 3.7: Developed connecting rod with major dimensions - - - 49

Fig. 3.8: (a) Core rod for the big hole (b) Mould locking system - - 50

Fig. 3.9: Sectional view of the mould assembly - - - - 50

Fig. 3.10: Manufacturing process flow chart of the connecting rod - - 52

Fig. 3.11: Forces on a connecting rod- - - - - - 59

Fig. 3.12: Inertia bending forces - - - - - - 61

Fig 3.13: Photograph Toyota Model 12 valve engine- - - - 72

Fig. 4.1: XRD pattern of Coconut shell ash - - - - - 76

Fig. 4.2: FTIR spectrum of Coconut shell ash - - - - 77

Fig. 4.3: Plot of Density with percent of Coconut shell ash - - - 79

Fig. 4.4: Variation of the Hardness values with wt% coconut shell ash particles- 89

Fig. 4.5: Variation of the Strength with wt% coconut shell ash particles - 89

Fig. 4.6: Variation of the Impact energy with wt% coconut shell ash particles - 93

Fig. 4.7: Variation of Wear rate with wt% of Coconut shell ash particles - 96

Fig. 4.8: Variation of Coefficient of Friction with wt% of Coconut shell ash particles - - - - - - - - 98

Fig. 4.9: DTA/TGA of Al-Si-Fe alloy - - - - - - 100

Fig. 4.10: DTA/TGA of Al-Si-Fe alloy/15wt%CSAP - - - - 101

Fig. 4.11: Average corrosion rate Al-Si-Fe/Coconut shell ash (CSAp) - - 102

Fig. 4.12: Tensile strength and Yield strength test result. - - - 105

Fig. 4.13: Regular connecting rod (Fuel consumption kW/h analysis) - - 107

Fig. 4.14: MMC Connecting Rod (Fuel Consumption/Kwh analysis) - - 108

Fig. 4.15: Variation of the Fuel Consumption/Kwh with Engine power - 108

Fig. 4.6: Variation of Brake force with Engine speed - - - - 109

LIST OF TABLES

Table: 2.1: Comparison of steel and MMC connecting rods - - 28

Table: 3.1: Basic constructional parameters of the (Small end) of the connecting rod - - - - - - - - - 43

Table 3.2: Basic constructional parameters of the (Big end) of the connecting Rod - - - - - - - - 44

Table: 3.4: Basic constructional parameters (rod shank) of the connecting rod 47

Table: 3.4: Summary of result of force acting on connecting rod - - 68

Table 4.1: The density of the composites - - - - - 74

Table 4.2: XRF analysis of Coconut shell ash - - - - 75

Table 4.3: Identified Patterns List of Coconut shell ash - - - 78

Table 4.4: Identification Peaks of the FTIR analysis - - - - 81

Table 4.5: Result of the tensile strength (N/mm^2) - - - - 104

Table 4.6: Result of the Yield Strength at 0.2% UPSET - - - 105

Table 4.7: Hardness test Result of the Composite Connecting Rods (BHN) - 106

Table 4.8: Value of impact energy test results conducted on composite Connecting rods (Joules) - - - - - 107

LIST OF PLATES

Plate: 2.1. Some Industrial Applications or AMCs (a) brake rotors for high speed train (b) automotive braking systems (c) automotive pushrods (d) cores for HV electrical wires. - - - - - 19

Plate 3.1: Photograph of Coconut shell - - - - - 31

Plate 3.2: Photograph of Coconut shell ash particles - - - - 31

Plate 3.2: Isometric view of connecting rod - - - - 53

Plate 3.3: Isometric view of the rod - - - - - - 54

Plate 3.4 (a) Casting profile of the connecting rod. - - - 56

Plate 3.4: (b) Casting profile of the connecting rod. - - - - 56

Plate 3.5: Boring of the connecting rod on the lathe. - - - - 57

Plate 3.6: Milling side faces of the connecting rod. - - - - 57

Plate 3.7 (a) Alignment on machine (Model NO. 335 – IG) - - - 58

Plate 3.7 (b) Squarness on machine (Model NO. 335 – IG) - - - 58

Plate 3.8a: Photograph of Regular connecting rod - - - - 71

Plate 3.8b: Photograph of MMCs connecting rod - - - - 71

Plate 4.1: Photograph of the cast composites - - - - - 78

Plate 4.2: SEM/EDS spectrum of Coconut shell ash - - - - 80

Plate 4.3: Profile of other test results - - - - - - 106

LIST OF MICROGRAPHS

Micrograph 4.1: SEM/EDS spectrum of the aluminium alloy - - 82

Micrograph 4.2: SEM/EDS spectrum of the aluminium alloy with 3wt%CSAp - 83

Micrograph 4.3: SEM spectrum of the aluminium alloy with 6wt%CSAp - 83

Micrograph 4.4: SEM spectrum of the aluminium alloy with 9wt%CSAp - 84

Micrograph 4.5: SEM spectrum of the aluminium alloy with 12wt%CSAp - 84

Micrograph 4.6: SEM spectrum of the aluminium alloy with 15wt%CSAp - 85

Micrograph 4.7: SEM Fractograph of the aluminium alloy - - - 92

Micrograph 4.8: SEM Fractograph of the aluminium alloy reinforced with 15wt% CSAp - - - - - - 92

Micrograph 4.9: SEM spectrum of the Worn surface of the aluminium alloy at 50N, 2.0m/s and 4000m - - - - - 94

Micrograph 4.10: SEM spectrum of the Worn surface of the aluminium alloy with 9wt%CSAp at 50N, 2.0m/s and 4000m - - 95

LIST OF APPENDICES

Appendix I: Table the density of the composites - - - - 122

Appendix II: Experimental Calculations - - - - - 129

Appendix III: Regular connecting rod (Fuel consumption kw/h analysis) - 133

NOMENCLATURE

A	Area (Surface area) (cm^2)
Al_2O_3	Aluminium Oxide
AMCs	Aluminium –Matrix Composites
CFAMCs	Continuous Fibers Reinforced Aluminium Matrix Composites
CSAp	Coconut shell ash particles
D	Density in (g/cm^3)
D_{eb}	Distance between connecting rod bolts (mm)
d_{ep}	Crank pin diameter (mm)
F	Brake load (N)
GFN	Grain Fineness Number
HBN	Brinell Hardness Number
b_{sec}	Sectional breath (mm)
^0C	Degree centigrade
id_{se}	Small end inside diameter (mm)
L_{se}	Length of small end (mm)
L_{sec}	Sectional length (mm)
L_{be}	Length of big end (mm)
L	Torque arm length (m)
L_{sec}(max)	Maximum sectional length (mm)
MFAMC	Monofilament Reinforced Aluminium Matrix Composites
N	Newton
OD_s	Small end outside diameter (mm)
P_b	Brake horse power (Bhp) (Kw)

PMMCs	Particulate Reinforced Metal Matrix Composites
r_{tew}	Radial thickness of end wall (mm)
SEM/EDS	Scanning Electron Microscope/Energy Dispersive Spectrometer
SFAMCs	Short Fiber and Wisker Reinforced Aluminium matrix composites
SIC	Silicon Carbide
T	Torque (N-m)
t_{sh}	Shell thickness (mm)
t_{ft}	Flange thickness (mm)
W	Weight of sample (mg)
π	3.142
mm	Millimetre
N	Newton

CHAPTER ONE

INTRODUCTION

1.1. BACKGROUND TO THE STUDY

The term "composite" broadly refers to a material system which is composed of a discrete constituent (the reinforcement) distributed in a continuous phase (the matrix) and which derives its distinguishing characteristics from the properties of its constituents from the geometry and architecture of the constituents, and from the properties of the boundaries (interfaces) between the different constituents (Clyne, 2000 and lkechukwuka, 1997). Composite materials are usually classified on the basis of the physical or chemical nature of the matrix phase, e.g., polymer matrix, metal-matrix and ceramic composites. In addition there are some reports to indicate the emergence of intermetallic matrix and carbon-matrix composites (Surappa and Rohatgi, 1981).

Aluminium is the most popular matrix for the metal matrix composites (MMCs). Aluminium alloys are quite attractive due to their low density, their capability to be strengthened by precipitation, their good corrosion resistance, high thermal and electrical conductivity and their high damping capacity (Whitehouse et al., 1991). Aluminium matrix composites (AMCs) have been widely studied since the 1920s and are now used in sporting goods, electronic packaging, amour and automotive industries (Skibo *et al*, 1988 and Donne *et al*, 1990). The unique thermal properties of aluminium based composites such as metallic conductivity with a low coefficient of expansion and high operating temperature and whose values can be tailored down to zero.

They offer a large variety of mechanical properties depending on the chemical composition of the aluminium matrix. The following reinforcements Al_20_3, SiC, C,

$Si0_2$, B, BN, B_4C are usually used in aluminium matrices (lkechukwuka, 1997, Skibo *et al,* 1998 and Lloyd, 1999). As proposed by the American Aluminium Association, AMCs should be designated by their constituents: accepted designation of the matrix/ abbreviation of the reinforcement's designation/arrangement and volume fraction in % with symbol of type (shape) of reinforcement. For example, aluminium alloys AA6061 reinforcement by particulates of alumina. 11% volume fraction. is designated as "AA6061/Al_20_3/11p" (Ikechukwuka, 1997, Rohatgi *et al*., 1988, Zhou and Xu, 1997).

Particulate reinforced metal matrix composites (PMMC) are currently being used as structural components in many aerospace and automotive applications. The increasing demand for PMMCs is due to the unique mechanical properties achieved in the metal when ceramic particulates are used as reinforcement phases. PMMCs usage in other automotive applications include:

- Automotive and heavy goods vehicles.
- Braking systems, piston rods, frames, pistons, piston pins, valve spring caps.
- Brake discs, disc brake calipers, brake pads
- Accumulator plates.
- Military and civil air industries

Axle tubes, reinforcements, blade and gear box casings, fan and compressor blades, turbine blades, aerospace industry, frames, reinforcements, aerials and joining elements.

Particulate reinforced metal matrix composites (PMMCs) are currently being used as structural components in aerospace, automotive and industrial applications. Discontinuously reinforced metal matrix composites have received much attention because of their improved specific strength, good wear resistance and modified

thermal properties unattainable in either of the starting (monolithic) materials (Ritnner, (2000), Wahab *et al*, 2009). These materials have emerged as the important class of advanced materials giving engineers the opportunity to tailor material properties according to their needs. Essentially these materials differ from the conventional engineering materials from the view point of homogeneity (Varajappa and Ghandrmohan, 2005).

PMMCs combine the ductility and toughness of the metal matrices with the high strength and stiffness of the ceramic reinforcement to achieve properties unattainable in either of the starting materials. PMMCs often have high strength to weight ratios, which is an important consideration in weight sensitive applications. Other distinctive properties of PMMCs include good thermal stability and excellent wear resistance (Aigbodion, 2007).

Dispersing small particulates (less than 1μm) in a metal increases its strength, typically by Orowan type strengthening mechanisms. Traditionally high modulus ceramic particulates such as silicon carbide (SiC) and alumina (Al_2O_3) have been used as reinforcements purposely for stiffness enhancement, plus strengthening. It is however, known that other property benefits can be achieved by carefully controlling the matrix properties, the reinforcement properties, and the interface formed between them.

1.2 STATEMENT OF RESEARCH PROBLEM

i. The demand for high level performance of the automotive connecting rod for rigidity, weight reduction (light weight) and ability to withstand tremendous loads puts conventional steel or aluminium alloy connecting rods to the limits of their material strengths particularly the effect of combustion gas loads in the combustion area.

ii. The life span (service life) of the connecting rod is affected due to corrosive action of the combustion products. Abnormal combustion is a serious problem for connecting rods (Schreier, 1999).

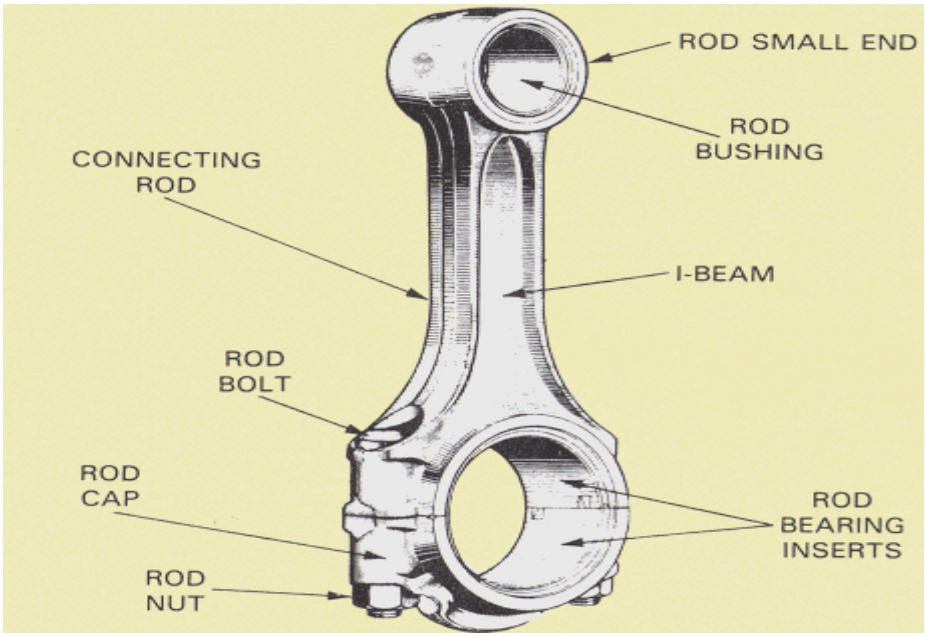


Fig: 1.1. Typical Connecting rod (Schrier, 1999)

To obtain optimum performance from composite materials, there is an advantage in selecting the shape and size of the reinforcement material to suit the application. It is apparent that different material types and shapes will have advantages in different matrices. For instance, silicon carbide whiskers have been particularly effective in toughening Al_20_3 and Si_3N_4. Both silicon carbide whiskers and silicon carbide grit have been effective in increasing the modulus of aluminium alloys (Ikechukwuka, 1999 and Clyne, 2001).

Thus researchers have worked out separately how to reinforce SiC, Al_20_3 (i.e. carbides, nitrides and oxides) TiB_2, boron and graphite into the aluminium matrix. By these reinforcements the composites have high densities and are also expensive.

The ever-increasing demand for low cost reinforcement in a composite material, stimulate the interest towards utilization of by-products from industries as reinforcements. They are readily available and are naturally renewable at lower cost.

1.3 THE PRESENT RESEARCH

The present research focus on the development of metal matrix/coconut shell ash particulate composite for automotive applications with particular interest in the connecting rod out of the numerous research problems.

1.4 AIM AND OBJECTIVES OF THE STUDY

The aim of this work therefore is to develop a metal matrix/coconut shell ash particulate composite for automotive applications with particular interest in the connecting rod.

The specific objectives are to:

i) carry out characterization of the coconut shell ash, and use it with aluminuim alloy to produce MMC.

ii) determine the physical and mechanical properties (such as density and porosity) of the developed composite and also study microstructure, and the various phases using the scanning electron microscope/energy dispersive spectrometer (SEM/EDS) and X-Ray diffraction meter (XRD)

iii) study the corrosion properties of the MMC, and carry out wear test on the MMC,

v). construct the connecting rod with the MMC, and test the performance of the rod

1.5 SIGNIFICANCE OF THE STUDY

The significance of this work is to further exploit the properties, characteristics and potentials of aluminium alloy/coconut shell ash in order to complement its existing areas of application, as well as to determine new areas of application particularly in the production of connecting rods. This research will add value to the abundant coconut shells in Nigeria for the production of metal matrix composites for the automotive and other industries, and reduce the environmental problems of disposal of the agricultural waste by open burning which leads to CO_2carbon dioxide and methane emissions.

The research will reduce the cost of reinforcement in metal matrix composites since coconut shells are available in large quantities and can be regarded as renewable products. The results that will be obtained in this research can act as a starting point for both industrial designers and researchers to design and develop MMC components using this agricultural waste in the production of automotive components, which will be a great benefit to Nigeria and the world at large.

1.6 SCOPE OF THE WORK

Experiments will be conducted under laboratory conditions to assess the physical, microstructural and mechanical properties of the developed metal matrix/coconut shell particulate composite for automotive applications, with particular interest in the connecting rod.

Experimental samples will be produced by the stir casting technique. The samples will be examined under the optical microscope, SEM/EDS and XRD to study the effect of particulate reinforcement on the mechanical properties of the composite.

CHAPTER TWO

LITERATURE REVIEW

2.1 METAL MATRIX COMPOSITE (MMCS)

This chapter reviews past works that are pertinent to the study of local materials for the production of composites. The works are on the metal matrix composite (MMC), aluminium alloy, and coconut shell, production techniques, thermal analysis of the MMC, reactivity in the MMC, and experimental techniques for investigating of physical and mechanical properties.

2.2 METAL MATRIX COMPOSITE (MMCs)

A great deal of research work has been carried out on composite materials at various levels and places which information can serve as a guide to this study.

Aluminium based alloys are widely used in applications where weight savings are important. However, the relatively poor wear resistance of aluminium alloys has limited their use in certain high friction environments (Naresh, 2006). Literature available on the subject reveals that most of the studies have been carried out to evaluate the wear behaviour of aluminium based particulate or whisker reinforced composites. It is generally agreed that various applications of AMCs such as aerospace (satellite struts), defense (electronic instrument racks), automotive (drive shafts and brake discs), sports goods (golf clubs and mountain bicycle frames), and marine (yacht fittings) are created by reinforcement and also the wear properties are improved remarkably by introducing hard intermetallic compounds into the aluminium matrix. The reinforcing materials are generally Silicon (SiC), aliminium oxide (Al_2O_3). Titanium Bromode (TiB_2) and graphite (Aigbodion. 2007).

The use of graphite reinforcement in a metal matrix has the potential to create a material with high thermal conductivity, excellent mechanical properties and

attractive damping behaviour at elevated temperatures. However, lack of wetability between aluminium and the reinforcement, and oxidation of the graphite lead to manufacturing difficulties and cavitations of the material at high temperature (Ejiofor and Reddy, 1997).

Alumina (Clyne, 2000) and other oxide particles like TiO_2, have been used as reinforcing particles in Al-matrix. Alumina has received attention as a reinforcing phase as it is found to increase the hardness, tensile strength and wear resistance of aluminium metal matrix composites. (Maruyama, 1998) Aigbodion and Hassan (2007), Clyne, (2001), Ejiofor and Reddy (1997) studied mica, alumina, silicon carbide, clay, zircon, and graphite as reinforcements in the production of composites. Numerous oxides, nitrides, borides and carbides were studied by Zedalis et al. (1991) as reinforcements for high temperature discontinuously reinforced aluminium (HTDRA). It has been inferred from their studies that HTDRA containing Totanium Carbide Ratanium Bromide (TiC TiB_2), Bromide Carbide (B_4C), Aluminium Oxide (Al_20_3), Silicon (SiC) and Silicon Nitride (Si_3N_4) exhibit the highest values of specific stiffness.

REINFORCEMENT (MMCs)

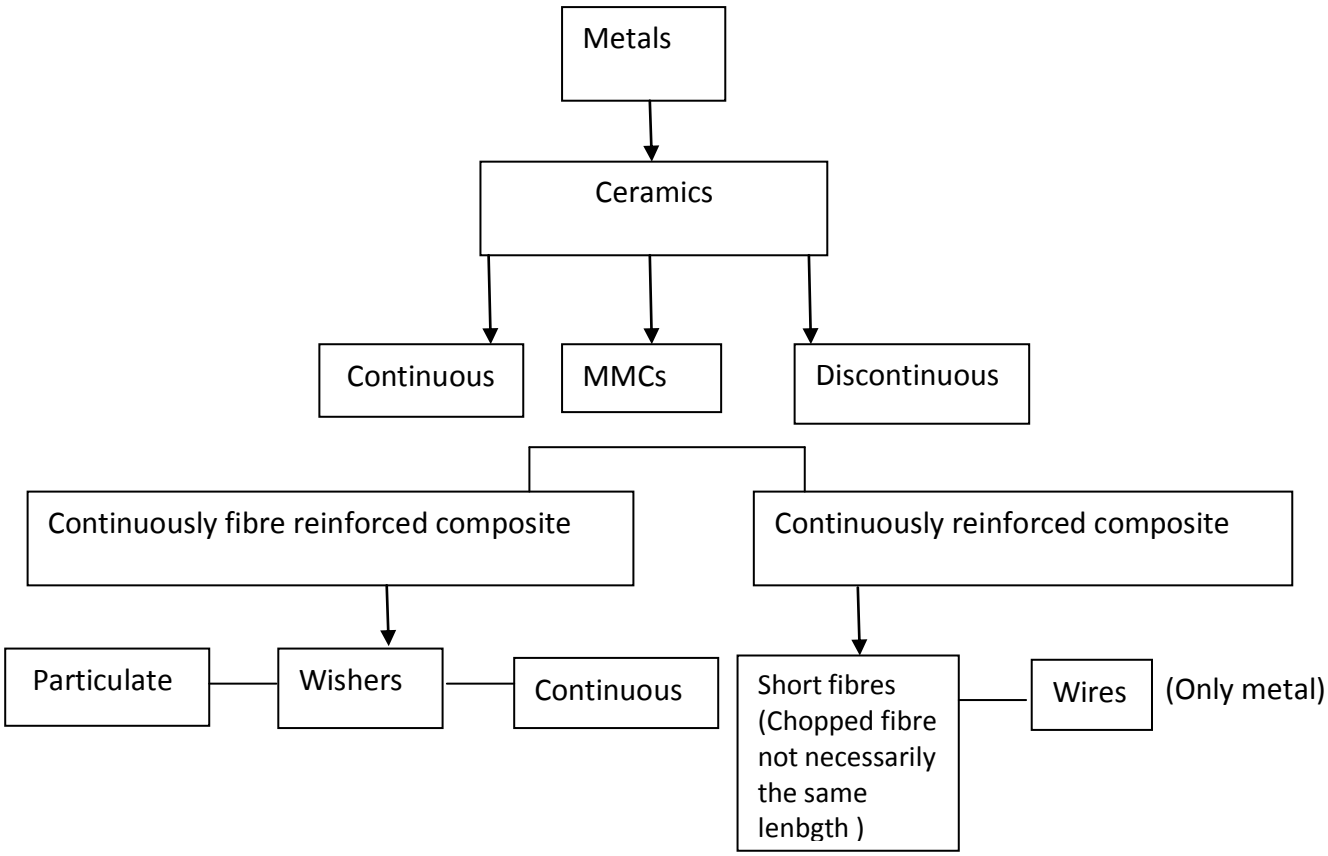


Fig. 2.1: Classification of Metal Matrix Composites (Kainer, 2006)

It has been proven that ceramic particles are effective reinforcement materials in aluminum alloy to enhance mechanical and other properties. The reinforcement in MMCs is usually of ceramic materials; these reinforcements can be divided into two major groups, continuous and discontinuous (Figure 2.1). The MMCs produced by the reinforcements are called continuously (fibre) reinforced composites and discontinuously reinforced composites (Clyne, 2000). However, they can be subdivided broadly into five major categories.

i. Continuous fibres,

ii. short fibres (chopped fibres, not necessarily of the same length),

iii. whiskers,

iv. particulate and wire (only for metal),

Fig 2.1. With the exception of wires, reinforcements are generally ceramics, typically these ceramics being oxides, carbides and nitrides. They are used because of their combinations of high strength and stiffness at both room and elevated temperatures. Common reinforcement elements are Silicon (SiC), Aliminium Oxide ($A1_20_3$), Titanium Bromode (TiB_2), boron and graphite will persist because many of the aspects cited above in addition to contamination from processing equipment and feedstock may vary greatly (Clyne, 2001). Since most ceramics are available as particles, there is a wide range of potential reinforcements for particle reinforced composites.

2.3 MECHANICAL PROPERTIES OF MMCs

Metal-matrix composites (MMCs) have emerged as a class of materials for advanced structural, aerospace, automotive, electronic, thermal management, and wear applications. The performance advantage of metal matrix composites is their tailored mechanical, physical, and thermal properties that include low density, high specific strength, high specific modulus, high thermal conductivity, and high abrasion and wear resistance. In general, the reduced weight and improved strength and stiffness of the MMCs are achieved with various monolithic matrix materials.

The attractive physical and mechanical properties that can be obtained with metal matrix composites, such as high specific modulus, strength and thermal stability, have been documented extensively (Aigbodion and Hassan, 2007). The various factors controlling the properties of particulate MMCs and the influence of the manufacturing methods on the MMCs properties have also been reviewed by several investigators (Ejiofor and Reddy, 1997). Improvement in modulus, strength, fatigue,

creep, thermal and wear resistance properties hava already been demonstrated for a variety of reinforcements (Aigbodion, 2007). Of these properties, tensile strength is the most convenient and widely quoted and is of central importance in many applications.

The strength of particle-reinforced composites is observed to be most strongly dependent on the volume fraction and particle size of the reinforcement. Dislocation strengthening will play a more significant role in the MMCs than in the unreinforced alloy due to the increased dislocation density.

The high temperature creep strength of metals is also greatly improved by the addition of a high temperature stable dispersed phase, due to grain boundary pinning. Grain refinement is not desirable in high temperature materials as it results in a higher rate of grain boundary sliding, which is a key mechanism of creep. For this reason dispersion strengthening is of particular importance in creep resistant metals such as the oxide dispersion strengthened super alloys (Maruyama, 1998).

2.4 PROPERTIES OF ALUMINIUM MATRIX COMPOSITES (AMCs)

The major advantages of AMCs compared to unreinforced aluminium alloy are as follows (Clyne, 2000; Surappa and Rohatgi, 1998, and Whitehouse *et al*, 1991):

- Greater strength
- Improved stiffness
- Reduced density (weight)
- Improved high temperature properties
- Controlled thermal expansion coefficient
- Thermal/heat management
- Enhanced and tailored electrical performance

- Improved abrasion and wear resistance
- Control of mass (especially in reciprocating applications)
- Improved damping properties.

These advantages are quantified for better appreciation. For example, elastic modulus of pure aluminium can be enhanced from 70GPa to 240GPa by reinforcement with 60% by volume of continuous alumina fibres. On the other hand incorporation of 60% alumina fibre in pure aluminium leads to decrease in the coefficient of expansion (Jayalakshmi *et al,* 2004). Similarly it is possible to process Al-9%Si-20% by volume SiC particulate composites having wear resistance equivalent or better than that or grey cast iron (Clyne, 2000). All these examples illustrate that it is possible to alter several technological properties of aluminium/aluminium alloy by more than two to three orders of magnitude by incorporating appropriate reinforcement in suitable volume fraction (Rohatgi *et al,* 1998 and Asthana, 1998). AMC material systems offer superior combinations of properties in such a manner that today no existing monolithic material can rival them (Whitehouse et al. 1991).

Over the years, AMCs have been tried and used in numerous structural, non-structural and functional applications in different engineering sectors (Jokinen and Rauta, 1992; lkechukwuka and Oguocha, 1997 and Lloyd, 1999). The driving force for the utilization of AMCs in these sectors includes performance, economic and environmental benefits. The key benefits of AMCs in the transportation sector are lower fuel consumption, less noise and lower airborne emissions (Lloyd. 1999). With increasing stringent environmental regulations and emphasis on improved fuel economy, use of AMCs in the transport sector will be inevitable (Surappa and Rohatgi, 1981).

AMCs are intended to substitute monolithic materials including aluminium alloys, ferrous alloys, titanium alloys and polymer based composites in several applications. In order that AMC substitution for monolithic materials in engineering systems is widespread, there is a compelling need to redesign the whole system to gain additional weight and volume savings (Lloyd, 1999 and Rohatgi et al 1988). In fact, according to the United Kingdom (UK) Advisory Council on Science and Technology, AMCs can be viewed either as replacements for existing materials, but with superior properties, or as a means of enabling radical changes in system or product design. American Society for Testing and Materials (ASTM Handbook Vol. 2) Moreover, by utilizing near-net shape forming and selective-reinforcement techniques. AMCs can offer economically viable solutions for a wide variety of commercial applications (Maruyama, 1998). Recent successes in commercial and military applications of AMCs are based partly on such innovative changes made in component design. Lack of adequate information and research have hindered the public from the utilization of service properties and possible usage of (AMMCs).

2.5 TYPES OF AMCs

AMCs can be classified into four types depending on the type of reinforcement (Clyne, 2000 and lkechukwuka *et al*, 1997).

- Particle reinforced aluminium matrix composites (PAMCs)
- Short fibre-and whisker-reinforced aluminium matrix composites (SFAMCs)
- Continuous fibre-reinforced aluminium matrix composites (CFAMCs)
- Monofilament reinforced aluminium matrix composites (MFAMs)

2.5.1 Particle Reinforced Aluminium Matrix Composites (PAMCS)

Particulate Reinforced Aluminium Metals or "Particle Reinforced Metals" (PAMC's) are combinations of a metal or alloy with a finite volume fraction of a roughly equiaxed second phase, generally ceramic, that is deliberately introduced into the metal in order to improve its properties. Frequent motivations are to raise the modulus, improve wear resistance, or lower the thermal expansion of aluminium while preserving its low density (silicon carbide particle reinforced aluminium serves as an example) (Clyne, 2000 and Maruyama 1998).

Generally, the improvements that are achieved in the properties of the metal are less extensive than with fibrous reinforcements. However, besides the lower cost, these materials present the additional advantages of having generally isotropic properties, and of being compatible with most metal working processes (e.g machining, deformation processes, welding), particularly when the volume fraction ceramic is below 30 percent (Jokinen and Rauta, 1992, Clyne, 2000).

Particulate reinforcements added to metals are generally ceramic in nature; although in some cases a refractory metal is used (tungsten in copper is an example). The reinforcing particles must, in order to be viable for a given metal, fulfill the following requirements: (Clyne, 2000 and Skibo *et al*, 1998)

(i) They must be comparatively inexpensive. This requirement generally defines both the nature and the form of the particulate reinforcements used in producing engineering PAMCs.

(ii) The matrix and the reinforcement must not be too mutually reactive (unless an in-situ composite is to be produced): given the intimacy or contact between matrix and reinforcement in the composite, the ceramic must thus be chemically stable in contact with the metal.

(iii) Generally, no interfacial reaction is desired, as matrix/particle bonding is in many systems inherently strong without reaction (i.e. it involves chemical bonds crossing the interface), and is weakened by a finite layer of brittle reaction product(s): hence, systems used are essentially those of low or non chemical reactivity.

These preconditions generally narrow the list of candidates for reinforcements to only a few possibilities. For the reinforcement of aluminium and its alloys, silica or reinforcements with a significant fraction of silicon (mullite, for example) are not optimal because of

(i) their reactivity with the matrix (aluminium and magnesium both reduce silica) and (ii) their relatively low elastic modulus compared with that of several alternative ceramics. The two main ceramic particles used as reinforcements for aluminium are: silicon and carbide, alumina (Clyne, 2000), Skibo *et al*. 1998).

2.5.2 Short Fibre and Whisker-Reinforced Aluminium Matrix Composites (SFAMCS)

These contain reinforcements with an aspect ratio greater than five, but are not continuous. Short alumina fibre reinforced aluminium matrix composite is one of the first and most popular AMCs to be developed and used in pistons. Whisker reinforced composites are produced either by powder metallurgy processing or by the infiltration route.

Mechanical properties of whisker-reinforced composites are superior compared to particle or short fibre reinforced composites. However, in recent years, usage of whiskers as reinforcements in AMCs is fading due to perceived health hazards and hence of late, commercial exploitation of whisker-reinforced composites

has been very limited. Short fibre reinforced AMCs display characteristics in between those of continuous fibre and particle reinforced AMCs (Clyne, 2000).

2.5.3 Continuous Fibre-Reinforced Aluminium Matrix Composites (CFAMCS)

In continuous fibre reinforcements, the reinforcements are in the form of continuous fibres (of alumina, silicon carbide or carbon). The fibres can either be parallel or pre-woven, braided prior to the production of the composite. AMCs having fibre volume fraction up to 40% are produced by the squeeze infiltration technique (Clyne, 2000).

2.5.4 Monofilament Reinforced Aluminium Matrix Composites (MFAMCS)

Monofilaments are large diameter (100 to 150μm) fibres, usually produced by chemical vapour deposition (CVD) of either silicon carbide or boron into a core of carbon fibre. Bending flexibility of monofilaments is low compared to multifilaments. Monofilament reinforced aluminium matrix composites are produced by diffusion bonding techniques and are limited to super plastic forming aluminium alloy matrices. In continuous fibre-reinforced aluminium matrix composites and mono filament reinforced aluminium matrix composites the reinforcement is the principal load-bearing constituent and the role of the aluminium matrix is to bond the reinforcement, transfer and distribute the load. These composites exhibit directionality and have low strength in the direction perpendicular to the fibre orientation (Ikechukwuka and Oguocha, 1997).

2.6 EFFECT OF CERAMIC REINFORCEMENTS ON THE BEHAVIOUR OF ALUMINIUM MATRIX IN AMCs

The presence of a relatively large (more than 10%) volume fraction of ceramic reinforcement (whisker, particle, short fibre and continuous fibre) profoundly affects the behaviour of aluminium matrix in aluminium matrix composites during manufacturing, heat treatment and their subsequent use in service. These changes include both intrinsic and extrinsic ones (Surappa and Rohatgi, 1981).

2.6.1 Intrinsic Effects of Ceramic Reinforcements

Intrinsic effects include microstructural changes, heat treatment characteristics and thermal stresses. These changes significantly alter and expand the physical, mechanical and tribological property limits of aluminium alloy (Clyne, 2000).

The presence of ceramic reinforcement can alter the solidification behaviour of aluminium alloys in several ways. Ceramic reinforcement can serve as a barrier to diffusion of heat and solute, catalyze the heterogeneous nucleation of phases crystallizing from the melt, restrict fluid convection and induce morphological instabilities in the solid-liquid interface.

Aluminium matrix composites often experience fabrication temperature in excess of 500^0C, and large thermal residual stresses are included on cooling. The magnitude of thermal residual stresses developed is related to many variables including the type of reinforcement, volume fraction, diameter and aspect ratio. For example, thermal residual stresses (tensile) of more than 100 MPa are present in the matrix of Al-30% by volume SiC particulate composites. Mechanical behaviour of AMCs is profoundly affected by thermal residual stresses. The presence of residual stresses caused by ceramic reinforcements results in a symmetrical yielding, and also affect fatigue and creep behaviour (Maruyama, 1998).

2.6.2 Extrinsic Effects of Ceramic Reinforcement

Incorporation of ceramic reinforcement in aluminium alloys leads to significant improvement in the sliding wear resistance of AMCs as measured by the pin-on-disc set up against a hardened steel disc (Zhou and Xu, 1997).

In recent years the extrinsic effect of SiC reinforcement in AMCs has been beneficially utilized in brake disc/brake pad tribo couples. When the AMCs brake disc slides against the brake pad adherent tribo layers are formed on the surface of the AMCs disc at the contact region (Donne *et al*, 1990). Tribolayers thus formed, further enhance the wear resistance of the AMC discs. Tribolayers consisting of mixed oxides are formed due to the transfer of material from the brake pad on to the AMCs disc during sliding (Surappa and Rohatgi, 1981, Clyne, 2000).

2.7 APPLICATIONS OF AMCS

AMCs now have a proven track record as successful "high-tech" materials in a range of applications. AMCs utilization provides significant benefits including performance benefits (component lifetime, improved productivity), economic benefits (energy savings or lower maintenance cost) and environmental benefits (lower noise levels and fewer air-borne emissions). Engineering viability of AMCs in a number of applications has been well documented. AMCs having different types of reinforcements (whiskers, particles, short fibres and continuous fibres) have been produced both by solid state and liquid state processing (Surappa and Rohatgi, 1981, lkechukwuka and Oguocha, 1997). The various and numerous applications are mentioned below and shown in plate 2.1(a, b, c &d)

Brake rotors for German high-speed trains ICE-1 and ICE-2 were developed by Knorr Bremse AG and made from a particulate reinforced aluminium alloy (AlSi7Mg+SiC particulates) supplied by Duralcan. Compared to conventional parts

made out of cast iron weigh 120 kg per piece: the 76kg of the AMC rotor offers an attractive weight saving potential. The braking systems (discs, drums, calipers or back-plate) of the New Lupo from Volkswagen were made from particulate reinforced aluminium alloy supplied by Duralcan.

AMCs continuous fibre reinforced pushrods were produced by Duralcan for racing engines. These pushrods weigh 40% as much as steel ones; they are stronger and stiffer and have high vibration damping, AMC wires were also developed by Duralcan for the core of electrical conductors. The unique properties of this type of conductor offer substantial performance benefits when compared to the currently used steel wire reinforced conductors.

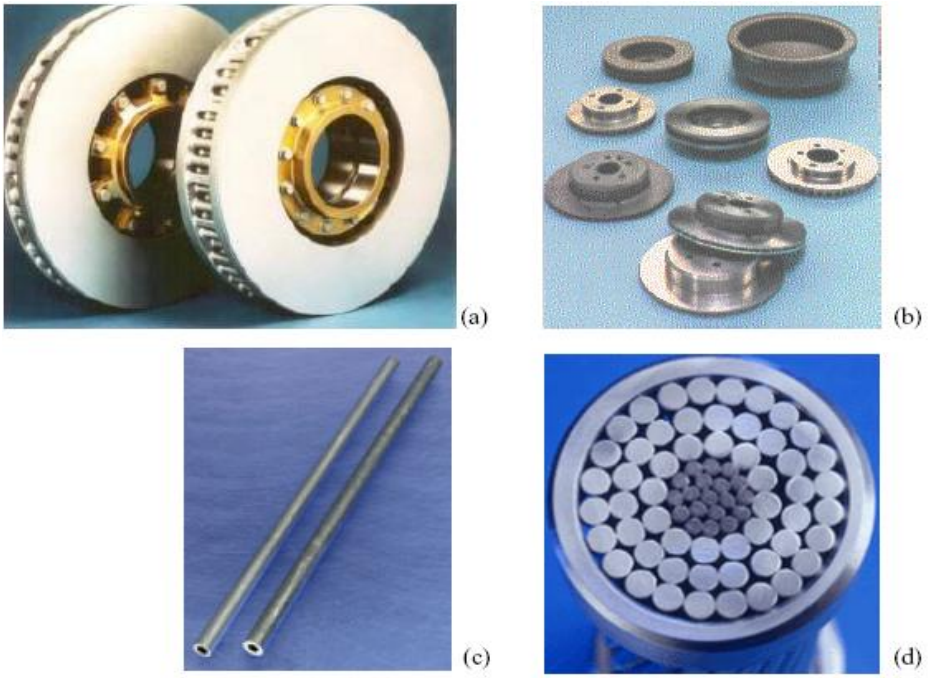


Plate 2.1: Some Industrial Applications of AMCs (a) brake rotors for high speed train (b) automotive braking systems (c) automotive pushrods (d) cores for HV electrical wires. (Sources: Surappa *et al*, 1981 and Ikechukwuka, 1997).

2.8 REVIEW OF PAST WORKS.

Prasad and Krishna (2010) worked on the fabrication and characterization of A356.2-rice husk ash (RHA) composite using the stir casting technique. In the study, metal matrix composites (MMC's were prepared by addition of 2, 4, and 8% by weight RHA particulates through the stir casting technique. Mechanical properties like density and hardness for the composites were determined. It was observed that as the percentage of RHA particles increased the density of the composites decreases and there is slight increase in the hardness.

Aigbodion *et al* (2010) worked on the potential utilization of solid waste bagasse ash. In the study, bagasse ash was chemically and physically characterized in order to evaluate the possibility of its use in industry.

Fabricated aluminium composite using a recycled aluminium automotive component and had chosen discarded engine blocks (Al-Si alloy) as a matrix for the composite. The recycled aluminium composite brake disc was found to have significant weight reduction which is about one-third of the conventional cast iron brake disc.

Rohatgi *et al* (1998), studied the application of fly-ash in synthesizing low cost metal matrix composites for automotive and other engineering applications. The work summarizes attempts of incorporating fly ash material content, cost, and weight on selected industrial components while also improving selected properties.

Harun *et al* (2006), studied the effect of fly ash particle reinforcements on the microstructure, porosity and hardness in Al-(Si-mg) cast composites. The composites were fabricated by the stir casting process and characterized by optical microscopy, an image analyzer, scanning electron microscopy, and hardness measurements. The results showed that particle contents affected the porosity and hardness of the

composites. An increase in the fly ash content increases the porosity in the composites, with the matrix alloy reinforced with 15% by weight of fly ash particles having the highest porosity and lowest hardness.

Ejiofor and Reddy (1997), reviewed developments in the molten processing of particulate Al-Si alloy composites and their respective properties. Existing and emerging processing innovations were discussed.

Bienia *et al*. (2003), reported that the addition of fly ash increased the corrosion rate of an Al-Si (4xxx) alloy in 3.5% by weight NaCl solution at a pH of 7. They attributed the decrease in corrosion resistance of the composite to increased galvanic corrosion between the Si liberated in the reaction between silica in fly ash particles and liquid aluminium. Furthermore, the deterioration of corrosion resistance of the composite was also attributed to the porosities created in the matrix by the introduction of fly ash particles

Nath *et al.* (1989), observed that Al-Mg and Al-Cu composites exhibited superior corrosion resistance to their composites reinforced with mica particles. The inferior corrosion resistance of the mica reinforced composites was attributed to the distortion of the passive protective films and provision of pit nucleation sites by the mica particles.

Candan *et al.* (2004), reported the addition of SiC particles to Al-4 w alloy in 3.5 wt by weight NaCl solution. They postulated that the Mg_2Si phase generated from a two-step reaction between liquid Al and SiC hindered the passage of electrons thus improving the corrosion resistance of the composites.

Kiourtsidis et al. (1998), noted that although SiC was not directly responsible for the enhanced pitting corrosion of aluminium AA2024 composites in 3.5% by weight NaCl solution, intermetallic phases surrounding the particles initiated pitting

attack of the material. They attributed the pits adjacent to the interdendritic zone to galvanic couples between the cathodic Al_2Cu and anodic α-phases.

Aylor *et al.* (1985), reported that the presence of SiC in AA6061 matrix did not increase the susceptibility of the composites to pitting attack in marine environments. Pits however occurred at the SiC/Al interface.

Aigbodion (2007) has used Kankara clay (alumino-silicate) in reinforcing Al-Si alloy. Biennia *et al* (2003) used fly ash in reinforcement of the aluminium matrix. Naresh (2006), worked on the development and characterization of metal matrix composite using red mud and industrial waste for wear resistance applications. Aigbodion and Hassan (2010) used the vortex method in the production of aluminium alloy matrix composites reinforced with bagasse ash particles. They reported good dispersion and recovery of the particles in the composite castings. In order to carry out further research in this noble area, is what has motivated the present research, which is the utilization of coconut shell ash in the reinforcement of aluminium alloy for automotive applications.

2.9 NIGERIA COCONUT

Commercial coconut production is mainly located in the southern part of Nigeria and dates back to the early 1960s, when the Nigerian Government started a massive agricultural diversification plan. Today, coconut is one of the world's most important fruit crops. Nigeria is one of the largest producers and exporters of coconut in the world. The industry provides employment to more than half a million people and livelihood to an estimated one million people (Prasertsan and Sajjakulnukit, 2006). The crop is used for a myriad of purposes from an ingredient in food products to engine lubricants. Moreover coconut is becoming an increasingly important

agricultural product for tropical countries around the world as a new source of energy-biofuel.

Until recently, the remaining 90% of the plant (empty fruit bunches, fibres, fronds, trunks) was discarded as waste, and either burnt in the open air or left to decay in waste ponds. This way, the coconut processing industry's waste contributed significantly to CO_2 and methane emissions (Butler, 2006). The later point might bring about various negative effects such as pollution from agrochemicals, erosion of soil, biomass and biodiversity; poisonings, chronic diseases resulting from pesticides in food, and unstable market prices, unpredictable income for farmers, disproportionate inflation rates between urban and rural sectors, debts, loss of culture, knowledge and traditional values, dependence on cash and technology (Bamgboye and Jekayinfa, 2006).

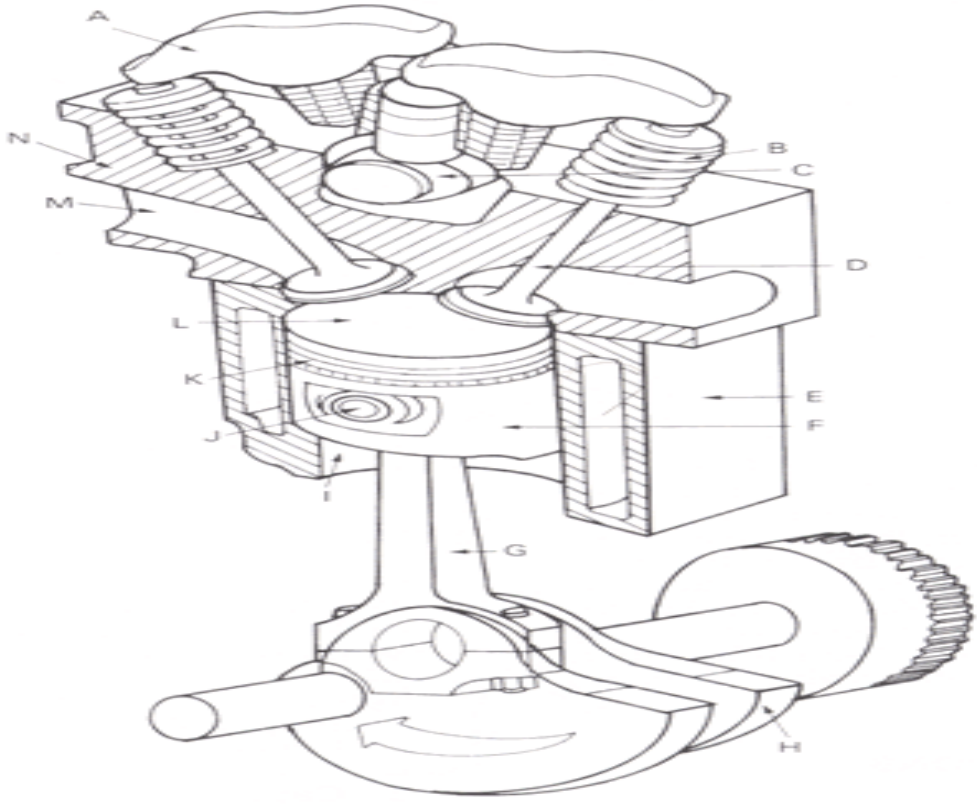
Presently, in Nigeria the coconut shell is used as a source of fuel for boilers. Unfortunately, the coconut shell contains silicates that form scale in boilers if too much shell is fed to the furnace, thus limiting the amount of coconut shell that can be utilized in boilers. Residual coconut shell is disposed of as gravel for plantation roads maintenance. Blacksmiths also buy the coconut shell to use as fuel material in their casting and forging operations (Butler, 2006).

Several companies have carried out studies to ascertain the viability of using coconut shell based biomass fuels. This development will further push towards higher demand for coconut in the next fifteen years (Butler, 2006). Going through available information on the utilization of coconut shell, it is seen that the use of coconut shell ash as reinforcement material for preparation of MMCs has not been explored.

2.10 CONNECTING ROD.

The connecting rod is said to be the most integral part of an engine. The connecting rod must be able to withstand tremendous loads and transmits a great deal of power, therefore it is no surprise that a failure in a connecting rod can be one of the most costly and damaging failures in the engine.

Schreier (1999), outlined the fundamental parts of an engine as shown in Fig 2.2: Surface L is where combustion occurs, air enters through M, and H is the shaft through which power is accumulated and delivered from the engine. Combustion occurs at the top surface of the piston F and pushes the connecting rod G downwards, causing the shaft to move in a circular motion. It is easy to see that the connecting rod harnesses all of the power produced in combustion, and converts it into something useful: in this case, spinning the shaft.



A. Rocker arm
B. Valve spring
C. Camshaft
D. Valve
E. Engine block
F. Piston
G. Connecting rod
H. Crankshaft
I. Cylinder wall or Sleeve
J. Con-rod pin
K. Piston ring
L. Piston crown
M. Exhaust manifold or port
N. Top cylinder

Fig. 2.1: Typical application of a connecting rod in an engine (Schreier, 1999)

2.10.1. Forces on Connecting Rod (I)

A connecting rod is subjected to a thrust load because of the fuel explosion on top of the piston. The connecting rod, therefore, can be treated as a column with pin ends.

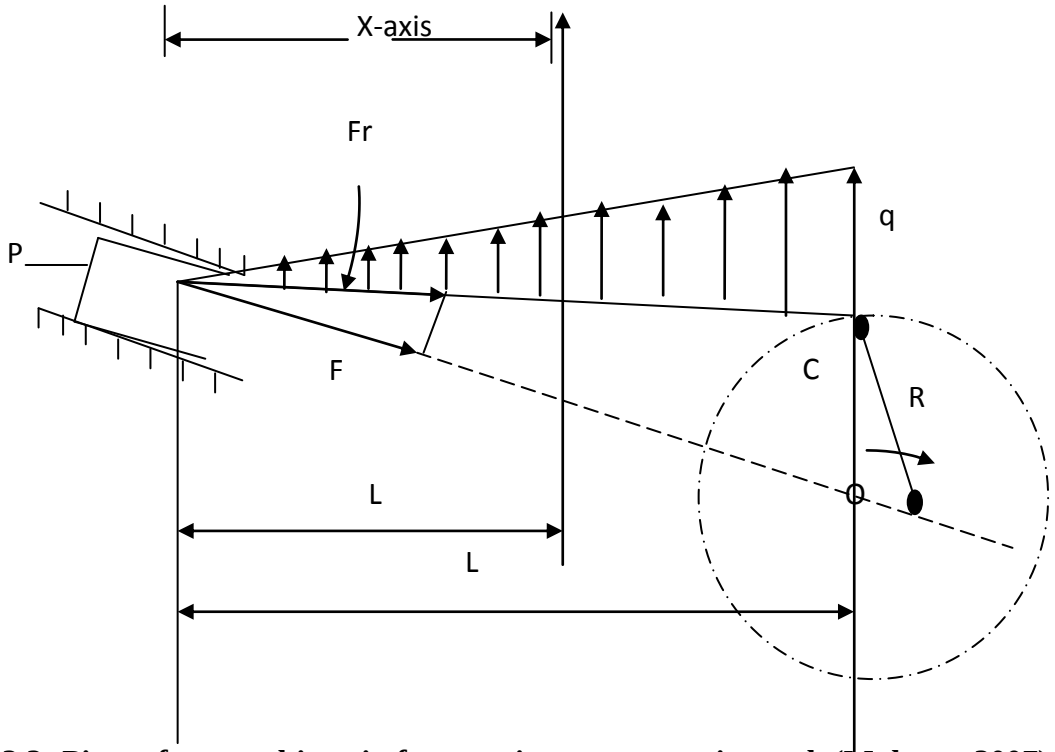


Fig. 2.2: Piston force and inertia force acting on connecting rod. (Mubeen, 2007)

The angular acceleration further imposes inertia force on the connecting rod which varies from zero at the piston pin (where the angular acceleration is zero) to a maximum at the crank pin end (where angular acceleration is maximum). This inertia force acts transversely on the connecting rod, causing a bending moment on it. The inertia force is shown distributed on the length of connecting rod in Figure 2.3, hence outlined two types of forces acting on the connecting rod as Mubeen (2007):

$$Fr = \frac{\delta_c A_c}{\dfrac{\delta_y}{4n\pi^2 E\left(\dfrac{L}{K}\right)^2}} \quad - - - - - - - - \quad (2.1)$$

where

F_r = effective axial force on connecting rod derived from gas pressure

A_c = cross-sectional area of connecting rod

L = centre to centre length of connecting rod

k = radius of gyration of cross-section of connecting rod

σy = yield strength of connecting rod material

n = column end factor

E = modulus of elasticity of connecting rod.

Further analysis assumes that the connecting rod pin -end is in the plane of oscillation as shown in Figure 2.3. On the other hand, in the plane perpendicular to the plane of oscillation, its ends are better regarded as fixed because of the length of the small end bearing covering 1.5 x diameter of gudgeon pin and the length of the large end bearing at the crank end is even larger. The section of the connecting rod is normally an I –section with pin-ended behaviour about the x-axis (Fig.2. 4), and the fixed-ended behaviour about y –axis. According to Mubeen (2007), from theory of columns, it is known that a fixed column is four times stiffer than the pin-ended column. For using equation (2.1), however, k will be k_{xx} where columns behave as pin ended about the xx-axis.

Equation (2.1) can in fact be used as a design equation directly if A_c and k_{xx} are substituted properly. The proposed I-section for connecting rod is shown in Fig. 2.4. Other typical sections that suit the manufacturing process (forging) are also shown in the same Figure 2.4 (a)

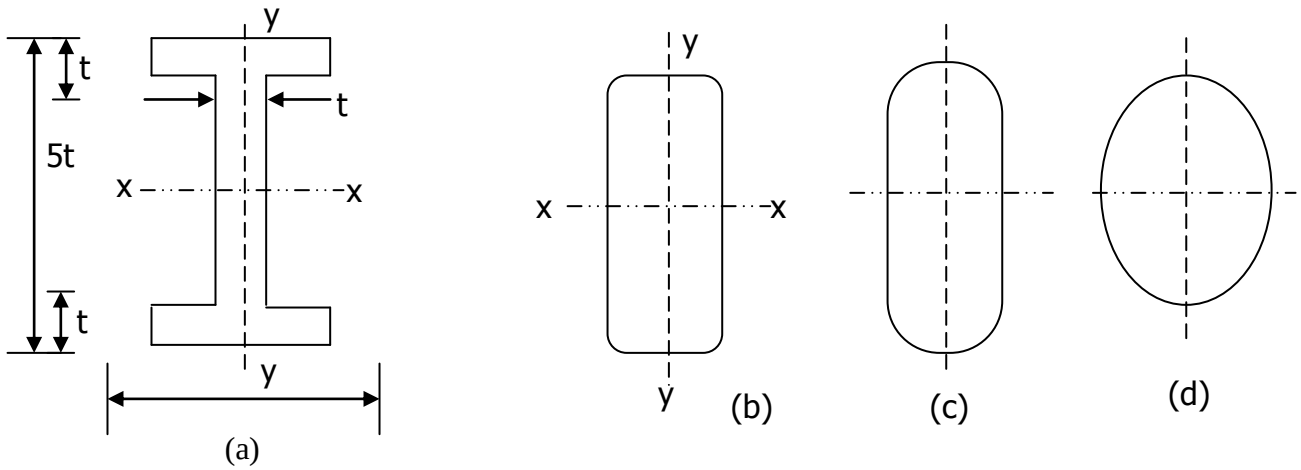


Fig 2.3: Connecting rod sections. The I –section is shown at (a)

It is a good proposition to make the I –section of connecting rod equally strong about the xx and yy axis.

$$Fr\ I_{xx} = \frac{419}{12} t^4$$

$A_c = 11t^2$

$K_{xx}^2 = 3.17t^2$

It is to be further noted that the coefficient of $(L/k)^2$ is constant for a given material and end conditions. The equation is written as:

$$Fr = \frac{\sigma c Ac}{1\ a\left(\frac{L}{k}\right)^2} \quad - - - - - - - \quad (2.2)$$

Ac is a constant whose value for forged steel is 1/7500 and for cast iron it is 1/1600 for pin ended conditions. Mubeen (2007), now if F_r, σ_c and L are known, the values of A_c and k_{xx} can be substituted and the value of t can be calculated. σ_c will be prescribed as permissible compressive stress. The force F_r is given by Mubeen (2007) as:

$$Fr = \frac{F}{1 - \left(R/L\right)^2 \sin^2} \quad -- \quad - - - - - - \quad (2.3)$$

Table: 2.1: Comparison of steel and MMC connecting rods (Sala, 2001).

	Mass (kg)	Variation (%)	Strength (N)	Specific strength ($N/kg/10^3$	Variation (%)	Stiffness (N/mm^2)	Specific stiffness (N/mmkg) 10	Variation (%)
Steel	0.130	-	61780	498	-	21960	192	-
MMC	0.088	-32	52570	597	+20	21870	248	+29

Sala (2001), stressed that the comparison in terms of specific performance as in Table 2.1, shows that the specific characteristics of the MMC connecting rod are remarkably higher than those of its steel counterpart, and could be further improved through technology optimization.

CHAPTER THREE

MATERIALS AND METHODS

3.1 EXPERIMENTAL PROCEDURE

The section describes and discusses the materials, equipment and all the techniques used in this research, which include production of the composites, micro structural analysis, thermal analysis, determination of mechanical properties and wear characteristics, corrosion tests and development of a prototype connecting rod and testing it.

3.2 MATERIALS

Pure aluminium wire was obtained from Northern Aluminium Company (NOCACO), Kaduna, Nigeria, manufacturers of electrical cables and wires and conduit pipes. The coconut shells were obtained from coconut sellers in Kaduna; silicon and iron powder were purchased from a chemical shop in Kaduna, Nigeria.

3.3 EQUIPMENT

Equipment used in this research are- a

i. pyrometer,
ii. mechanical stirrer,
iii. crucible,
iv. electrical resistance furnace,
v. Avery Denison impact tester (Charpy),
vi. Rockwell hardness tester,
vii. Tinus-Olsen tensile test machine,
viii. grinding and polishing machine,
ix. X-ray diffractometer (XRD) machine,

x. scanning electron microscope with energy dispersive spectrometer(SEM/EDS),

xi. X-ray fluorescent XRF,

xii. DTA/TGA machine

xiii. pin- on- disc machine.

3.4 METHOD

3.4.1 The Processing and Chemical Analysis of the Coconut Shell Ash

Coconut shells were ground to form coconut shell powder, the powder was packed in a graphite crucible and fired in an electric resistance furnace at a temperature of 1300^{o}C to form coconut shell ash (CSAp) (Plates 3.1-3.2). The particle size analysis of the coconut shell ash particles was carried out in accordance with BS1377:1990 (Bienia *et al*, 2003) About 100g of the coconut shell ash particles were placed in a set of sieves, arranged in descending order of fineness and shaken for 15minutes which is the recommended time to achieve complete classification. The particles that were retained in the BS 100µm were used in this study because the fine reinforcement particle size is among several factors responsible for increase in tensile strength and hardness value of composites. It was also carried out in accordance with recommended standard on similar works (Rohatgi and Guo (1997), Prasad and Krishna (2010), Aigbodion and Hassan (2010).



(a)



(b)

Plate 3.1: Photograph of Coconut shell



(c)



(d)

Plate 3.2: Photograph of Coconut shell ash particles

Plates (3.1 and 3.2) are identified as:

(a) Coconut shell

(b) Crushed coconut shell

(c) Coconut shell powder

(d) Coconut shell ash particles

The mini pal compact energy dispersive X-ray spectrometer (XRF) was used for the elemental analysis of the coconut shell ash. The system is controlled by a PC running the dedicated mini pal analytical software (Bienia *et al*, 2003).

A FTIR-8400S Fourier transform infrared spectrophotometer (SHIMADZU) was used for the functional groups present in the coconut shell ash. A spectrometer

and detector capable of measuring functional groups to the predetermined minimum detectable level were employed. The system includes a personal computer with compatible software that provides real-time updates of the spectral profile during sample collection and spectral collection, using a FTIR system at 1 cm^{-1} resolution, 22 metre path length, and a broad band MCT detector. The data analysis was performed using appropriate reference spectra, whose concentrations can be verified using CTS spectra (Bienia *et al,* 2003).

3.4.2 Specimen Preparation

The production of the composites was done by the double stir-casting method (Fig 3.1). Initially, Al-7%Si weight of alloy was charged into the graphite crucible furnace and heated to about 750 ºC, untill the entire alloy in the crucible was melted and 2% by weight iron powder was added. The reinforcement particles (CSA) were preheated to 800^{O}C for 1 hour before incorporation into the melt. After the molten metal was fully melted, 0.05% by weight degassing tablets (hexachloroethane) were added to reduce the porosity. Simultaneously, 1% by weight magnesium was added to the melt in order to enhance the wetabability between coconut shell ash particles and the alloy melt.

It was noticed that without the addition of magnesium, the particles of coconut shell ash were rejected. The stirrer made of stainless steel was lowered into the melt slowly to stir the molten metal at the speed of the speeds seem too high for stirring (500 -700) rpm. The preheated CSA particles were added into the molten metal during the stirring time. The stirring rate continued for another 5mins, even after the completion of particle feeding. The mixture was poured into the mould which was also preheated for 30 min to obtain uniform solidification. Moulds can be preheated by exposure to direct flame, or in an oven, but preheating in an oven until

the molten metal is ready for pouring was chosen and it is much more desirable(Metal Handbook,1970). Using this process, 0, 3, 6, 9, 12 and 15% by weight CSA particle- reinforced composites were produced.

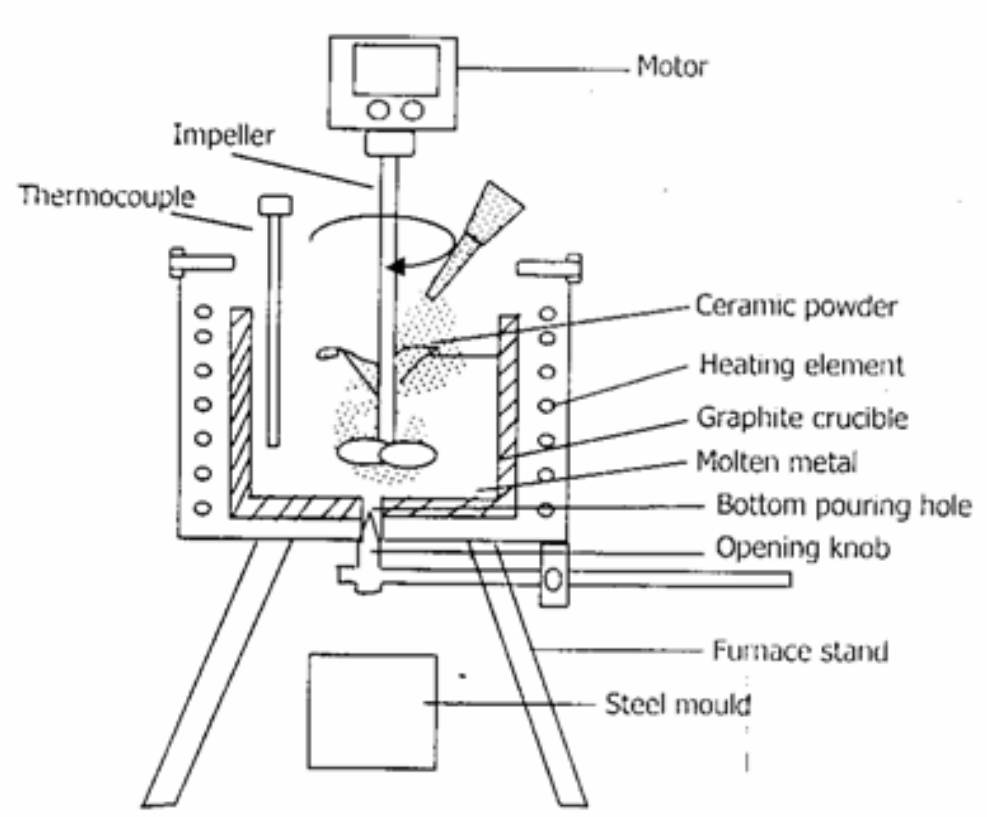


Fig. 3.1: Schematic drawing of Stir-Casting (Clyne, 2000)

3.4.3 Density Measurement

Density measurements were carried out on the coconut ash and composite samples using Archimedes's principle. The buoyant force on a submerged object is equal to the weight of the fluid displaced. This principle is useful for determining the volume and therefore the density of an irregularly shaped object by measuring its mass in air and its effective mass when submerged in water (density = 1 gram/cc). This effective mass under water was its actual mass minus the mass of the fluid displaced. The difference between the real and effective mass therefore gives the mass of water displaced and allows the calculation of the volume of the irregularly shaped object.

The mass divided by the volume thus determined gives a measure of the average density of the samples. The density of the sample was then estimated from equation 3.1 (Maruyama, 1998):

3.4.4 X-RAY Diffractometer (XRD) Analysis

The XRD analysis of the coconut shell ash and the developed composites was carried out using Philips X-ray diffractometer at the Department of Chemical and Metallurgical Engineering, University of Witwatersrand, Johannesburg, South Africa. The X-ray diffractograms was taken using Cu Kα radiation at a scan speed of 3^{o}/ min. The samples were rotated at precisely one-half of the angular speed of the receiving slit, so that a constant angle between the incident and reflected beams is maintained. The receiving slit is mounted in front of the counter on the counter tube arm, and behind it is usually fixed a scatter slit to ensure that the counter receives radiation only from the portion of the specimen illuminated by the primary beam. The intensity diffracted at the various angles was recorded automatically on a chart and the appropriate (Ɵ) and (d) values were then obtained.

3.4.5 Microstructural Analysis

The microstructure of the coconut shell ash, cast samples and surface morphology of the wear debris were studied using a JOEL JSM 5900LV scanning electron microscope equipped with an Oxford INCA^{TM} energy dispersive spectroscopy system at the Department of Chemical and Metallurgical Engineering, University of Witwatersrand, Johannesburg, South Africa. The samples were firmly held on the sample holder using double-sided carbon tape before putting them inside the sample chamber. The SEM was operated at an accelerating voltage of 20 Kv as indicated by Aigbodion and Hassan, (2010).

3.4.6 Hardness Testing

The hardness values of the samples were determined according to ASTM E18-79, (2000) using the Rockwell hardness tester on "B" scale (Frank Well test Rockwell Hardness Tester, model 38506) with a 1.56mm steel ball indenter, minor load of 10kg, and major load of 100kg and hardness value of 101.2HRB on the standard block. Before the test, the mating surface of the indenter, plunger rod and test samples were thoroughly cleaned by removing dirt, scratches and oil and calibration of the testing machine using the standard block. The samples were placed on anvils, which act as supports for the test samples. A minor load of 10kg was applied to the sample in a controlled manner without inducing impact or vibration and zero datum position was established, and the major load of 100kg was then applied. The reading was taken when the large pointer came to rest or had slowed appreciably and dwelled for up to 2 seconds. The load was then removed by returning the crank handle to the latched position and the hardness value read directly from the semi automatic digital scale.

3.4.7 Tensile Test

The tensile test on the samples were conducted on the Tinus-Olsen tensile testing machine at a strain rate of $2x10^{-3}S^{-1.}$ The test pieces were machined to the standard shape and dimensions as specified by the American Society for Testing and Materials (ASTM D, 2000). The sample was locked securely in the grips of the upper and lower jaws of the testing machine. A small load was initially applied to seat the sample in the jaws and then the load was increased until failure occurred. The values of the load and the extension were recorded and were used in obtaining the stress-strain graph.

3.4.8 Impact Strength Test

The impact test of the sample was conducted using a fully instrumented Avery Denison test machine. Charpy impact tests were conducted on notched samples. A standard square impact test sample measuring 75 x 10 x 10 mm with notch depth of 2 mm and a notch tip radius of 0. 02 mm at angle of 45^{o} was used (ASTM D, 2000). The precision of the machine is 0-25 Joules.

3.4.9 Wear Test

A pin-on-disc test apparatus was used to investigate the dry sliding wear characteristics of the composites as per ASTM G99- 95 standards (Korkut, 2008, Basavarajappa *et al,* 2006). The disc used is En-32 steel hardened to 62 HRC, 120 mm track diameter and 8 mm thick, with surface roughness of 10l . The initial weight of the samples was measured using a single pan electronic weighing machine with an accuracy of 0.01 g. During the test, the pin is pressed against the rotating disc. The wear tests were conducted by varying applied load from 10 to 50N at a constant speed of 2.0m/s and sliding distance of 4000m.

The wear of the samples was studied as a function of the percentage volume of reinforcement, applied load and sliding velocity. The formula used to convert the weight loss into wear rate is (Basavarajappa *et al,* 2006):

$$\text{Wear rate} = \frac{\Delta W}{S} \quad \text{- - - - - - - - (3.1),}$$

where, ΔW is the weight difference of the sample before and after the test in g, S is total sliding distance in m.

3.4.10 Thermal Analysis

Thermal decomposition (TA) was observed in terms of global mass loss by using a TA Instrument TGA Q50 thermogravimetric analyzer. The apparatus detects the mass loss with a resolution of 0.1 as a function of temperature. The samples were evenly and loosely distributed in an open sample pan of 6.4 mm diameter and 3.2 mm deep with an initial sample weight of 8-10 mg. The temperature change was controlled from room temperature (25±3°C) to 900°C at a heating rate of 10°C/min.

High purity argon was continuously passed into the furnace at a flow rate of 60 mL/min at room temperature and atmospheric pressure. Before the start of each run, the argon was used to purge the furnace for 30 min to establish an inert environment in order to prevent any unwanted oxidative decomposition. The TG and DTA curves were obtained from TGA runs using universal analysis 2000 software from TA Instruments.

3.4.11 Corrosion Test

The standard immersion corrosion test was used to investigate the weight loss and corrosion rates of the composite materials in specified electrolytes. Test samples were polished using several grades of emery paper ranging from 240 to 600 grit, rinsed in distilled water and methanol, and dried, then weighed using an electronic weighing balance. The sample weights were measured in grams to 4 decimal places. After weighing, the samples were immersed in 3.5 wt. % NaCl solution for corrosion tests. The plastic threads should be attached to a wooden support as shown in Fig 3.2 and the solution-to-sample surface area ratio was 312.5 ml cm^{-2}. After each immersion test, the samples were extracted from the electrolyte and cleaned in 70 wt. % HNO_3 (specific gravity = 1.4134) for 1 to 5 minutes as specified by ASTM G1 (Aylor and Moran, 1985). The corrosion products on the surface of the samples were

removed by rubbing gently against a soft wet nylon sponge drenched in water. The specimen should then be cleaned in methanol.

The standard immersion corrosion test was used to investigate the weight loss and corrosion rates of the composite materials in specified electrolytes. Test samples were polished using several grades of emery paper ranging from 240 to 600 grit, rinsed in distilled water and methanol, and dried, then weighed using an electronic weighing balance. The sample weights were measured in grams to 4 decimal places. After weighing, the samples were immersed in 3.5 wt. % NaCl solution. The plastic threads should be attached to a wooden support as shown in Fig 3.2 and the solution-to-sample surface area ratio was 312.5 ml cm^{-2}. After each immersion test, the samples were extracted from the electrolyte and cleaned in 70 wt. % HNO_3 (specific gravity = 1.4134) for 1 to 5 minutes as specified by ASTM G1 (Aylor and Moran, 1985). The corrosion products on the surface of the samples were removed by rubbing gently against a soft wet nylon sponge drenched in water. The specimen should then be cleaned in methanol.

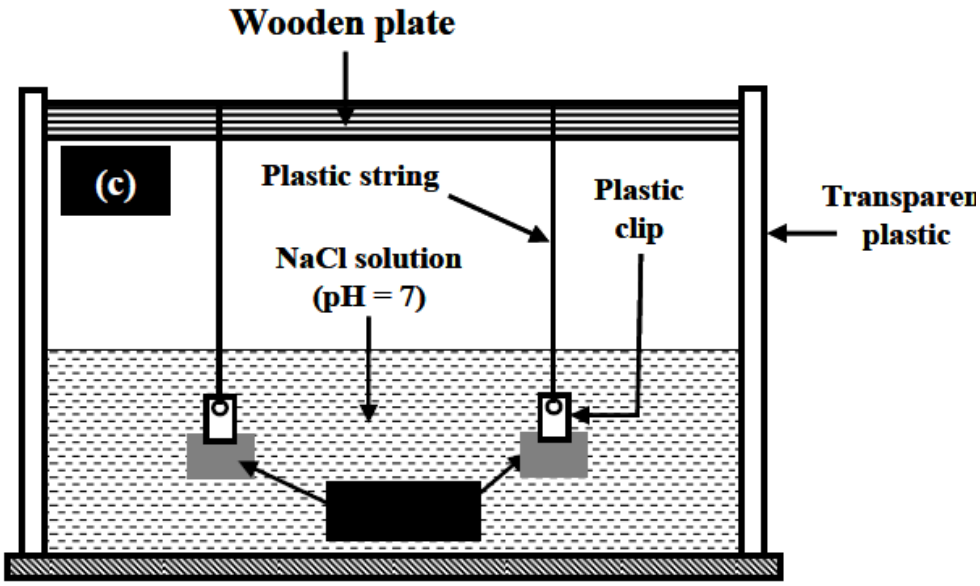


Fig 3.2: Sketch for the Corrosion Test Apparatus. (Candan and Bilgi, 2004)

The samples were placed in an air furnace maintained at 100^{o}C for 2 hours and subsequently cooled to room temperature at the rate of 0.625^{0}C/min and re-weighed. The exposure time was varied from 1, 3, 6, 9, 12, and 15 days (giving a cumulative total exposure time of 46 days for each sample). The cleaning procedure was observed after each exposure. To account for metal loss resulting from cleaning of the samples, the weight loss of uncorroded control sample was obtained using the same cleaning procedure. Weight loss data was obtained by subtracting weights obtained after each exposure to the electrolyte from the initial weights before the exposure. The corrosion rate of each sample in mm/year was determined using the expression of Aylor and Moran (1985):

$$Mm/yr = 87.6W/DAT, \quad - \quad - \quad - \quad - \quad - \quad - \quad (3.2)$$

Where *W is* weight loss is in mg, *D* is density in g/cm^{3}, *A* is surface area in cm^{2}, and τ is time in hours.

3.4.12 **Design of the Connecting Rod** (Basic consideration)

The basis for the choice of the MMC connecting rod dimension is for it to be tested on a Toyota starlet of 12 valve engine model E series**.**

Engine specifications it is a four stroke, four cylinder petrol engine type with the following parameters;

Bore x stroke; 73.0mm x 77.4mm

Displacement; 1,295cc

Compression ratio; 5:1

Standard output range of the engine is from 65hp (48kw) to 82hp (61kw) at 600 rpm with a torque of 98N-m at 3000 rpm to 7716ftlb 104N-m) at 5,200 rpm.

This engine can run in both carbureted and fuel injected versions.

The specific pressure on the joint surface between the bushing and small end of the connecting rod is according to Demidov and Kolchin (1984).

$$P = \frac{\Delta_{\Sigma}}{\left[\frac{\left(d_e^2 + d_e^2\right)/\left(d_e^2 + d^2\right) + \mu}{E_{cr}} + \frac{\left(d^2 + d_p^2\right)/\left(d^2 - d_p^2\right)\mu}{E_b}\right]} \quad - \quad - \quad - \quad (3.3)$$

where:

de, d and dp are the outer and inner diameters of the small end and the inner diameter of the bushing in table (3.1) respectively, (mm)

Poisson's ratio $\mu = 0.3$ of the steel connecting rod.

Elasticity modulus of steel connecting rod $E_{cr}=2.2 \times 10^5$ Gpa

Elasticity modulus of the bronze $E_b = 1.15 \times 10^5$ Gpa

Stress on the external fiber

$$\sigma'aj = \left[2M_{j\omega em}\frac{6r_m + h_e}{\left(2r_m + h_e\right)} + N_{j\omega em}\right]\frac{10^{-6}}{l_{se}h_e}, \quad - \quad - \quad - \quad - \quad - \quad (3.4)$$

Stress on the internal fiber according to (Demidov and Kolchin, 1984) is given by.

$$\sigma'ij = \left[-2M_{j\varphi em}\frac{6r_m + h_e}{h_e\left(2r_m + h_e\right)} + N_{j\varphi em}\right]\frac{10^{-6}}{l_{s.e}h_e} \quad - \quad - \quad - \quad - \quad (3.5)$$

where:

$h_e = (de - d)/2$ is the thickness of the small end wall, (m);

$i_{s.e}$ = the length of the small end, (m).

Including coefficient K, the stresses are

$$\sigma aj = \left[-2M_{j\omega em}\frac{6r_m + h_e}{h_e\left(2r_m + h_e\right)} + N_{j\omega em}\right]\frac{10^{-6}}{l_{s.e}h_e} \quad - \quad - \quad - \quad - \quad (3.6)$$

$$\sigma'ij = \left[-2M_{j\omega em}\frac{6r_m + h_e}{h_e\left(2r_m + h_e\right)} + KN_{j\omega em}\right]\frac{10^{-6}}{l_{s.e}h_e}$$

The specific pressure on the contact surface between the bushing and small end is:

$$P = \frac{\Delta_{\Sigma}}{d\left[\frac{\left(d_e^2 + d_e^2\right)/\left(d_e^2 + d^2\right) + \mu +}{E_{cr}} + \frac{\left(d^2 + d_p^2\right)/\left(d^2 - d_p^2\right) - \mu}{E_b}\right]} \quad - \quad - \quad (3.7)$$

where:

Poisson's ratio of the stress from the total interference on the small end internal surface

$\mu = 0.3$

1_{xx} and 1_{yy} = Moment of inertia of the section about *X* – axis and *Y*- axis respectively and

K_{xx} and K_{yy} = radius of gyration of the section about *X*- axis and *Y*- axis respectively. (also Fig 2.3 and 2.4)

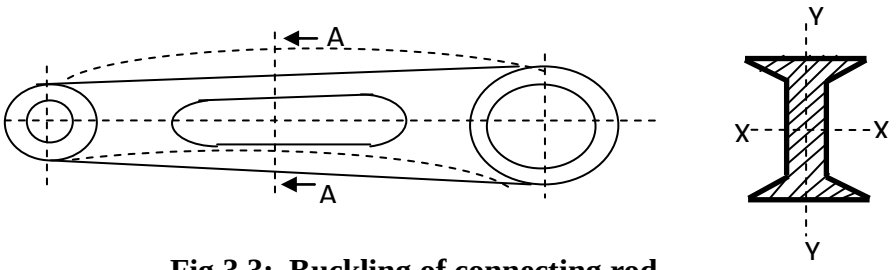


Fig 3.3: Buckling of connecting rod

According to Rankin's formula,

w_{cr^-} about *X*- axis = $\frac{\sigma_c xA}{1 + a\left(\frac{l}{K_{kk}}\right)2} = \frac{\sigma_c xA}{1 + a\left(\frac{l}{K_{kk}}\right)z}$ .. (∴ For both ends hinged, L=I)

and W_{cr} - about *Y*- axis = $\frac{\sigma_c xA}{1 + a\left(\frac{L}{K_{kk}}\right)2} = \frac{\sigma_c xA}{1 + a\left(\frac{l}{zK_{yy}}\right)2}$ (∴ For both ends fixed,

$L = \frac{1}{2}$

In order to have a connecting rod equally strong in bucking about both axes, the bucking loads must be equal, i.e

$$\frac{\sigma_c xA}{1+a\left(\frac{l}{K_{kk}}\right)2}=\frac{\sigma_c xA}{1+a\left(\frac{l}{zK_{yy}}\right)2} \text{ or } \left(\frac{1}{K_{xx}}\right)2=\left(\frac{l}{2K_{yy}}\right)2$$

:. $K^2_{xx} = 4K^2_{yy}$ or Ixx= $4I_{yy}$ (:. I = AxK^{2}2 - - - (3.8)

where,

A = Cross-sectional area of the connecting rod, (mm^2)

l = Length of the connecting rod, (mm).

σ_c = Compressive yield stress, (N-m)

W_{cr} = Crippling or buckling load, (N or KN)

This shows that the connecting rod is four times stronger in buckling about the *Y*-axis than about *X*- axis. If $I_{xx} > 4\ I_{yy}$, then bucking will l occur about *Y*- axis and if about I_{yy}, bucking will occur about the the *X*- axis. In actual practice, I_{xx} is kept slightly less than 4 I_{yy}. It is usually taken between 3 and 3.5 and the connecting rod is designed for bucking about the *X*-*X* axis. the design will always be satisfactory for buckling about the *Y* –Y axis. The most suitable section for the connecting rod is the *I* section with the proportions as shown in fig.3.4a.

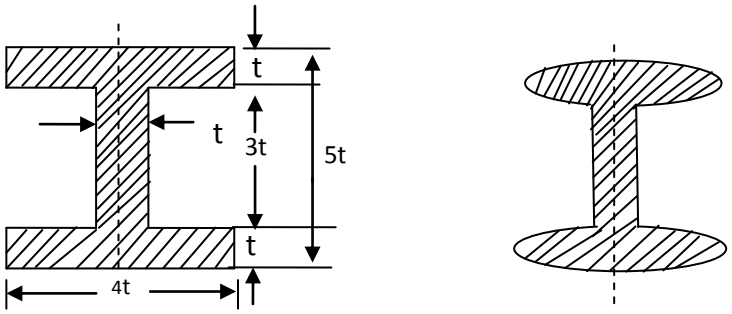
Area of the section = 2 (4 t x t) + 3t x t = 11 t^2

:. Second moment of area about X- axis,

$$= \quad 1_{xx}=\left[2x\frac{1}{12}tx(4t)3+\frac{1}{12}(3t)t3\right]=\frac{131}{12}t^4$$

And the Second moment of area about the *Y* – axis,

$$1_{xx}=\left[2x\frac{1}{12}tx(4t)3+\frac{1}{12}(3t)t3\right]=\frac{131}{12}t^4$$



(a) (b)

Fig. 3.4 I-section of connecting rod.

The basic constructional parameters of the connecting rod are given in tables (3.1) and (3.2) for the small end and big ends respectively, and table (3.3) for the rod shank of the connecting rod. Similarly, the design diagram of the connecting rod assembly and the developed connecting rod with major dimensions are given in figures (3.5) and (3.6) respectively.

Table: 3.1. Basic constructional parameters of the Small end of the connecting rod. (Demidov and Kolchin, 1984).

Description	Ratio	Petrol engine	Diesel engines
Piston pin diameter dp		16mm	
Small end inside			
Diameter $id_{se:}$ without bushing		$Id_{se} \approx$ dp	$Id_{se} \approx$ dp
With bushing id_{se} (b)	$Id_{se}(b)/dp$	0.95 – 1.03	0.95 – 1.03
Small end outside			
Diameter OD_{se}	Od_{se}/dp	1.15 – 1.90	1.20 – 1.95
Length of small end L_{se}	$L_{se}/L_{sec}(max)$	0.66 – 1.07	0.66 – 1.07
Radial thickness of end wall rt_{ew}	Rt_{ew}/dp	0.19 – 0.30	0.19 – 0.30

Table 3.2. Basic constructional parameters of the (Big end) of the connecting rod. (Demidov and Kolchin, 1984).

Description	Ratio	Variation limits
Crank pin diameter dep	D_{cp}/L_{sec}(max)	0.99-1.02
Shell wall thickness t_{sh}: Thin- walled	T_{alt}/dcp	0.10 – 0.17
Thick- walled	t_{sh}/ dcp	0.35
Length of big end L_{be}	L_{be}/dcp	0.82 – 0.99
Distance between connecting rod bolts D_{eb}	D_{cb}/dcp	1.25 – 1.45

Material for the mould

The recommended material for permanent moulds for casting aluminum alloy is gray iron (Metal Handbook, 1970). However, steel is also widely used to produce permanent moulds for casting as shown in figures (3.8 (a), and (b) as the core rod for the big hole, and the mould locking system respectively and also figure (3.8) as the sectional view of the mould assembly, hence for this work, medium carbon steel is used to produce the moulds for the following reasons (Jain, 1985):

1. It can withstand the pouring temperature of aluminum alloys.
2. The effects of high temperature will not limit the use of medium carbon steel
3. It can easily be shaped and polished to give a smooth surface
4. It is cheap and readily available

Material for the MMC Connecting rod

The material used for the production of the connecting rod which is to be tested in the Toyota-12 valve engine is a composite of aluminum alloy with coconut shell ash particles at 6 – 9wt% composition using the double stir casting method

which was earlier used in the production of the test specimen and selecting the best composition.

Mould cavity for the connecting rod

A connecting rod is made up of three parts- the big end, the small end and the shank. The relative values of the basic constructional parameters of the three parts used to calculate mould cavity are shown in Tables (3.1. and 3.2)., while table (3.3) shows that most of the parameters depend on the piston pin diameter (dp) and the crank pin diameter (dcp) respectively which are the basis of the connecting rod design. The piston diameter (dp) is equivalent to the small end inside diameter (id_{se}) of the connecting rod is 16mm. In order to avoid the problem of exceeding or falling below the specified limits, all dimensions are taken on average value of relative values in the column for petrol engines, since Toyota starlet 12 valve engine uses petrol.

3.4.13 Small end of the Connecting rod

Demidov and Kolchin (1984) recommended the following assumption;

Piston pin dia. (d_p) $\approx$ small end inside dia. (id_{se}) without standing

$Dp \approx id_{se} = 16mm$

Outside diameter of the small end (od_{se})

$$\frac{Od_{se}}{Dp} = \frac{1.15 + 1.90}{2} = 1.525$$

$Od_{se} = 16 \times 1.525 = 24.4mm$

Length of small end (L_{se})

$$\frac{L_{se}}{L_{sec}(max)} = \frac{0.66 + 1.07}{2} = 0.865$$ (calculate L_{sec} (max) =30mm}

$L_{se} = 30 \times 0.865 = 25.95mm$

Radial thickness of end wall rt_{ew}

$\frac{rt_{ew}}{dp} = \frac{0.19 + 0.30}{2} = 0.245$ (assumed dp = 16mm)

$rt_{ew} = 16 \times 0.245 = 3.92mm$

3.4.14 Big end of the Connecting rod

Crank pin diameter d_{cp}

$\frac{d_{cp}}{L_{sec}\ (max)} = \frac{0.99 + 1.02}{2} = 1.005$ (calculate L_{sec}(max) = 30mm

$D_{cp} = 30 \times 1.005 = 30.15mm$

Shell wall thickness t_{sh}

$\frac{t_{sh}}{d_{cp}} = \frac{0.10 + 0.17}{2} = 0.135$ (from above d_{cp} = 30.15mm)

$t_{sh} = 30.15 \times 0.135 = 40.05mm$

Length of the big end L_{be}

$\frac{L_{be}}{d_{cp}} = \frac{0.82 + 0.99}{2} = 4.05mm$

$L_{be} = 30.15 \times 0.905 = 27.15mm$

Distance between connecting rod bolts D_{cb}

$\frac{D_{cb}}{d_{cp}} = \frac{1.25 + 1.45}{2} = 1.35$

$D_{cb} = 30.15 \times 1.35 = 40.5mm$

3.4.15 Connecting rod shank

In addition to the connecting rod length L_{CR} the basic design parameter of the connecting rod shank includes the dimension of its middle section as shown in (Fig. 3.4).

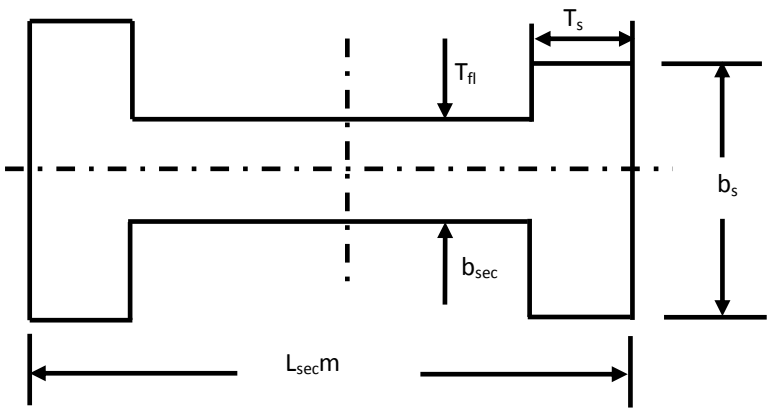


Fig. 3.5: Sectional view of section A-B

$L_{sec}(max)$ = maximum sectioned length

b_{sec} = sectional breadth

t_{sh} = shell thickness

t_{fl} = flange thickness

$t_{sh} \approx t_{fl}$ (Kolchin and Demidov, 1984)

Table: 3.3. Basic constructional parameters (rod shank) of the connecting rod (Demidov and Kolchin, 1984).

Dimension of section	Ratio	Petrol engine	Diesel engine
L_{sec}	L_{sec}/OD_{se}	0.62 – 1.07	0.62 – 1.07
L_{sec} (max)	L_{sec} (max/L_{sec}	1.01 – 2.03	1.01 – 2.03
b_{sec}	b_{sec}/L_{sec} (max)	0.64 – 0.83	0.69 – 0.98
$t_{sh} \approx t_{fl}$		3.5 – 5.0	5.0 – 9.0

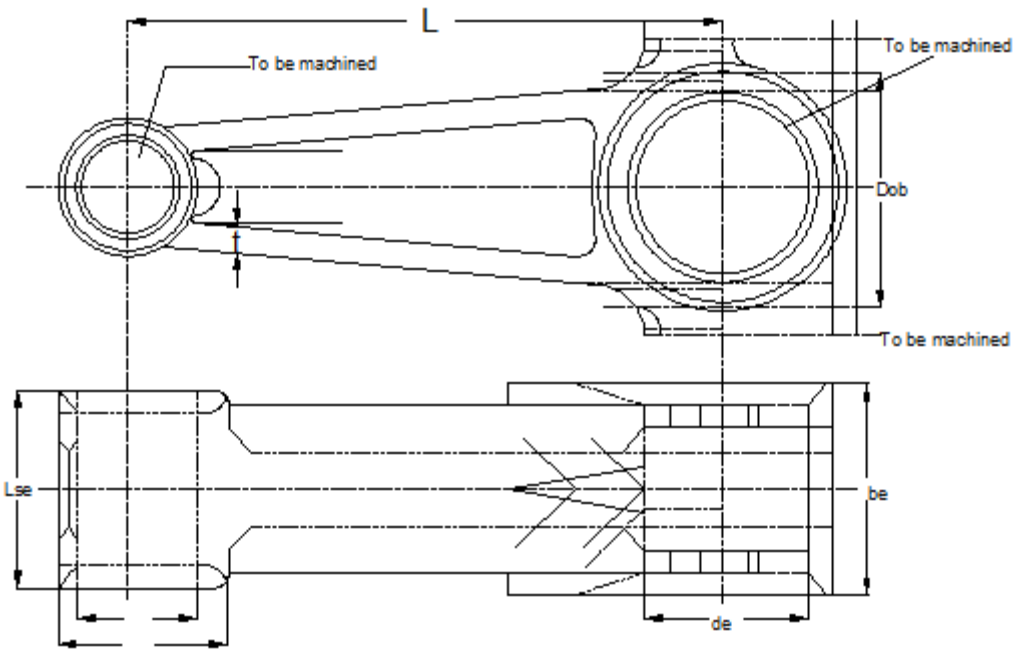


Fig. 3.6: Design diagram of a connecting rod assembly

Small end of the connecting rod Assumption by (Demidov and Kolchin, 1984)

Piston pin dia (d_p) ≈ small end (id_{se}) without bushing $d_p \approx id_{se}$ = 16mm

Outside diameter of the small end **(Od_{ac})**

$$= \frac{OD_{se}}{dp} = \frac{1.15 + 1.90}{2} = 1.525$$

OD_{se} = 16 x 1.525 = 24.4mm

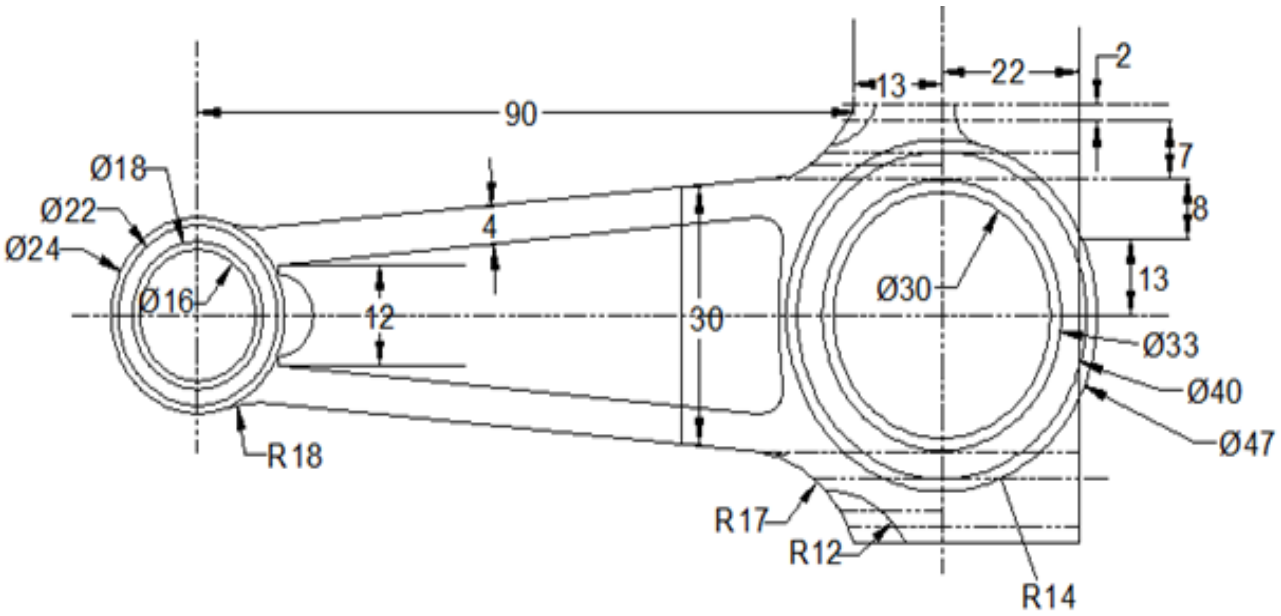
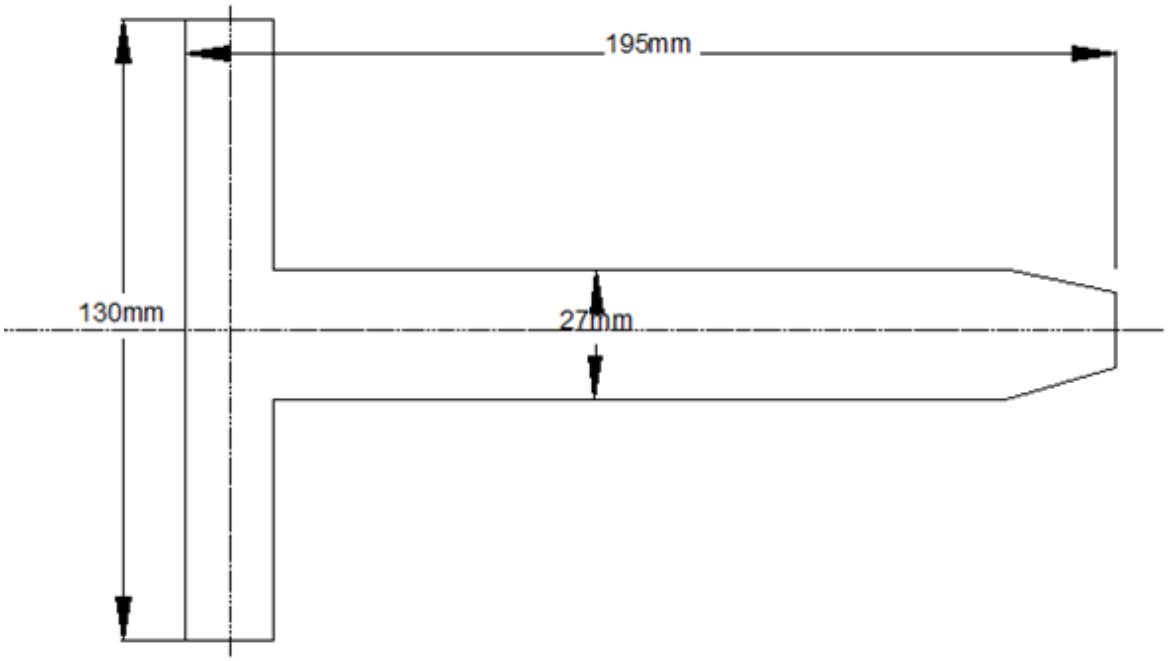
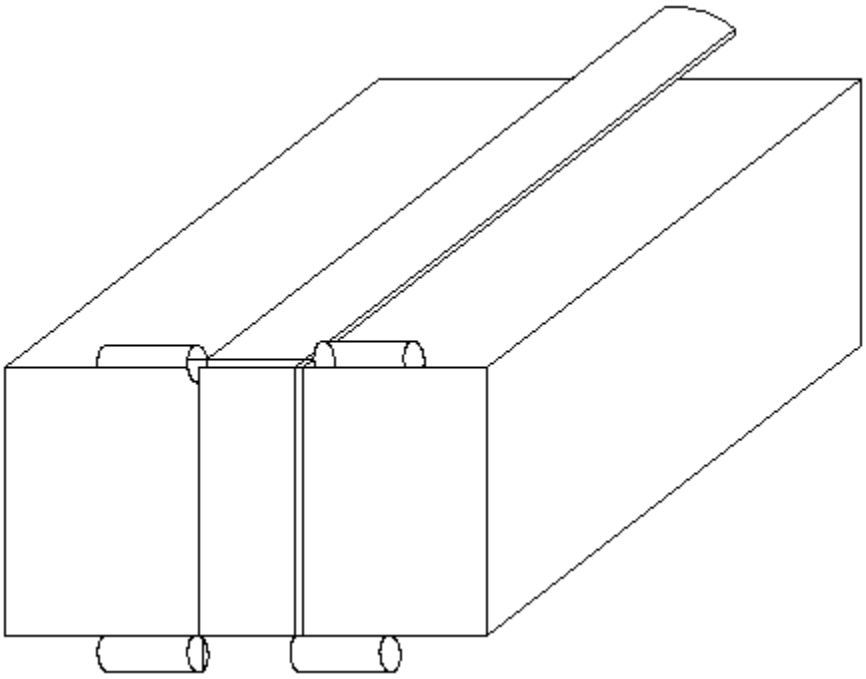


Fig. 3.7: Developed connecting rod with major dimensions (All dimensions in mm)



(a)



(b)

Fig. 3.8: (a) Core rod for the big hole (b) Mould locking system

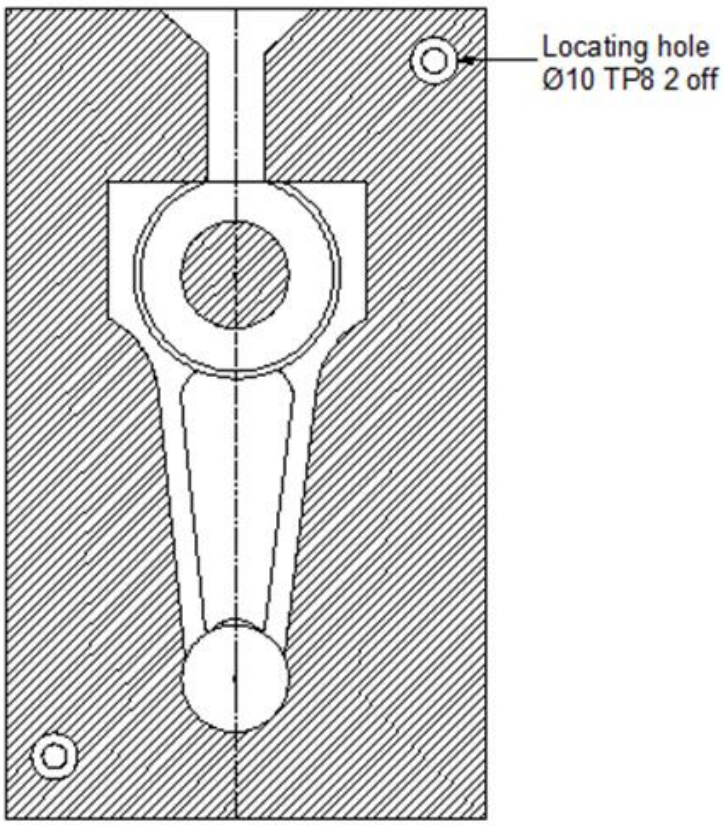


Fig. 3.9: Sectional view of the mould assembly

3.4.16 Casting Process

The material used for the casting is Al-SiC-Fe/ Coconut shell ash particles (CSAp). The production of the MMC was done by the double stir-casting method. Initially the material Al-Si Al-7% SiC composite was charged into the furnace and heated to about 750^0C till the entire alloy in the furnace melted and 2wt% iron powder was added. The reinforcement (CSA) was preheated to 800^0C for 1 hour before incorporation into the melt. After the molten metal was fully melted, 0.05% of degassing tablet was added to enhance wettability between the coconut shell ash particles and the alloy melt.

The mechanical stirrer was lowered slowly to stir the molten metal at a speed of 500-700 rpm and the preheated coconut shell ash particle reinforcement (CSAp) was added to the melt at a constant rate during the stirring process. The entire mixture was poured into a mould and its arrangement as shown in Fig. 3.8 (a) and (b) and Fig 3.9 respectively which was heated for 30 minutes to obtain uniform solidification of the casting using 0, 3, 6, 9 and 15 % by weight of reinforcement, the composite connecting rod was produced choosing 6-9% of the coconut shell ash particles (CSAp) that are within the standard values for impact energy for connecting rod applications (Rohatgi and Guo, 1997).

After removal of the casting from the mould it was trimmed and went through different stages of machining process i.e. turning, facing,, drilling, grinding operation and finally tapping the M8 holes (Refer to Plates 3.3a and 3.3b)

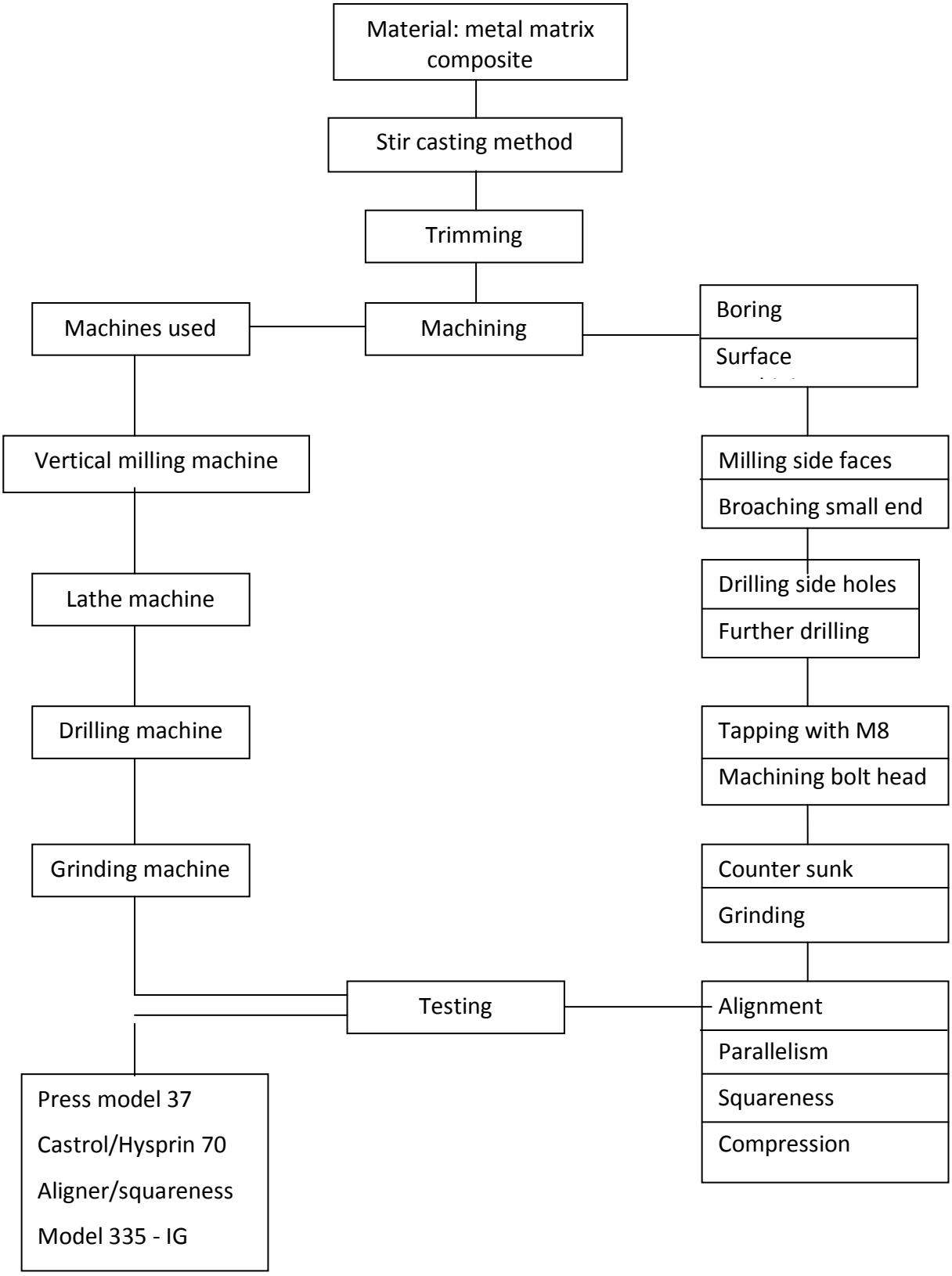


Fig. 3.10: Manufacturing process flow chart of the connecting rod

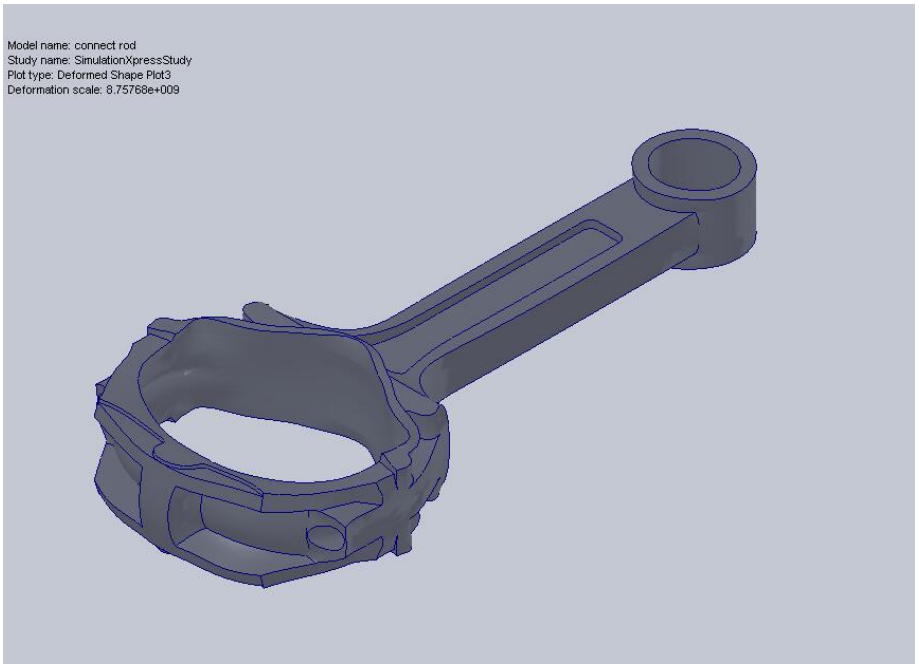


Plate 3.3a: Isometric view of connecting rod

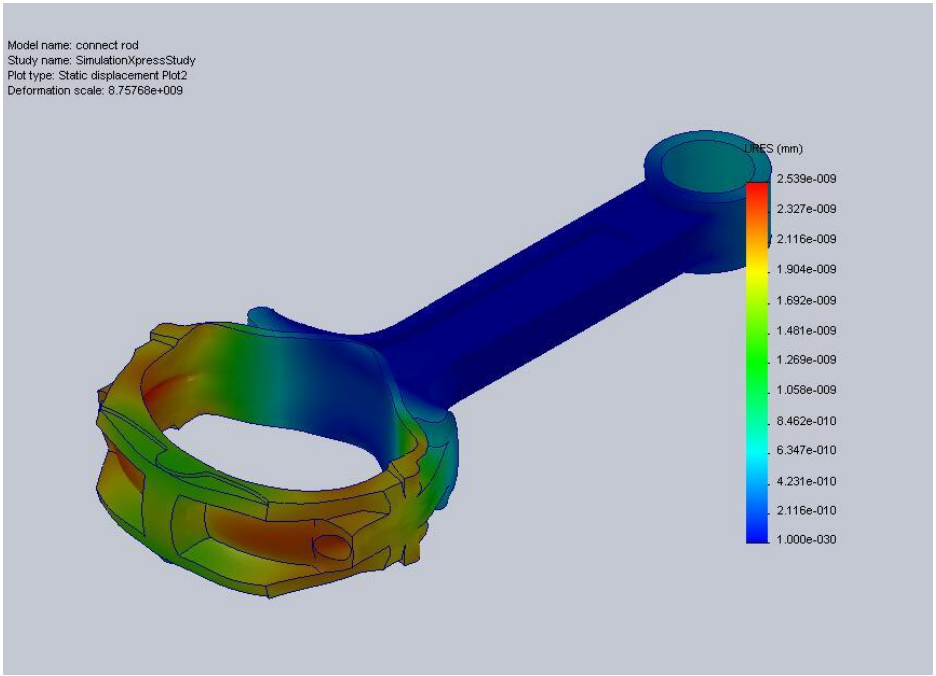


Plate 3.3b: Isometric view of connecting rod

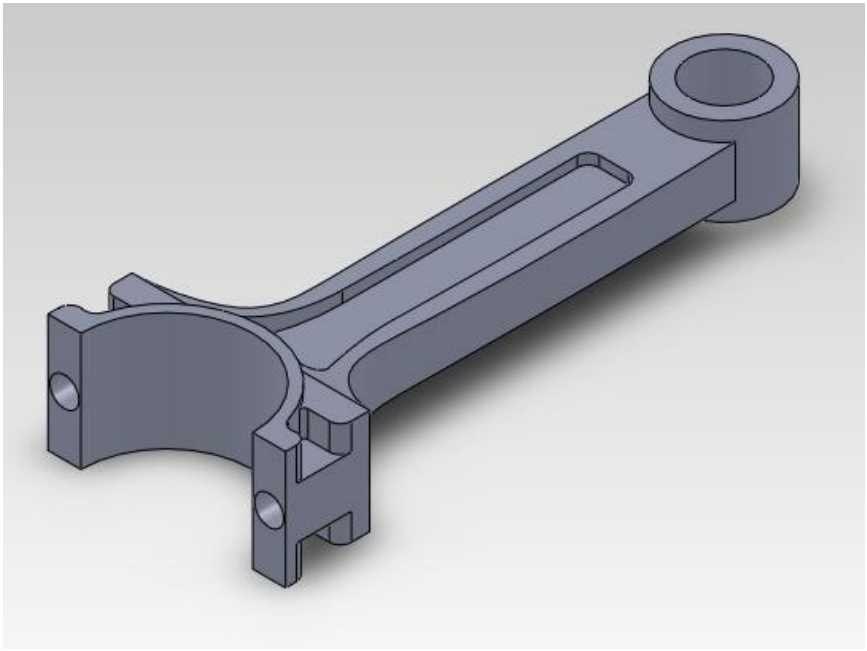


Plate 3.4a: Isometric view of the rod open

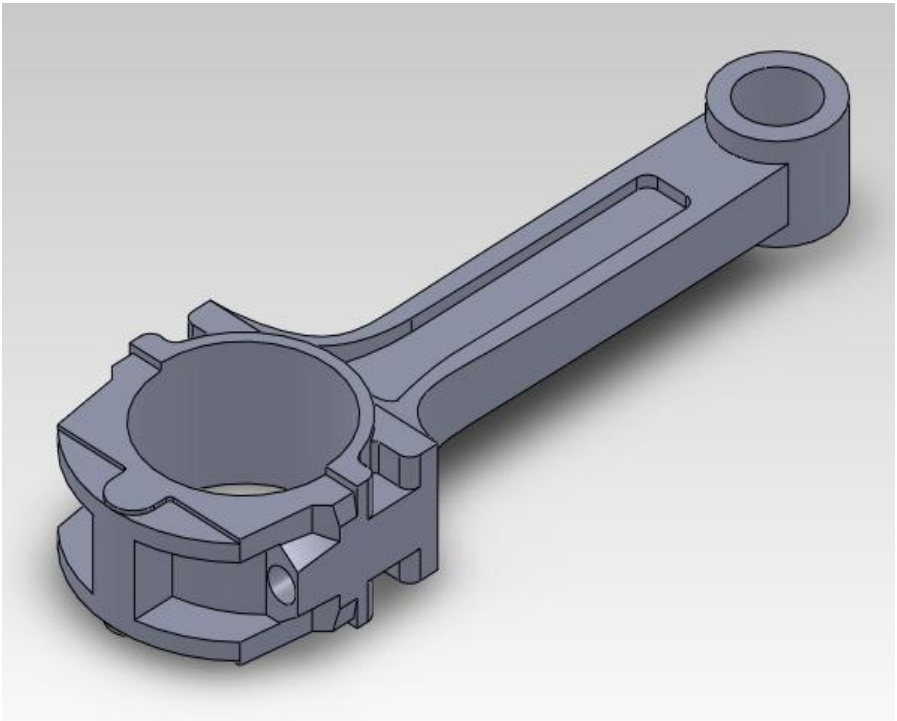


Plate 3.4b: Isometric view of the rod closed

3.4.17 Fabrication (Casting and Machining) of the Connecting Rod

The connecting rod was produced by stir casting. Its function is to join the piston to the crankshaft and convert the linear movement of the piston to rotary motion of the crank shaft. Because of the complex movement of the rod, its weight is kept low to ease the problem of balancing but the rod must have adequate strength to withstand the forces to which it is subjected.

Mould preheating and pouring

The entire mixture was poured into a mould which was heated for 30 minutes to obtain uniform solidification of the casting. The pouring lip of the pot was held as close as possible to the gate so that the free fall of the molten metal is at minimised in order to prevent gas absorption, by the cascading melt, and entrapment of atmospheric air flowing down the sprue (Fig.3.8 (a) , 3.8 (b) and Fig.3.9). The sprue was kept full to prevent the formation of the vortex which will otherwise form on top of partially filled sprue. Using 0, 3, 6, 9, and 15% by weight of reinforcement; the composite connecting rod was produced. After the pouring process was complete, the casting was allowed to remain in the mould for some reasonable time before ejection. Ejection was achieved by removing the core rod (Fig.3.7 (a), and then the mould was declamped and the die opened. Casting was removed from the mould by gently tapping sideways and upper part of the gating system with a soft hammer (Plates 3.4 (a) and 3.4 (b).

After removal of casting from the mould it was trimmed and went through different stages of machining process, i.e. turning, facing, drilling, grinding operation, and finally tapping M8 holes on the connecting rod (Plates 3.5 and 3.6).



(a) Profile 1



(b) Profile 2

Plate 3.5: Casting profiles of the connecting rod.

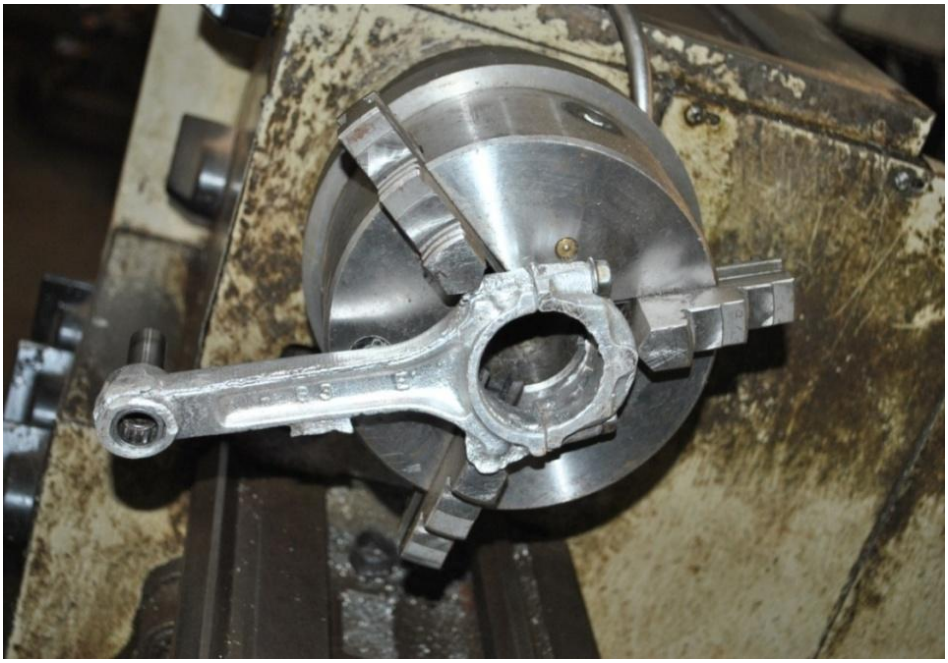


Plate 3.6: Boring of the connecting rod on the lathe.

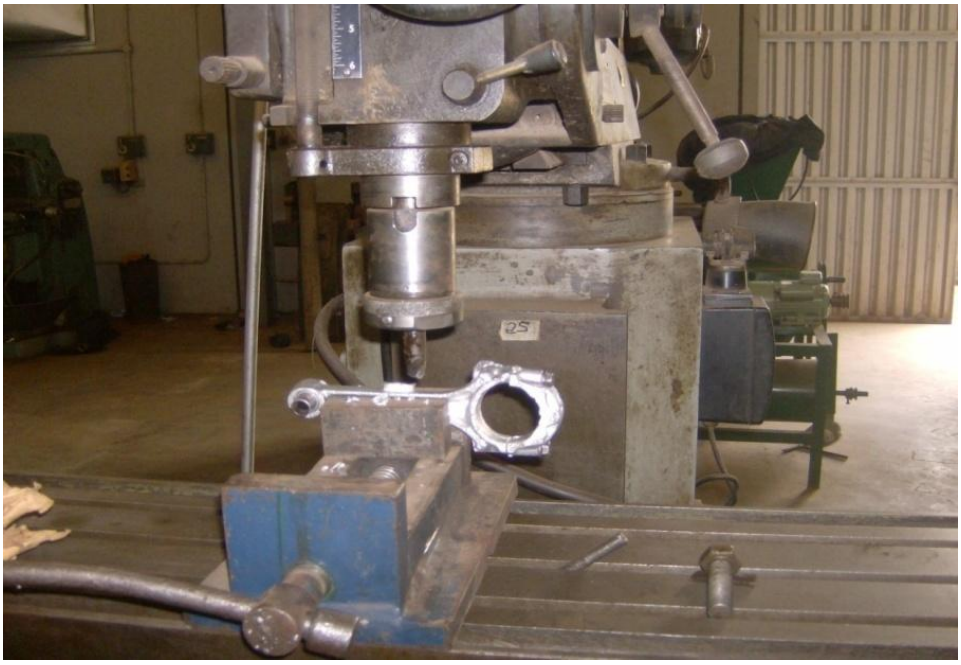


Plate 3.7: Milling side faces of the connecting rod.



Plate 3.8 (a) Alignment on machine (Model NO. 335 – IG)



Plate 3.8 (b) Squarness on machine (Model NO. 335 – IG)

3.4.18 Forces Acting on the Connecting Rod (ii)

A connecting rod is subjected to the following forces;

1. Force due to gas or steam pressure and inertia of reciprocating parts.
2. Inertia bending force, and
3. Force acting on a horizontal plane

Expressions for the forces acting on a connecting rod PC are shown in (fig.3.10).

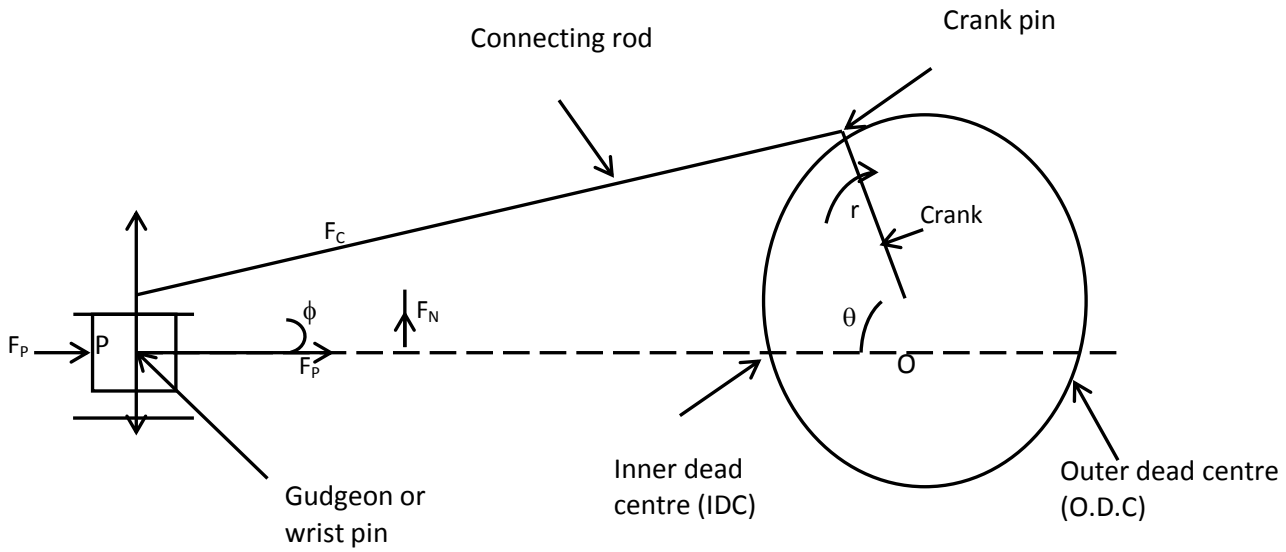


Fig. 3.11: Forces on a connecting rod

The forces acting on a connecting are:

P = Pressure of gas or steam

A = Area of piston

M_R = Mass of reciprocating parts

= Mass of piston, gudgeon pin etc. + 1/3 rd mass of connecting rod,

ω = Angle of inclination of the connecting rod with the length of stroke

ϕ = Angle of inclination of the connecting rod with the line of stroke

θ = Angle of inclination of the crank from inner dead centre,

r = Radius of crank

l = Length of connecting rod, and

n = ratio of length of connecting rod to radius of crank = l/r

Force on the piston due to pressure of gas or steam,

FL = Pressure x Area = p x A

FI = Mass x acceleration= m_R x ω^2 x r$\left(\cos t\, \theta \frac{\cos 20}{n} \right)$ - - - - (3.9)

where,

FI = Inertia force of reciprocating parts.

F_P = Force due to pressure of gas or steam ± inertia force = $F_L \pm F_1$

In the connecting rod, force F_P gives rise to a force F_C and a thrust F_N on the sides of the cylinder walls fig. 3.3.26, i.e. force in the connecting rod at any instant.

$$FC = \frac{F_P}{COS\Phi} = \frac{F_P}{\sqrt{1 \frac{\sin^2 \Phi}{n^2}}} \quad - \quad - \quad - \quad - \quad - \quad - \quad (3.10)$$

3.4.19 Inertia Bending Forces

In the connecting rod PC, a crank OC, rotates with a uniform angular velocity ω rad/s. Also in CQNO as shown in fig. 12.

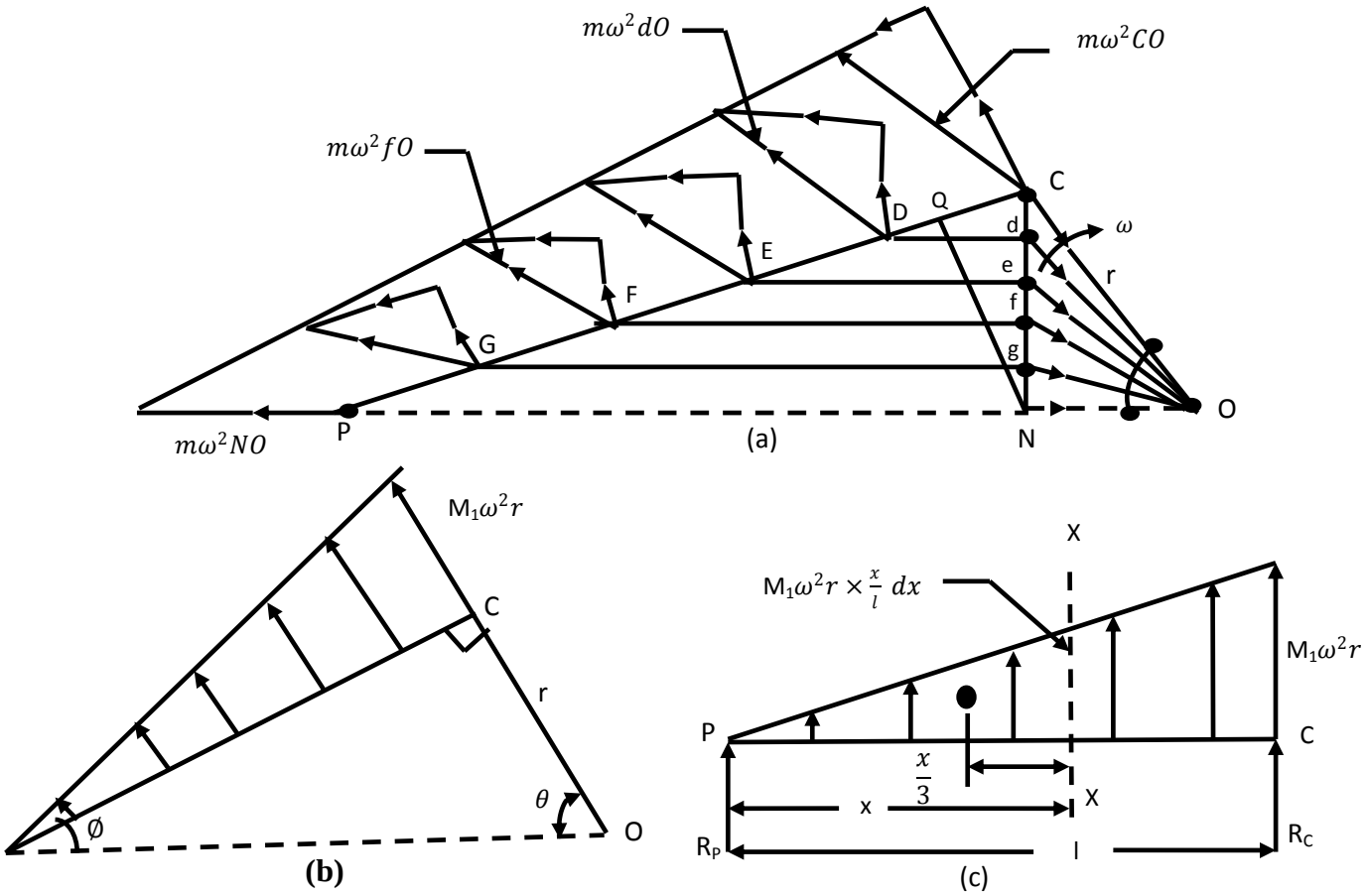


Fig. 3.12: Inertia bending forces (Khurmi and Cupta, 2010).

Points G, F, E and D Fig. (3.12 (a)) are gudgion pin position at each stage and resultant inertia forces (parallel and perpendicular) components acting on the connecting rod. That is:

(i) Parallel (or longitudinal) components on the connecting rod. (FC)

(ii) Perpendicular (or transverse) component produces bending action (also called whipping action)

(i) CO represents acceleration of C towards O

(ii) NO represents acceleration of P towards O

The Acceleration of other points such as D, E, F and G etc. on the connecting rod PC can be found, i.e., dO, eO, fO and gO represent the acceleration of D, E, F and G all towards O.

The inertia force acting on each point will be as follows:

Inertia force at C = m x ω^2 x CO

Inertia force at D = m x ω^2x dO

Inertia force at E = m x ω^2 x eO, etc.

According to Kurmi and Gupta (2010) the variation of the inertia force on the connecting rod is linear and is like a simply supported beam of variable loading as they made the assumption that the connecting rod is of I cross-section and has mass m_1 kg. per unit length, and that the inertia force per unit length at the crank pin. = m_1 x ω^2r.

The inertia force per unit length at the gudgeon pin = 0

Inertia forces due to a small element dx at a distance x from the gudgeon pin P,

$$dF_I = m_I \times \omega^2 r \times \frac{x}{l} \times dx$$

Resultant inertia force,

Kurmi and Gupta (2010) give the resultant force

$$FI = \int_0^i m_1 \; x \; w^2 r \; X \; \frac{x}{l} \; x \; dx = \frac{m_1 \; x \; \omega^2 r}{l} \left[\frac{x^2}{2} \right]_0^1$$

$$= \frac{m_1 \; x \; l}{2} \; x \; \omega^2 r \; \frac{m}{2} \; x \; \omega^2 r \; - \; - \; - \; - \; - \; - \qquad (3.11)$$

Reactions of inertia force at the two ends of the connecting rod.

$R_P = {}^1/_3 \; F_I$, and $R_C = {}^2/_3 \; F_I$

The bending moment acting on the rod at section X – X at a distance x from p,

$M_X = R_P \times x = *m1 \times \omega^2 r \times {}^x/_l \times {}^1/_2 x \times {}^x/_3$

$$= {}^1/_3 \; F1 \times x \; \frac{m_1 l}{2} \; x \; \omega^2 r \; x \; \frac{x^3}{31^2}$$

Therefore $R_P = {}^1/_3 \; F_I$

(Multiplying and dividing the latter expression by l)

$$= \frac{F_1 \, x \, \chi}{3} - F_1 \, x \, \frac{x^3}{3l^2} = \frac{F_1}{3}\left(x - \frac{x^3}{l^2} \right) - \quad - \quad - \quad - \quad - \quad - \qquad 3.12$$

For maximum bending moment, differentiate M_X with respect to x and equate to zero, i.e.

$$= \frac{d_{MX}}{dx} 0 \text{ or } \frac{F_1}{3}\left[1 - \frac{3x^2}{l^2} \right] = 0 \qquad - \qquad - \qquad - \qquad - \qquad -$$

3.13

$$= \text{ or } \quad 3x^2 = l^2 \; x = \frac{\ell}{\sqrt{3}}$$

Substituting this value of x in equation (7), given the maximum bending moment,

$$M_{max} = \frac{f_1}{3}\left[\frac{\ell}{\sqrt{3}} - \frac{\left(\frac{\ell}{\sqrt{3}} \right)^3}{l^2} = \frac{f_1}{3}\left[\frac{\ell}{\sqrt{3}} - \frac{\ell}{\sqrt[3]{3}} \right] \right] - \quad - \quad - \quad - \quad - \quad 3.14$$

$$= \frac{f_1}{3} \, x \, \frac{21}{\sqrt[3]{3}} = \frac{2 \; f_1 \; x \; l}{\sqrt[9]{3}}$$

$$= 2 \, x \, \frac{m}{2} \, x \, \omega^2 r \; x \; \frac{1}{\sqrt[9]{3}} \; m \; x \; \omega^2 r \; x \; \frac{1}{\sqrt[9]{3}} \; ..... \left(f_1 = \frac{m}{2} \, x \, \omega^2 r \; x \right) - \quad 3.15$$

The general practice is to design the connecting rod by assuming the force in the connecting rod (F_C) is equal to the maximum force on the piston due to pressure of gas or steam (F_L), neglecting piston inertia effects and then check for bending stresses due to the inertia force (i.e. whipping stress).

Experimental calculation on regular connecting rod.

To determine the dimensions of the I-section of the connecting rod for a petrol engine with the following data.

Diameter of the piston = 110mm

Mass of the reciprocating parts = 2kg

Length of the connecting rod from centre to centre = 325mm

Stroke length = 150mm

R.P.M = 2500

Possible over speed of 2500 r.p.m

Compression ratio = 4:1

Maximum explosion pressure = 2.5N/mm^2

D = 110mm = 0.11m; M_R = 2kg;

I = 325mm = 0.325m; stroke length = 150mm = 0.15m;

N_{min} = 1500 r.p.m; N_{max} = 2500 r.p.m; *compression ratio = 4:1; p = 2.5N/mm^2

R radius of crank,

$$R = \frac{Stroke\ length}{1} = \frac{160}{2} = 75mm = 0.075m$$

R ratio of the length of connecting rod to the radius of crank,

$$n = \frac{l}{r} = \frac{325}{75} = 4.3 \quad - \quad - \quad - \quad - \quad - \quad - \quad - \quad 3.16$$

Maximum force on the piston due to pressure,

$$FL = \frac{\pi}{4}\ x\ D^2\ x\ p = \frac{\pi}{4}(110)^2\ 2.5 = 23760N$$

and maximum angular speed,

$$\omega_{max} = \frac{2\pi\ x\ N_{max}}{60} = \frac{2\pi\ x\ 2600}{60} = \frac{261.8rad}{s} \quad - \quad - \quad - \quad 3.17$$

Maximum inertia force of reciprocating parts

$$F_I = M_R\ (\omega_{max})^2 r\ Cos\theta + \left(\frac{Cos2\theta}{n}\right) \quad - \quad - \quad - \quad - \quad - \quad 3.18$$

Inertia force of reciprocating parts is maximum, when the crank is at the inner dead centre, i.e. when $\theta = 0^0$

Therefore $F_I = M_R (\omega max)^2 r \left(1 + \frac{1}{n}\right)$

$= 2 (261.8)^2 \text{ x } 0.075 \left(1 + \frac{1}{4.3}\right) = 12672N$ - - - - 3.19

The connecting rod is designed by taking the force in the connecting rod (F_C) equal to the maximum force on the piston due to gas pressure (F_L).

Therefore force in the connecting rod, FC = F_L = 23760N

Thickness of flange and web = t = 6.8mm = 0.0068m **ans.**

Bending stress due to inertia force on the connecting rod.

M1 = volume x density = Area x length x density

$= A \text{ x } l \text{ x } p = 11t^2 \text{ x } l \text{ x } p$

$= 11 (0.0068)^2 \text{ 1 x } 7800 = 3.97kg.$

Maximum bending moment (taking p = 7800kg/m^3)

$M_{max} = m \omega^2 r \text{ x } \frac{1}{\sqrt[9]{3}} = m_1 \omega^2 r \text{ x } \frac{l^2}{\sqrt[9]{3}}$ - - - - - 3.20

$= 3.97 (261.8)2 (0.075) \text{ x } \frac{(0.325)^2}{\sqrt[9]{3}} = 138.3 N - m$ - - - - 3.21

And section modulus,

$Z_{xx} = \frac{1_{xx}}{5t/2} = \frac{419t^4}{12} x \frac{2}{5t} = \frac{419}{30} t^3$ - - - - - 3.22

$= \frac{419}{30} (0.0068)^3 = 4.4 x 10^{-6} m^2$ - - - - - 3.23

Maximum bending or whipping stress due to inertia bending forces

$\sigma_{c(max)} = \frac{M_{max}}{Z_{xx}} = \frac{138.3}{4.4x10^{-6}} = 31.4 \text{ x } 10^6 \text{ N/m}^2$- - - - 3.24

Maximum compressive stress in the connecting rod will be,

$$\sigma_{c(max)} = \frac{320}{6} + 31.4 = 84.7 \text{ MPa}$$

Experimental calculation on MMCs connecting rod.

Data available:

Diameter of piston = 73mm

Mass of reciprocating parts = 2kg

Length of connecting rod from centre to centre = 120mm

Length of stroke = 77.4mm

RPM = 1100

Compression ratio = 5:1

Taking density P = 2.86g/cm^3 = 0.00286kg/cm^3

Maximum explosion pressure = 2.5 N/mm^2

D = 73mm = 0.073m

M_R = 2kg

I = 120mm = 0.12m

Length of stroke = 77.4mm = 0.0774m

N (min) = 800rpm, N (max) = 1100 rpm

Compression ratio = 5:1

Pressure P = 2.5 N/mm^2

Radius of crank = $\frac{\text{stroke length.}}{2} = \frac{77.4\text{mm}}{2} = 38.7\text{mm}$

Ratio of the length of connection rod to the radius of the crank

$$n = \frac{i}{r} = \frac{120}{38.7} = 3.1$$

Maximum force on the piston due to pressure

$$F_L = \frac{\pi}{4} x D^2 \text{ x pressure}$$

$$= \frac{\pi}{4}(73)^2 x 2.5 \frac{N}{mm2} \text{ x mm x mm} = 10464.8 \text{ N} \quad - \quad - \quad - \quad 3.25$$

Maximum angular speed

$$W_{max} = \frac{2\pi\ x\ N\max}{60} = \frac{2\pi x 1100}{60} = 115.2 \text{ rad/s} \quad - \quad - \quad - \quad 3.26$$

Maximum inertia force of reciprocating parts

$F_I = M_R (W_{max})^2_r (\cos\theta + \underline{\cos 2\theta})$

The inertia force of reciprocating parts is maximum when the crank is at inner dead centre i.e $\theta = 0$

$$F_L = M_R (W_{max})^2 r \left(1 + \frac{i}{n}\right)$$

$$= 2 (115.2)^2 \text{ x } 0.0387 \left(1 + \frac{1}{3.1}\right) - \quad - \quad - \quad - \quad - \quad 3.27$$

$= 26542.08 \text{ x } 0.05118387 = 1358.53\text{N}$

The connecting rod is designed such that the force in the connecting rod (FC) is equal to the maximum force on the piston due to gas pressure (F_L)

Therefore the force in the connecting rod:

FC = F_L is shown in the summary of result of force acting on connecting rod table (3.4).

Thickness of flange and web t = 6.8mm = 0.068m. Bending stress due to inertia on the connecting rod

MI = Volume x density

= Area x l x p $\quad$ $A = 7.3\ t^2$

Taking density $p = 0.00286 \text{kg/m}^3$

MI = A x l x p = 7.3 x l x p

= A x 1 x P = 7.3 x 1 x P

$= 7.3 (0.0068)^2 \text{ x l x } 0.00286 = 965 \text{ x } 10^{-6} \text{ kg}$

Maximum bending moment

$$M_{max} = m\ w^2 r \text{ x } \frac{1}{\sqrt[9]{3}} = miW^2 r \text{ x } + \frac{12}{\sqrt[9]{3}} \quad (m = mi \text{ x } l)$$

$$= 2.63 (115.2)^2 \text{ x } (0.0387) \text{ x } \left(\frac{0.120}{\sqrt[9]{3}}\right)^2 - \quad - \quad - \quad - \quad 3.28$$

$= 965 \times 10^{-6} (1152)^2 \times 0.0387 \times$ - - - 3.29

$= 965 \times 10^{-6} (1152)^2 \times \frac{(0.1202)^2}{15.588845727} = 0.012806553 \times \frac{(0.1202)^2}{15.58845727}$

$M_{max} = 11.87 N\text{-}m$

Section modulus

$$Z_{xx} = \frac{l_{xx}}{\frac{5t}{\sqrt{2}}} = \frac{419t2}{12} x \frac{2}{5t} \quad - - - - - \quad 3.30$$

$= \frac{419}{30}(0.0068)^3 = 4.4 \times 10^{-6} m^3$

Maximum bending or whipping stress due to inertia bending forces

$\sigma_b (max) = \frac{M_{max}}{Z_{xx}} = \frac{11.87}{4.4 \times 10^{-6}} = 26.98 Mp_a$

Maximum compressive stress in the connecting rod will be

σ_c (max) = direct compressive stress + maximum bending stress

$= \frac{320}{6} + 26.4 Mp_a = 35.3 Mp_a$

Table: 3.4. Summary of result of force acting on connecting rod

S/No	Description	Produced MMCs connecting rod
1.	Maximum force on the piston due to gas pressure F_L = Pressure x Area = P x A	10464.8N
2.	Force in the connecting rod FC= $\frac{FP}{COSQ}$	10464.8N
2.	$FC = F_L$	10464.8N
3.	Maximum inertia force of reciprocating parts F_I	1358.53N
4.	Maximum bending or whipping stress due to inertia bending forces σ_b (max)	$2.84 \times 10^{-6} N/m^2$
5.	Maximum compressive stress in the connecting rod σ_c (max)	$81.7 MP_a$
6.	Maximum bending moment M_{max}	124.76 N-m
7.	Maximum angular speed W_{max}	115.2 rad/s
8.	Ratio of the length of connecting rod to the radius of crank	3.1

3.5 FINISHING OPERATION (MACHINING)

After removal of the casting from the mould the connecting rod was trimmed and thereafter went through different stages of machining-turning, facing, milling, drilling and grinding and finally tapping the two holes with M8 tap.

Alignment, Squareness, and Parallelism.

Alignment, squareness and parallelism checks were carried out on the connecting rod using the Castrol/Hyspring 70, (model No. 37) machine and the machine aligner (model No. 335 – IG) see plate (3.7 (a), and plate.3.7 (b) to determine if the rod is bent or twisted and then take corrective measures.

The connecting rod was mounted on the aligner (Model No. 335 – IG) and press (Castrol/Hyspring 70 (model No. 37) to check it for boring and twisting and if the limit is exceeded (limit on bow = 0.05mm, and limit on twist = 0.10mm. (Rajput, 2008).

3.5.1 HEAT TREATMENT (solution-treatment and aging. "STA")

The produced composite were heat treated using the conventional method (solution heat treatment and ageing single thermal ageing)

Equipment

Equipment used in the heat-treatment process includes the, muffle furnace (Model No.SXL 0z 47-80, c 25) having a heating capacity of 1200^{o}C. Quenching media used was (water and air).

Method

The sample connecting rods were packed in the muffle furnace and heated to 496^{0}C for three hours. This is to allow precipitation to take place. At the end of the time the connecting rods were removed and quenched in water. The aging treatment was then carried out at 150^{0}C.

3.5.2 PERFORMANCE TEST ON THE CONNECTING ROD

Live engine test

A (stationary) engine was used for the performance test. The test was conducted according to the work Serag *et al,* (1989), and Repgen, (1988).

The engine used was a Toyota starlet of 12 valve model E series. The 2E is 1.3L single overhead camshaft (SOHC) version with three valves per cylinder. It is a four stroke, four cylinder compression ignition engine with the following parameters.

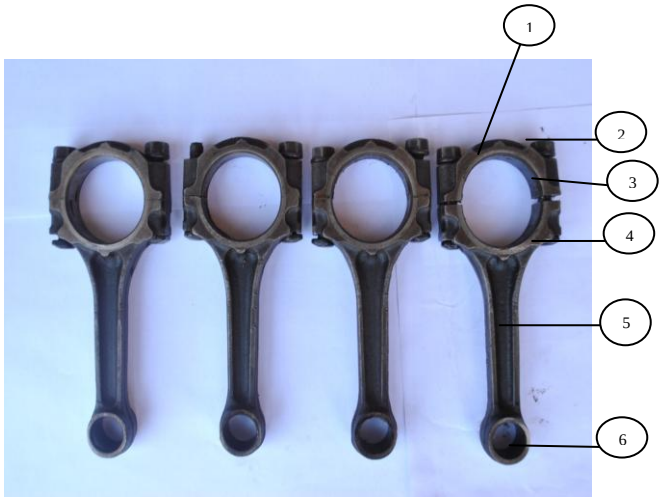
Bore x stroke; 73.0mm x 77.4mm

Displacement; 1,295cc

Compression ratio; 5:1

Standard output range of the engine is from 65hp (48kw) to 82hp (61kw) at 600 rpm with a torque of 98N-m at 3000 rpm to 7716ftlb 104N-m) at 5,200 rpm.
This engine can run in both carbureted and fuel injected versions.

Before the test the composite with coconut shell particles was used in the production of the connecting rod using the double stir-casting method which was earlier used in the production of the test specimen and selecting the best composition. After the casting, the connecting rod was machined and heat-treated. Also a regular connecting rod was purchased which serves as a control. The photographs of the connecting rods are shown in Plate 3.3(a) and 3.3(b) respectively.



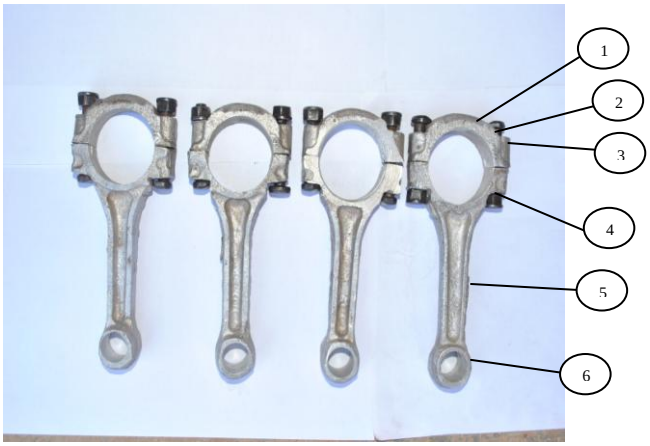


Plate 3.9a: Photograph of Regular connecting rod. **Plate 3.9 b: Photograph of MMCs connecting rod.**

Plate 3.3a and Plate 3.3b are part of the regular connecting rod and the MMCs connecting rod respectively

1. Rod small end
2. I-Beam
3. Rod cap
4. Rod bolt
5. Rod Nut
6. Rod big end (Bearing Inserts)

The engine was assembled, serviced and then test run to determine its performance with the regular connecting rods. For fuel consumptions a 100ml (0.1litre) of fuel was poured into the fuel chamber and the engine was turned on. A stop watch was used to determined the time over which the fuel was consumed. Observations were made of the temperature, speed, torque and brake horse power (Bhp) with the aid of a dynamometer and tachometer. Similar tests were performed by using 0.2, 0.25 and 0.3litres of fuel. The regular connecting rods were replaced with the MMC connecting rods for the same performance tests were carried out. Table's

10A (a)-10A (b) and Figures 3.44-3.45 and figure 4.22 show the regular connecting rod and MMC connecting rod test results respectively.

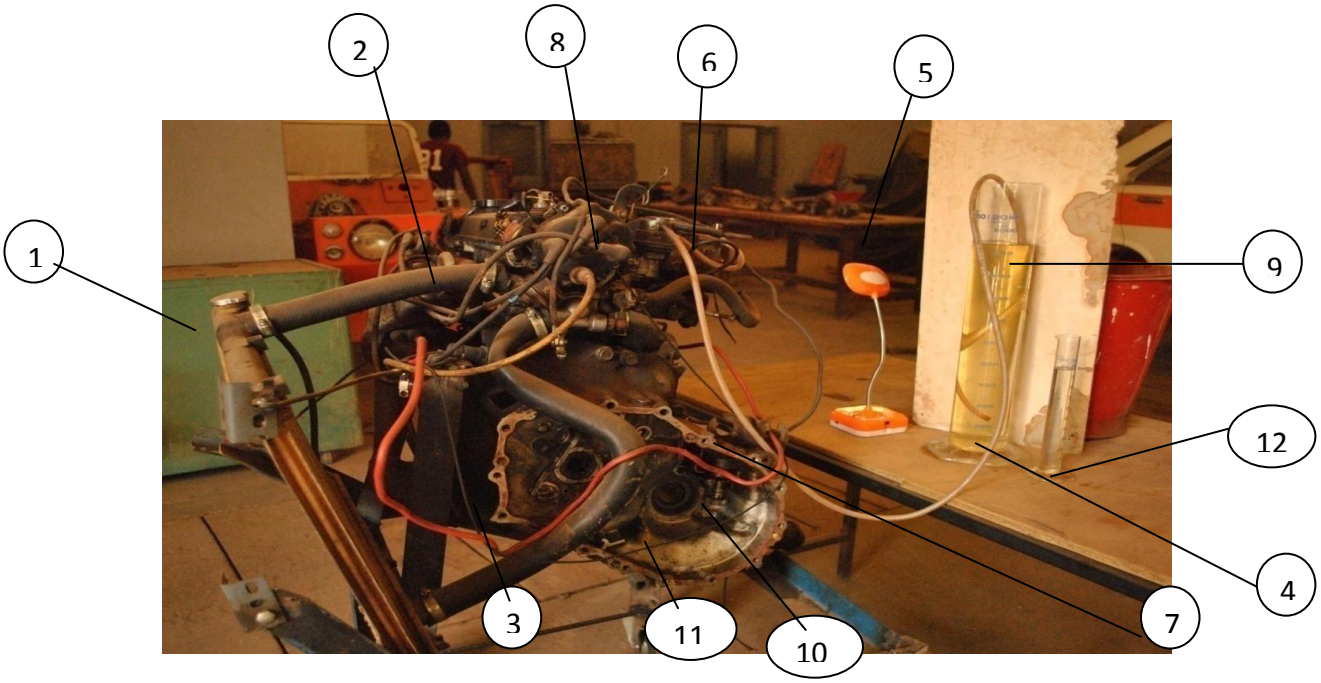


Fig 3.13: Photograph Toyota Model 12 valve engine.

(Automotive Laboratory,Kaduna Polytechnic 2013)

In Fig. 3.12 Some parts of the Toyota Model 12 valve engine are:

1. Radiator
2. Radiator upper hose
3. Radiator lower hose
4. Petrol hose connect to fuel pump
5. Petrol hose connect to carburator
6. Kick starter
7. Clutch housing
8. Distributor with high tension cable
9. Graduation cylinder
10. Exhaust pipe end
11. Engine Test Rig(bed)Graduation cylinder table

CHAPTER FOUR

RESULTS AND DISCUSSIONS

4.1 RESULTS

i. Microstructural analysis.

ii. Thermal analysis.

iii. Mechanical properties.

iv. Wear characteristics.

v. Corrosion tests

vi. Analysis on the developed prototype connecting rod, and tests on live engine.

4.2 CHARACTERIZATION OF THE COCONUT SHELL ASH

4.2.1 Particle size analysis of the coconut shell ash

From the particle size analysis the results, show that coconut shell ash particles have grain fineness number (GFN) of 75.08. The sample can be considered to be fine because the Grain Fineness Number (GFN) value of 100 is ranked the finest. Also, the sample can be considered to have met the AFS specification since four sieve-sizes, have the bulk of the retained samples on four consecutive sieves in descending order corresponding to 355μm, 180μm, 125μm, and 63μm size fractions respectively.

The particle size analysis of the coconut shell ash particles was carried out in accordance with BS1377:1990 (Ejiofor and Reddy, 1997, Bienia *et al,* 2003, Harun *et al,* 2006, Aigbodion *et al,* 2010).

4.2.2 Density of the coconut shell ash particle

The density of the coconut shell ash is 2.05g/cm^3 which means that coconut shell ash is a very light material. The values obtained fall within the range of densities

of fly ash, bagasse and silica which are 1.8 and 2.2 g/cm^3 respectively (Bienia *et al*, 2003, Aigbodion *et al*, 2010) and are currently used in metal matrix composites(Maruyama,1998).

Table 4.1: The density of the composites

wt%CSAp	Mass(g)	Volume(cm^3)	Density(g/cm^3)
0	5.50	1.93	2.85
3	6.00	2.12	2.83
6	5.00	1.82	2.75
9	5.58	2.07	2.70
12	6.20	2.31	2.68
15	5.89	2.21	2.66

4.2.3 Refractoriness of the coconut shell ash particles

The coconut shell ash was observed to have Seger Cone No. 22, with an equivalent temperature of 1500^{o}C. This means that coconut shell ash can withstand operating temperature of 1500^{o}C without any load (Kumar and Swamy, 2011).

4.2.4 XRF Chemical composition analysis of the coconut shell ash particles

The XRF chemical composition of the coconut shell ash is represented in Table 4.2. XRF. Analysis has confirmed that Silcon Oxide (SiO_2), Alumium Oxide (Al_2O_3), Manganes Oxide (MgO) and iron Oxide (Fe_2O_3) were found to be the major constituents of the ash. Silicon dioxide, iron oxide and alumina are known to be among the hardest substances. Some other oxides such as CALCIUM Oxide (CaO), K_2O, Na_2O and MnO were also found to be present in traces. The presence of hard elements like Silcon Oxide (SiO_2), Aluminium Oxide (Al_2O_3) and Iron Oxide (Fe_2O_3) suggests that, coconut shell ash can

be used as particulate reinforcement in various metal matrices. This result of XRF is in agreement with the results of the XRD obtained. Therefore, the present work suggests the possibility of using coconut shell ash as particulate in metal matrix composites since the chemical composition has close similarity with the XRF analysis of rice husk ash, bagasse ash and fly ash currently used in metal matrix composites (Bienia *et al,* 2003, Aigbodion *et al,* 2010, Kumar and Swamy, 2011).

Table 4.2: XRF analysis of the Coconut shell ash used

Element	Al_2O_3	CaO	Fe_2O_3	K_2O	MgO	Na_2O	SiO_2	MnO	ZnO
%	15.6	0.57	12.4	0.52	16.2	0.45	45.05	0.22	0.3

4.2.4 Compositional Analysis and Microstructure of the Coconut shell ash particles (CSAp)

From the XRD pattern(Figure 4.1) obtained, it was observed that the major diffraction peaks are 20.75°, 10.22° and 35.40°, and their inter-planar distances, 3.87Å, 8.66 Å and 2.54Å, and their relative intensities of X-ray scattering are 100.00, 61.90 and 8.44, and phases at these peaks are Quartz (SiO_2), Cordierite, syn ($Mg_2\ Al_4\ Si_5\ O_{18}$) and Moissanite (SiC), while each of these phases have a score of 44, 32 and 16 respectively (Table 4.3).

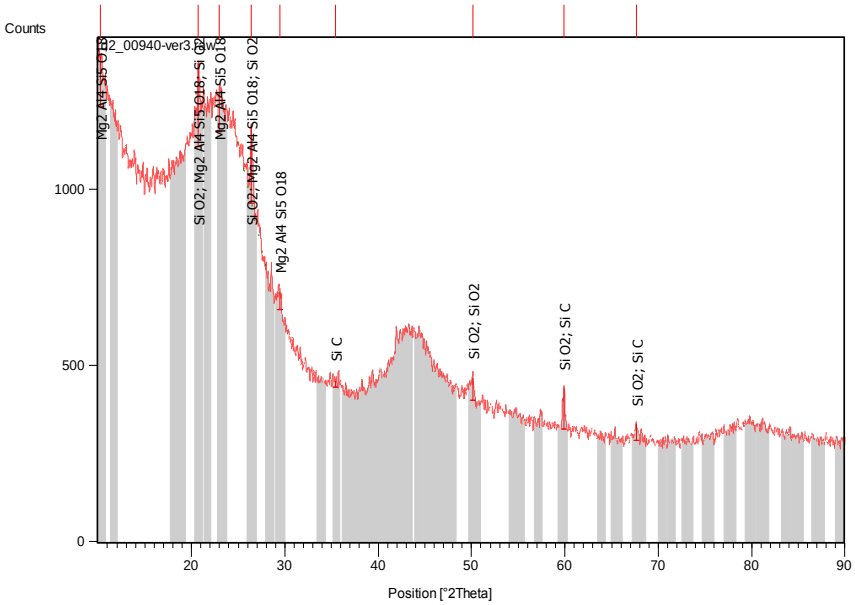


Fig. 4.1: XRD pattern of the Coconut shell ash used

The result showed that SiO_2 has the highest percentage of all the compounds and elements present as revealed by the XRD analysis. Complete mineralogical analysis carried out by X-ray difraction also revealed that the ash contains each of these elements C, O, Mg, Al, Si Fe, and none of these elements H, He, Li, Be, B, N, F, Ne, Na, P, S, Cl Zn, Ga, Ge, As, Se, Br, Kr, Rb, Sr, Y, Nb, Mo, Tc, Ru, Rh, Pd, Ag, Cd, In, Sn, Sb, Te, I, Xe, Cs, Ba, La, Ce, Pr, Nd, Pm, Sm, Eu, Gd, Tb, Dy, Ho, Er, Tm, Yb, Lu, Hf, Ta, which means that with the absence of all these other elements, coconut ash does not contain radioactive materials. This is in agreement with findings of Aigbodion and Hassan, (2010), Prasad and Krishna, (2010).

4.2.5 FTIR Analysis of the coconut shell ash particles

Twenty main peaks were detected in the *FTIR Analysis* of the coconut shell ash as visible in Figure 4.2. These peaks are shown in Table 4.3. This result has shown that the presence of quartz in the original ash gives rise to the IR spectrum in a series of bands located at 1132 and 443.64 cm^{-1}. The presence of mullite, in turn, is responsible for a series of bands at around 3797 cm^{-1}. The presence of carbon in

a series of bands at around 4091.15 4617.74 cm^{-1}. Quartz, mullite and the vitreous phase of the ash overlap in the area between 1220 cm^{-1} and 1434.12cm^{-1}. Hence, quartz, mullite, carbon and vitreous phases are confirmed to be present. However, the peaks in treated and untreated cases do not show any variations. This is in agreement with the earlier work of Ejilofor and Reddy, (1997), Kumar and Swamy (2011).

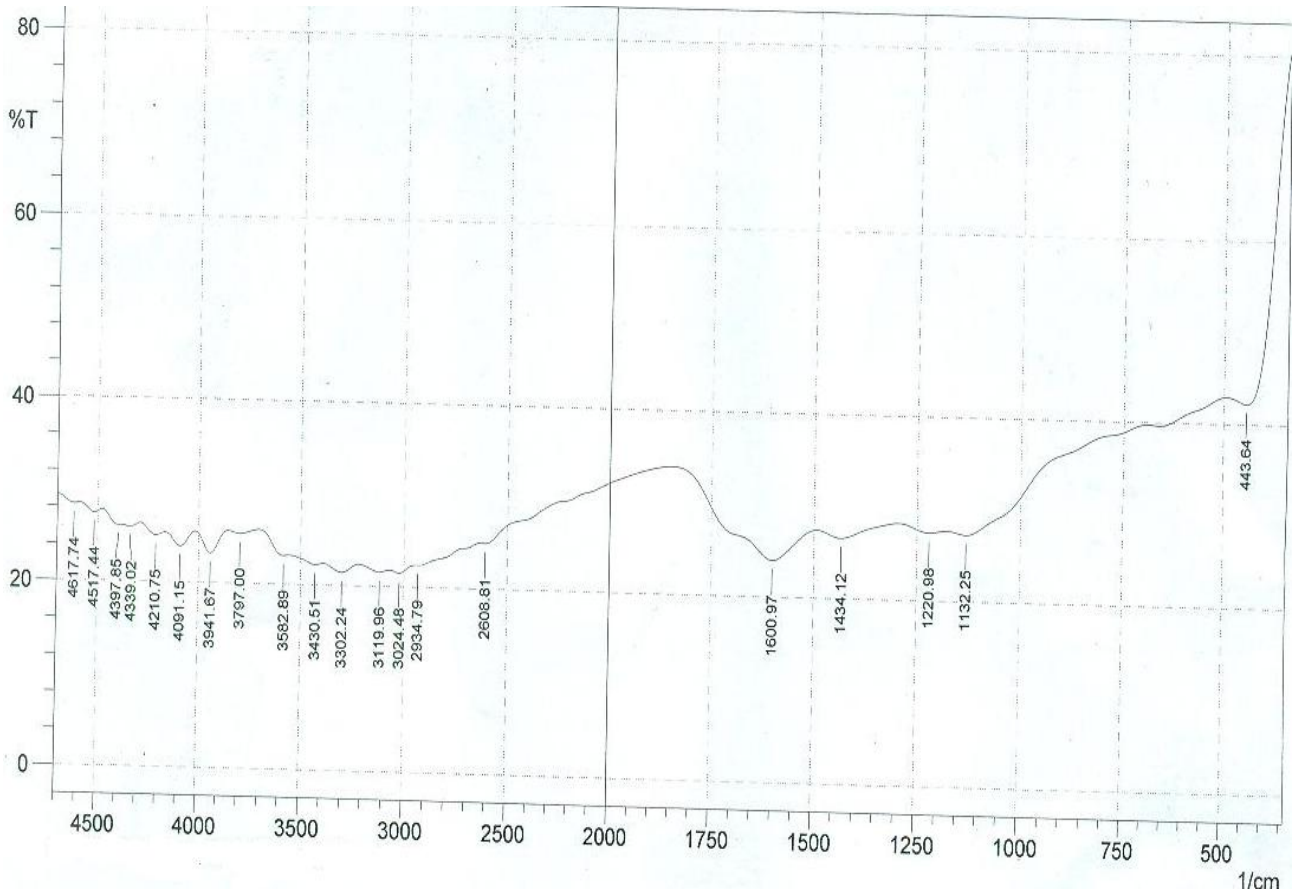


Fig. 4.2: FTIR spectrum of coconut shell ash

Table 4.3: Identification Peaks of the *FTIR analysis*

	Peak	Intensity	Corr. Intensity	Base (H)	Base (L)	Area	Corr. Area
1	443.64	42.2149	13.1434	494.76	339.48	45.9051	10.1546
2	1132.25	27.1942	1.5636	1179.51	692.47	231.175	2.8009
3	1220.98	27.3523	0.4785	1296.21	1180.47	64.5302	0.4347
4	1434.12	26.5234	1.1098	1492.95	1297.17	110.3001	1.5248
5	1600.97	23.953	5.3532	1848.83	1493.92	198.1139	14.825
6	2934.79	24.9316	0.268	2630.03	1849.8	414.8633	0.2663
7	2934.79	22.3717	0.082	2944.44	2630.99	196.7375	0.5234
8	3024.48	21.4832	0.5261	3070.78	2945.4	82.8073	0.5844
9	3119.96	21.5287	0.4499	3218.34	3071.74	96.8457	0.6531
10	3302.24	21.4044	0.9435	3390.01	3219.3	112.6911	1.6016
11	3430.51	22.1843	0.3504	3553.96	3390.97	105.2941	0.4467
12	3582.89	23.0736	0.5718	3703.45	3554.93	91.4995	0.8093
13	3797	25.3657	0.3682	3854.87	3704.41	89.1332	0.5007
14	3941.67	23.1722	2.4099	4016.89	3855.83	98.5847	3.24
15	4091.15	23.8574	1.5527	4165.42	4017.86	89.7741	1.9765
16	4210.75	24.9963	0.6758	4287.9	4166.38	72.2261	0.7304
17	4339.02	25.8493	0.3262	4381.45	4288.86	54.1344	0.2576
18	4397.85	26.8494	0.2859	4476.93	4382.42	54.2572	0.3228
19	4517.44	27.3549	0.5835	4588.81	4477.89	61.741	0.4816
20	4617.74	28.3067	0.3104	4700.68	4589.77	60.1765	0.3021

4.3 MACROSTRUCTURAL OBSERVATIONS



Plate 4.1: Photograph of the cast composites

Macrostructural observations revealed a reasonably uniform distribution of coconut shell ash particles in the aluminum alloy. The distribution of coconut shell ash particles is influenced by good wettability of the coconut shell ash by the molten metal and good interfacial bonding between coconut shell particles and matrix material (Plate 4.2) The good wet ability obtained in this study was as a result of the use of the degassing tablets combined with the double stirring method during casting which helped to avoid gravity segregation. This prevented the composite slurries from oxidation and breakdown of the gas layer. It was observed that during the casting of the composites that increasing the weight percentage coconut shell ash particles beyond 15% by weight made the composite slurry thick, and thus, the fluidity of the molten composite was reduced.

4.4 DENSITY OF THE COMPOSITES

The result of density measurements on the alloy and reinforced materials are shown in Figure 4.3 and Appendix Table A1.

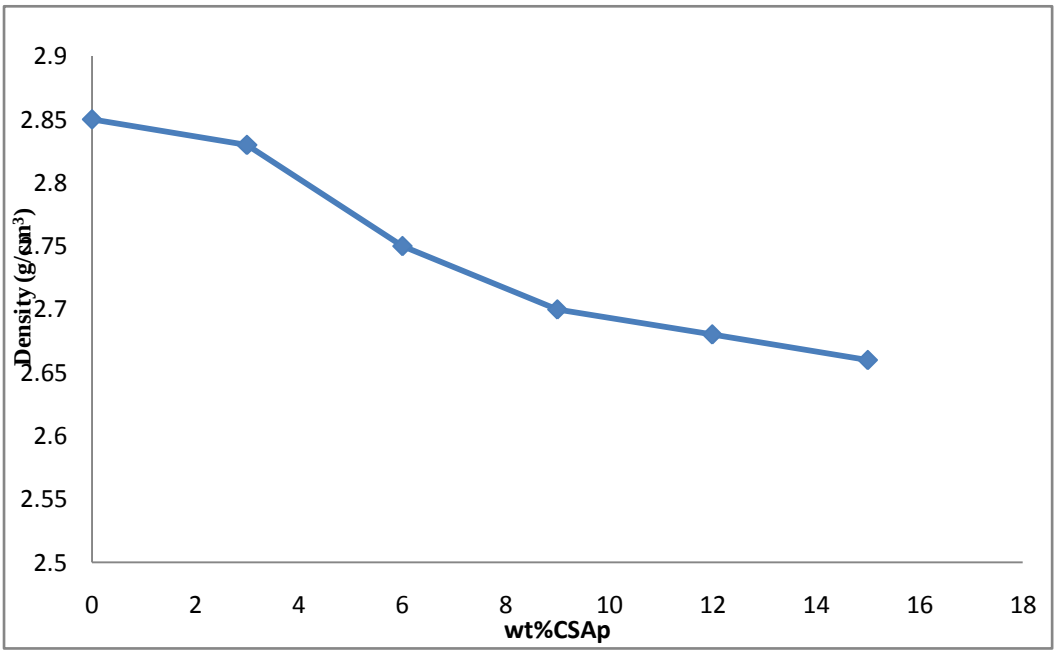


Fig. 4.3: Plot of Density with percent of Coconut shell ash

Morphologies of the coconut shell ash by SEM with EDS are shown in Plate 4.1.

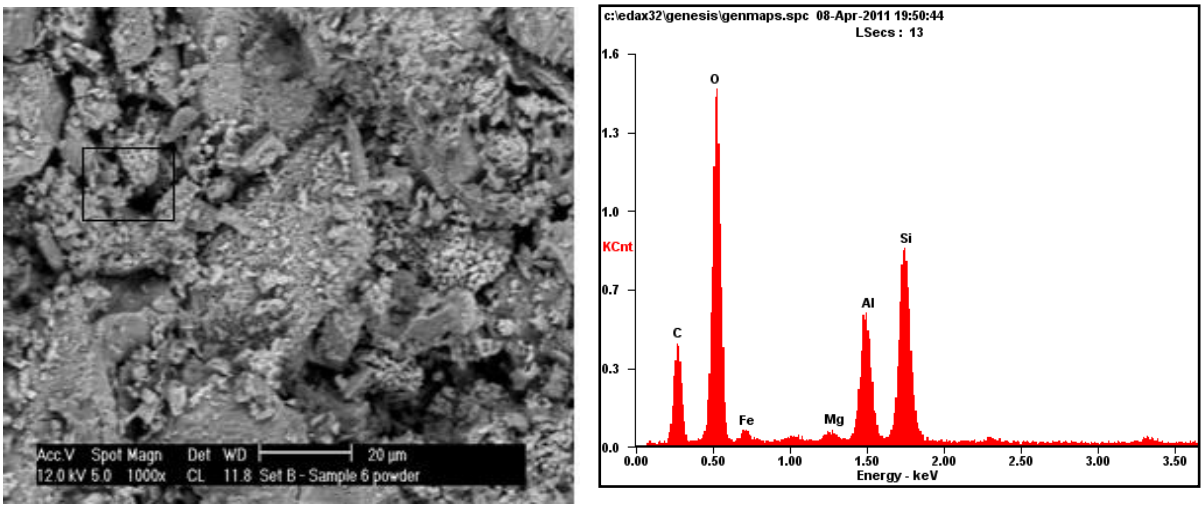


Plate 4.2: SEM/EDS spectrum of Coconut shell ash

The structure reveals that the size and shape of the particles vary; however, they can be sorted into two main groups – spherical and fibrous. The spherical particles consist mainly of Si, C and O. The fibrous ones contain Si and O as well as Mg, Al with small amounts of Fe as shown in the EDS scan (Plate 4.1). The results are consistent with XRD analysis of other biomass by Ejiofor and Reddy, (1997). The SEM result showed that both SiO_2 and SiC have a fine structure, the former having a finer one (Prasad and Krishna. 2010).

The results reveal that an increase in the percentage of coconut shell ash (CSAp) in MMCs decreases the material density; this is due to the fact that coconut shell ash particles are less dense than the aluminium alloy. The density of the reinforced coconut shell particle composites decreased from 2.86 g/ cm^3 at 0% by weight of CSAp addition to 2.66g/ cm^3 at 15% of CSAp addition. This shows that composites with light weight can be made with this ash. The result is in line with the earlier work of Prasad and Krishna (2010).

4.5 MICROSTRUCTURAL AND THE INTERFACIAL STUDY OF THE COMPOSITES

Table 4.4: Identified Patterns List of Coconut shell ash

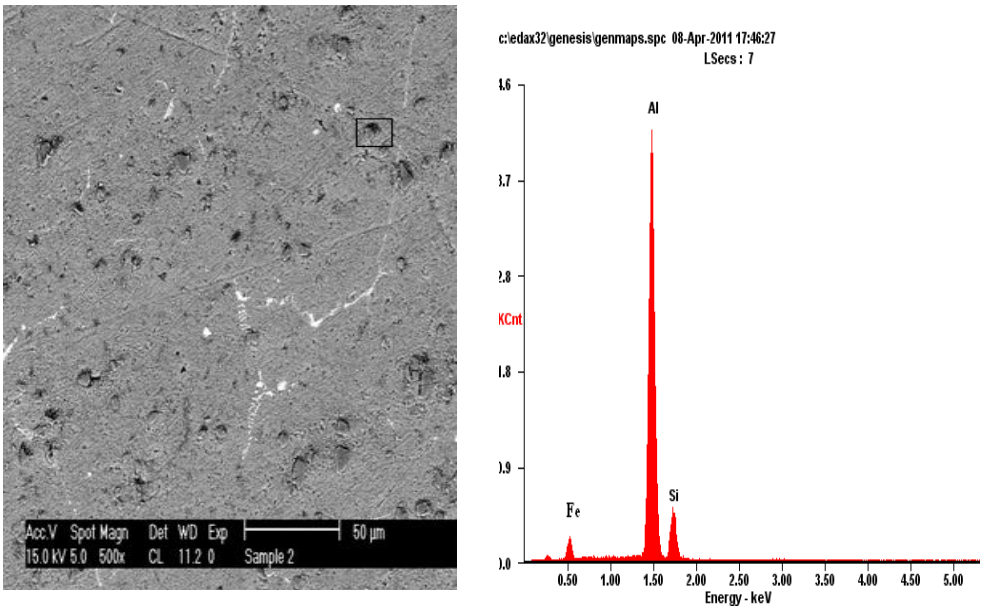
Visible	Ref. Code	Scorex	Compound Name	Displacement [°2Th.]	Scale Factor	Chemical Formula
*	00-043-0596	44	Silicon Oxide	0.000	0.912	SiO_2
*	00-013-0294	32	Cordierite, syn	0.000	0.590	Mg_2 Al4 Si_5 O18
*	01-089-1961	26	Quartz low, dauphinee-twinned	0.000	0.642	SiO_2
*	01-075-1541	16	Moissanite 6\ITH\RG	0.000	0.207	Si C

4.5.1 X-ray Diffraction Analysis (XRD)

The XRD pattern of the aluminium alloy and the alloy reinforced with coconut shell ash composites manufactured by the stir-casting method are shown in (Figure 4.1 and Table 4.3). From the figures it was observed that, the major phases of the aluminium alloy are Fe_3Si, Al_6Fe, Al and SiO_2 (Table 4.3). The composite shows smaller inter-planar distances and the phases are SiC; Fe_3C FeSi SiO_2 and C. In these diffractograms, one can evidently deduce the crystalline phases of the aluminium alloy from that of the composite material. The X-ray patterns show Fe_3Si, Al_6Fe, Al presence in the matrix aluminium alloy and evidence of the coconut shell ash particles in the composite.

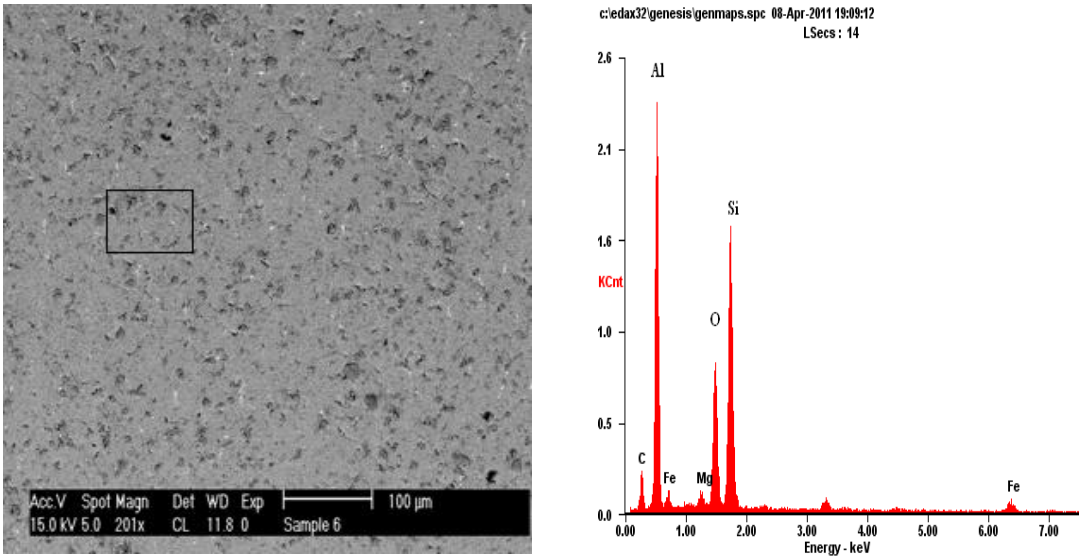
4.5.2 MICROSTRUCTURAL ANALYSIS OF COMPOSITES

The microstructure of the aluminium alloy and that of the aluminium alloy with coconut shell ash were analysed, using scanning electron microscopy/energy dispersive spectrometery. The microstructure of the aluminium alloy is shown in Micrograph 4.1. The structure reveals the eutectic phase containing Fe_3Si, Al_6Fe, in α-aluminum matrix

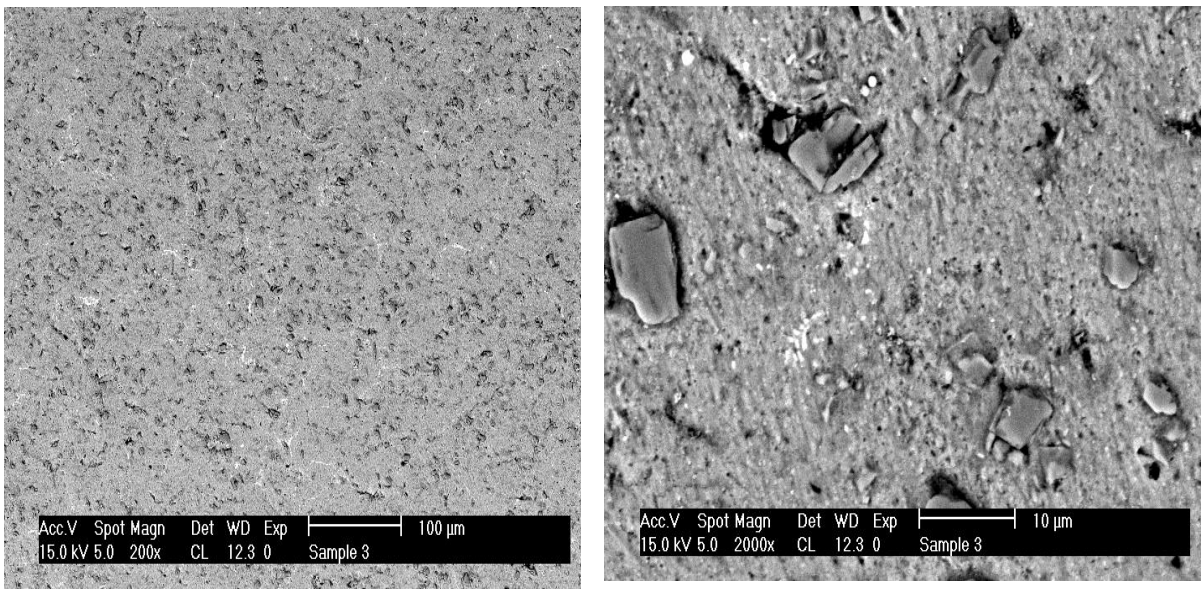


Micrograph 4.1: SEM/EDS Micrograph of the aluminium alloy

The microstructure of the composites can be seen in micrographs to 4.2-4.7.They reveal small discontinuities and a reasonably uniform distribution of coconut shell ash particles in the aluminum matrix. The ceramic phase is shown as the dark phase, while the metal phase is white (Micrographs 4.3-4.6).

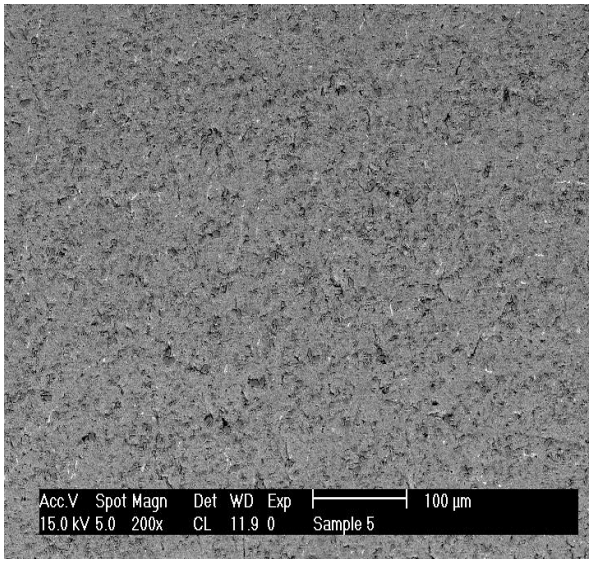


Micrograph 4.2: SEM/EDS Micrograph of the aluminium alloy with 3% by weight CSAp

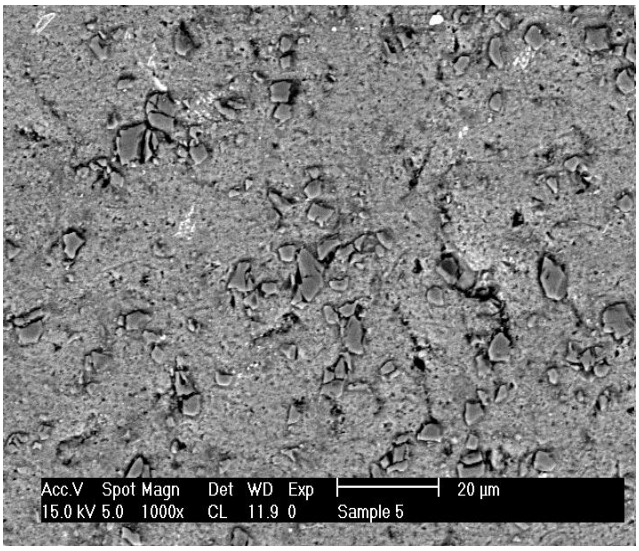


a) Lower magnification = 200 x b) Higher magnification = 2000 x

Micrograph 4.3: SEM Micrograph of the aluminium alloy with 6% by weight CSAp

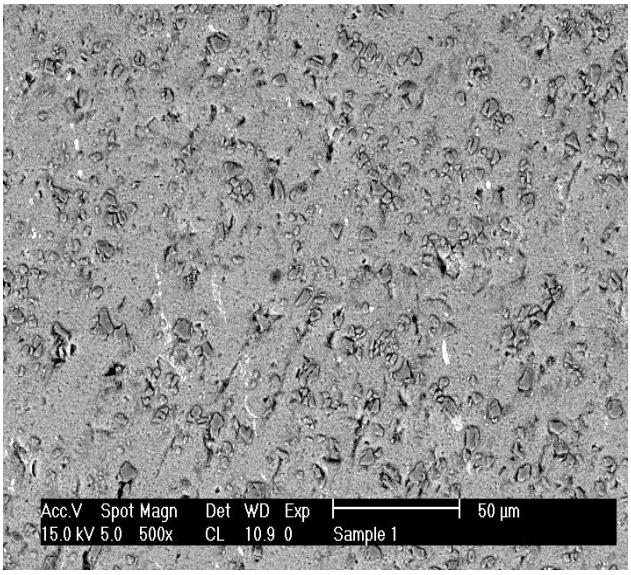


a) Higher magnification = 200 x

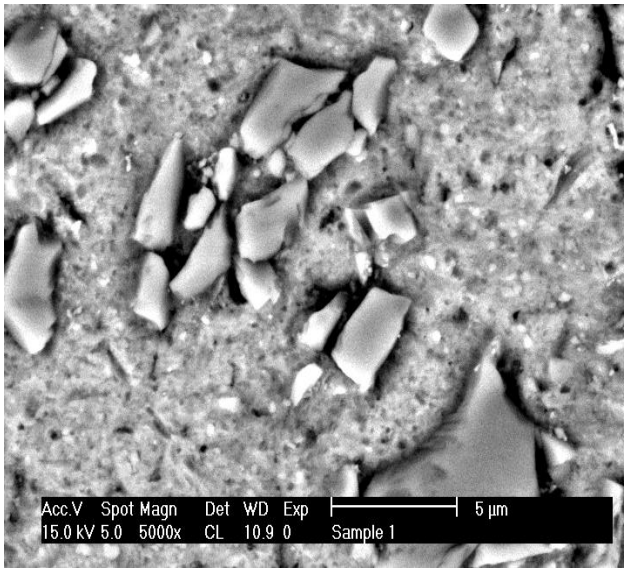


b) Lower magnification = 1000 x

Micrograph 4.4: SEM Micrographs of the aluminium alloy with 9% by weight CSAp

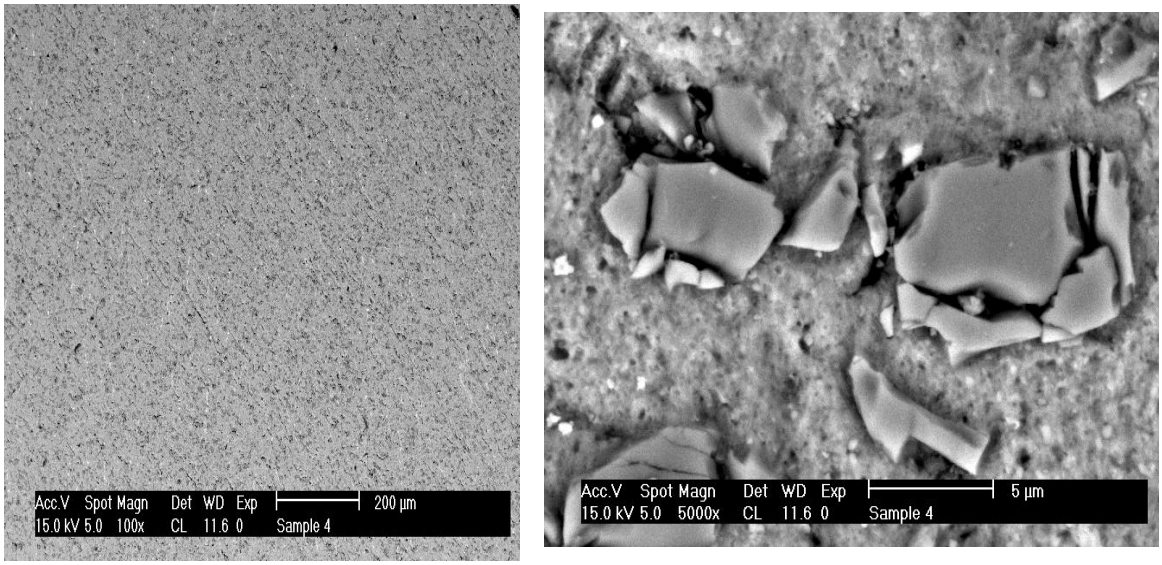


a) Lower magnification = 500x



b) Higher magnification = 5000 x

Micrograph 4.5: SEM Micrographs of the aluminium alloy with 12% by weight CSAp



a) Lower magnification = 100 x b) Higher magnification = 5000 x

Micrograph 4.6: SEM Micrographs of the aluminium alloy with 15% by weight CSAp

These structures are in agreement with phases studied by other researchers (Aigbodion and Hassan, 2007, Surappa and Rohatgi, 1981). The structure obtained in this work was made possible by activation of the coconut shell ash particles (CSAp) and proper selection of parameters for the casting process.

Electron transmission microscopy was used to make the analysis of the interfaces between coconut shell ash particles and the matrix. The presence of the considerable amount of silicon and iron in the matrix alloy ensured the formation of the required bonds between the components of the composite and matrix examined. Interfaces between the particles and the matrix, are free from intermediary phases and any precipitates, had an adhesive effect on component bonding. Moreover, they were characterized by a high cohesion (without micro-cracks) and strength of bonding. The microstructure of the composite clearly shows a uniform distribution of coconut shell ash in the aluminum alloy matrix such as cast composites (see plate 4.2).

In the composites examined, no effects of unfavourable phenomena were observed, which frequently form in the structures of cast composites, such as sedimentation or flowing out of the reinforcing phase, as well as the formation of particle agglomerates or gas blisters. This showed that there was good interfacial bonding between coconut shell ash particles and the matrix. Good retention of coconut shell ash particles was clearly seen in the microstructures of the composites. Satisfactory interfacial bonding was obtained by heating of coconut shell ash particulates prior to dispersion and addition of magnesium in small quantities during stirring, which improved wettability of coconut shell ash particles.

Scanning electron micrographs of a typical coconut shell ash particle which has retained the original shape of the coconut shell ash are shown in Micrograph. However, these particles are quite fragile and some particles tend to break down during handling, thereby loosing the hull like shape. In addition, aluminium dendrites, eutectic silicon and some small fragmented coconut shell ash particles can also be seen in the microstructure.

The chemical analysis was done by Energy Dispersive Spectrometer Energy dispersive spectrometer (EDS) using the sample prepared for Scanning Electron Microscope Scanning electron microscope (SEM). The analysis revealed the presence of silicon particles as a result of the reaction between the Coconut Shell Ash Coconut Shell ash (CSA) particles and molten Al alloy. The peak value shows the presence of Al and its compound on the surface. The unreinforced alloy reveals the presence of α-Al, Si and Fe as evident from the EDS spectra (Micrograph 4.2). From the EDS analysis of the composite (Micrographs 4.3) there are indications of some possible chemical reaction between aluminium melt and coconut shell ash particles which led to the release of Si, Fe, O and C.

The diversified chemical composition of coconut shell ash particles and its high reactivity can form compounds by chemical reactions between coconut shell ash particles and liquid aluminium during the synthesis of the composites. The reaction between CSAp-reinforcement containing silica and liquid aluminium can lead to the formation of alumina and silicon in the following reaction:

$4Al + 3SiO_2 = 2Al_2O_3 + 3Si$

The development of some primary silicon single crystals in the vicinity of coconut shell ash is seen in Micrograph 4.3.

Electron transmission microscopy was used for the analysis of the interfaces between coconut shell ash particles and the matrix. The presence of considerable amounts of silicon and iron in the matrix alloy ensured the formation of the required bonds between the components of the composite examined. Interfaces between the particles and matrix, are free from intermediary phases and any precipitates, had an adhesive effect on component bonding.

Moreover they were characterized by high cohesion (without micro-cracks) and strength of bonding.

The microstructure of the composite clearly shows a uniform distribution of coconut shell ash in the aluminium alloy matrix. In the composites examined no effects of unfavorable phenomena were observed, which frequently form in the structures of cast composites, such as sedimentation or flowing out of the reinforcing phase, as well as the formation of particle agglomerates or gas blisters. This showed that there was good inter facial bonding between coconut shell ash particles and matrix, good inter facial.

4.6 HARDNESS VALUES

Hardness of the developed composites increased with increase in percentage of coconut shell ash particles. It is noteworthy that the hardness value of coconut shell ash is 95.05HB, and the presence of the hard ceramic phase in the ductile matrix has resulted in the increase in hardness of the composite (Figure 4.10 and Appendix Table A2). For example the hardness values increased from 63.50HRB at 0% to 78.60HRB at 15% by weight of coconut shell ash particles. These increments are attributed to the increase in weight percentage of the hard and brittle phase of the coconut shell ash particles in the aluminium alloy. This hardness value of the coconut shell ash particles is obtained from the SiC, Al_2O_3, Fe_2O_3 and SiO_2 in the chemical makeup of the particles(Table 4.1). Also, the presence of coconut shell ash particles in the alloy, increases the dislocation density at the particle-matrix interfaces. This is as a result of differences in the coefficient of thermal expansion (CTE) between the hard and brittle reinforced particles, and soft and ductile metal matrix which results to elastic and plastic incompatibility between the matrix, and the reinforcement (Aigbodion and Hassan, 2010, Mohan *et al*, 2003).

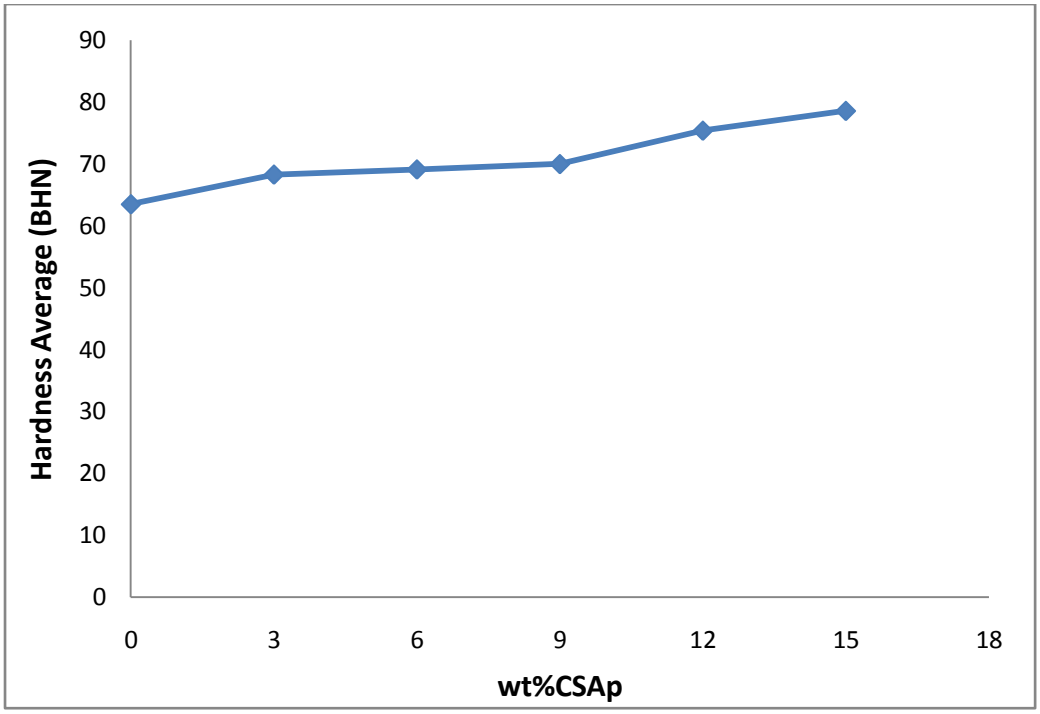


Fig 4.4: Variation of the Hardness values with wt% coconut shell ash particles.

4.7 TENSILE PROPERTIES

The results of the yield and tensile strength are shown in Figure 4.5 and Appendix Table A3.

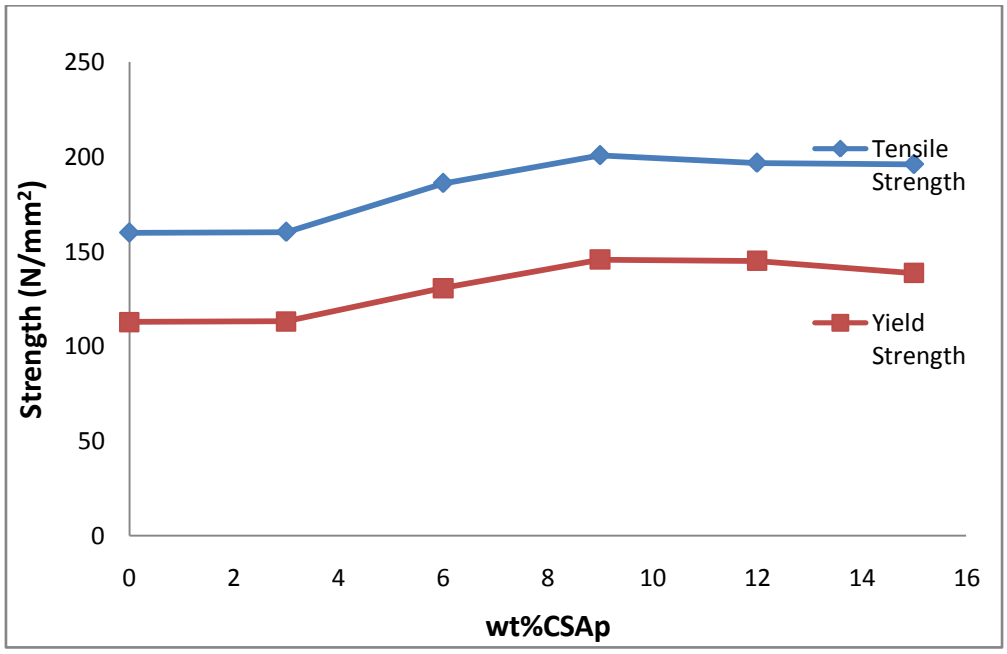


Fig. 4.5: Variation of the strength with wt% coconut shell ash particles

The 0.2% offset yield stress (YS) and ultimate tensile strength (UTS) of the composites are higher than those of the aluminium alloy matrix, and show a monotonic trend over the whole added reinforcement volume fractions, e.g. the yield and tensile strength increased by 28.38 and 24.86% at 12% by weight coconut shell ash particles(CSAp) respectively. With increasing volume fraction, more loads are transferred to the reinforcement which also resulted in a higher tensile strength. This behaviour is in agreement with the work carried out by Yung et al (2004). This result may be attributed to several factors including the good particle-matrix interfacial bonding, the fine reinforcement particle size and the strengthening effect of the coconut shell ash particles (CSAp) on the aluminium alloy matrix (Guo *et al*, 1996a, Guo *et al*, 1996b).

In general, when ceramic particles are introduced to a metal matrix by the casting method, particle-porosity clusters tend to occur due to the poor wettability and gas entrapment during mixing (Prasad and Krishna, 2011). However, the defect has not been found in the present study, which can be attributed to the good wettability of the CSAp with aluminium alloy melt which helped the dispersion process of the particles in the aluminium alloy melt (Rohatgi, 1994, Rohatgi and Guo, 1997).

The strengthening effect of CSAp is noticeable, with the hardness and tensile strength values of the composites. To understand the above improvement, it is desirable to discuss the strengthening mechanism in details. Generally, the mechanical properties of metallic materials are significantly affected by various factors, such as grain-boundaries, sub-structures, solid solutions, second phases, and so on. For the present materials, contributions from sub-structures and solid solution effects can be ignorable. Based on the structural information obtained above (Micrographs 4.2 to 4.7), the grain refinement of the matrix and the reinforcement contributed by CSAp

are the main reasons for the improvement of the hardness and tensile strength illustrated in Figure 4.5.

CSAp play an important role on the load transfer in the strengthening of the developed composites. As shown in Micrographs 4.3-4.7, they introduce large amounts of grain-boundaries, along which atomically bonded interfaces of aluminium alloy are generated. With a low volume fraction of CSAp, the grain size of the matrix is much bigger, so the Orowan bypass mechanism may operate within those large grains of aluminium alloy, as it happens in most traditional materials (Rohatgi *et al*, 1995, Rohatgi *et al*, 1998). With high CSAp fractions, however, aluminum grains that are getting smaller and smaller and induce grain refinement as illustrated above, the Orowan bypass mechanism will not operate because the matrix and the reinforcing agent present similar grain sizes. In this case, the load can be transferred directly through the interface. The above speculation is based on two facts:

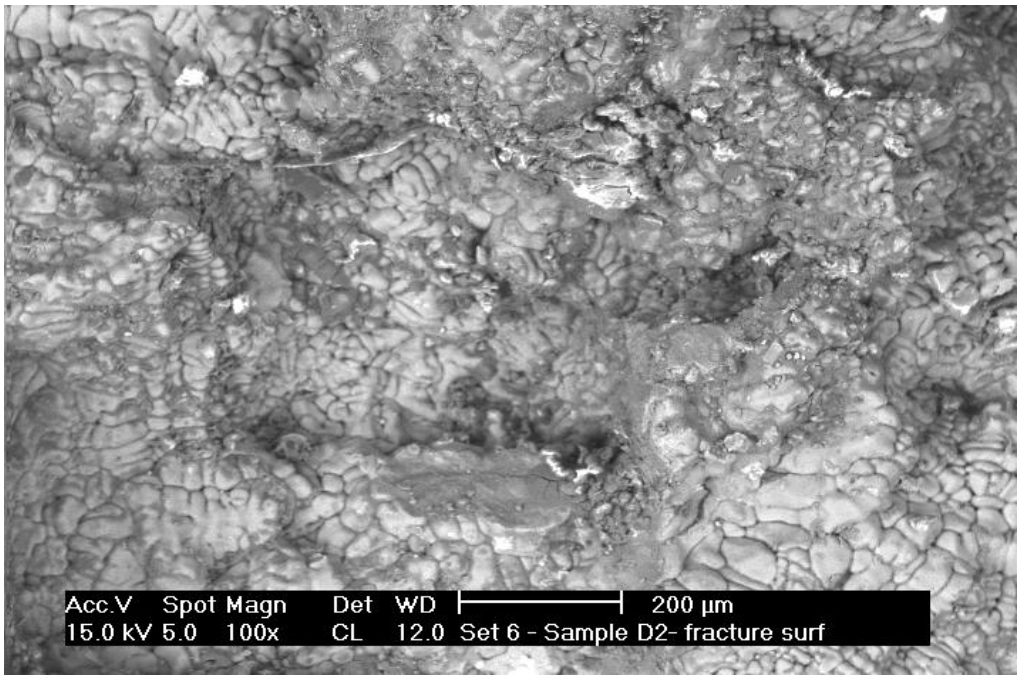
(i) large amount of atomically bonded interfaces have been observed in the experiments;

(ii) the material grain-boundary (GB) activities (sliding/rotation or dislocations emitting from GBs), rather than the dislocation pile-up and movement, are thought to mainly account for the deformation under applied stress.

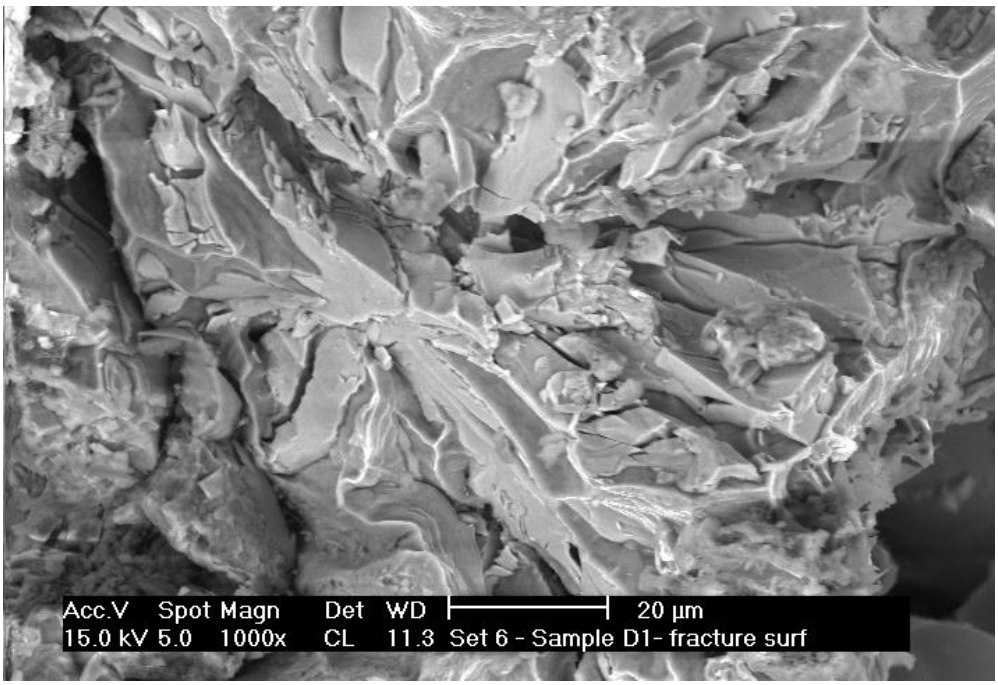
Thermal mismatch matrix and reinforcement have different coefficients of thermal expansion, therefore, during the cooling process, plastic deformation is produced in the matrix at the interface. This deformation can cause defect such as dislocations. Due to the increment of interfacial areas, the density of dislocation is also increased (Rohatgi *et al,* 1998, Itskos *et al,* 2011).

Micrographs 4.8-4.9 show the typical fractographs of the failed tensile samples. The composite samples display a mixed fracture mechanism on the fracture

surface: brittle fracture of the reinforcement particles and ductile tearing of the aluminium alloy matrix.



Micrograph 4.7: SEM Fractograph of the aluminium alloy



Micrograph 4.8: SEM Fractograph of the aluminium alloy reinforced with 15wt% CSAp

A primary difference between the fracture surfaces of the composites is the relative area fraction of the matrix to fractured particles. Another difference is the proportion of voids presented on the fracture surface. From Micrograph 4.7 and 4.8), it can be concluded that the dominant fracture mode of samples are particle cracking and matrix ductile tearing. Particle-matrix interfacial debonding cannot be found by fracture surface examination, which confirms the strong interfacial bonding between the CSAp and the aluminium alloy matrix (Itskos *et al*, 2011).

4.8 IMPACT STRENGTH

The results of impact energy tests are shown in Figure 4.12 and Appendix Table A5

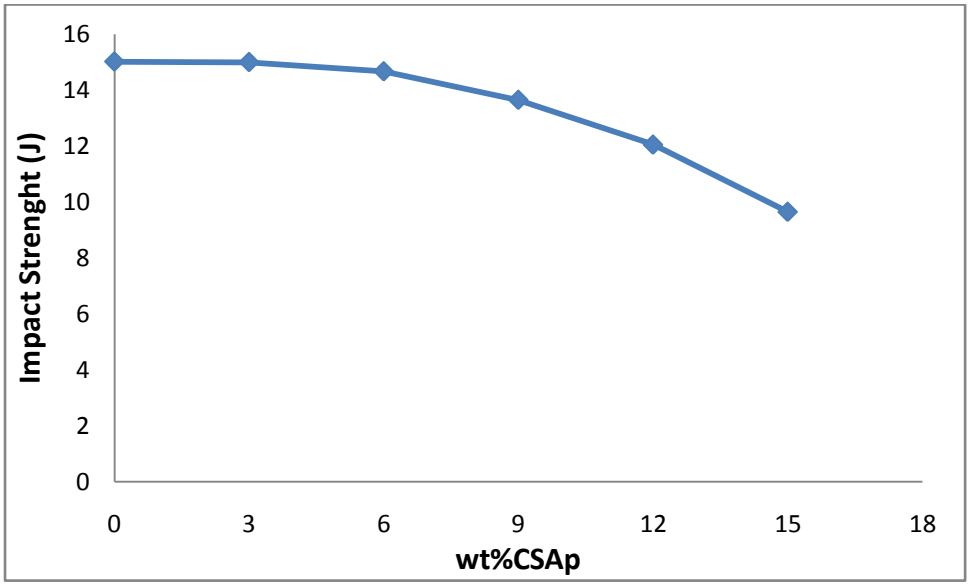


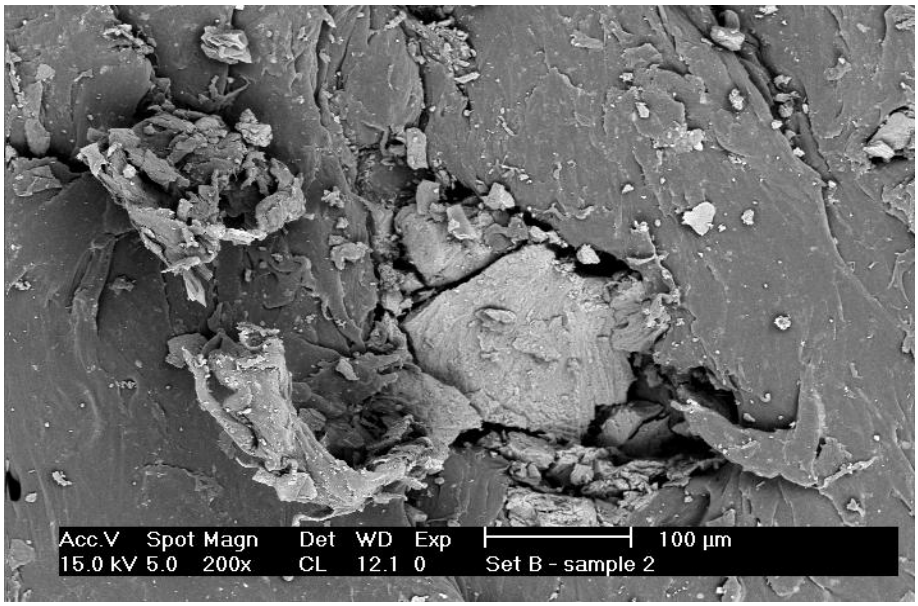
Figure 4.6: Variation of the Impact Strength with wt% coconut shell ash particles

The most interesting part of the present research is that the impact energy and % elongation decrease as the percent CSAp addition increases in the composites (Figure 4.6). The brittle nature of the reinforcing material (CSAp) is supposed to play a significant role in degrading the impact energy and % elongation of the composites. On the other hand, as can be suggested from the impact test, the elastic behaviour of

the matrix proportionately varies with the addition of the CSAp. As the loading of CSAp increases, the ability of the composite to absorb impact energy is supposed to have decreased to a great level, since there is less ratio of the matrix to particles. However, the impact energy results obtained at 6-9% by weight CSAp are within the standard values for impact energy for connecting rod applications as shown by the research of Rohatgi and Guo (1997).

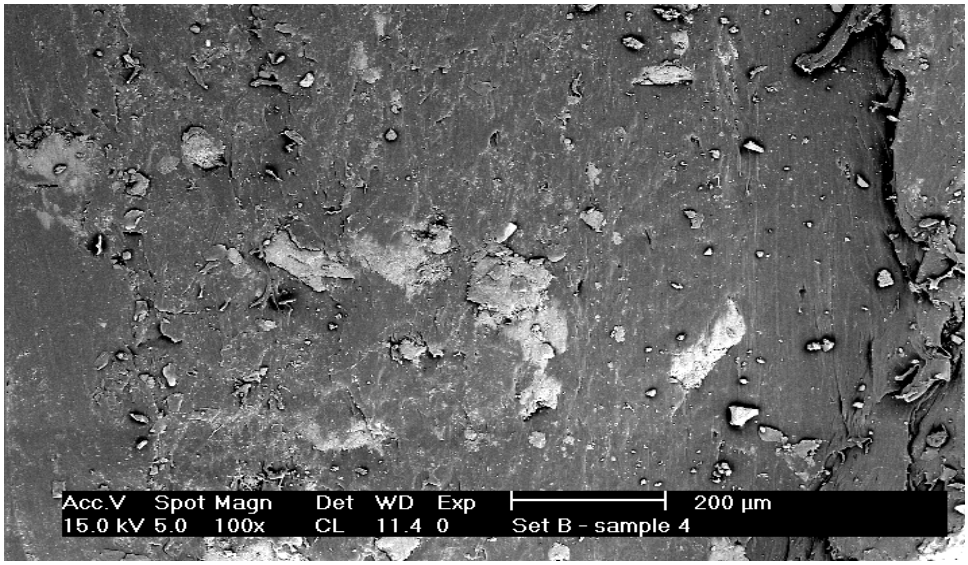
4.9 WEAR BEHAVIOUR

The SEM microstructure of the worn surfaces are shown Micrographs 4.9 and 4.10.



200 x

Micrograph 4.9: SEM Micrograph of the Worn surface of the aluminium alloy at 50N, 2.0m/s and 4000m. these represent wear test conducted by varying applied from 10 to 50N at a constant speed of 2.0m/s and a sliding distance of 4000m



100 x

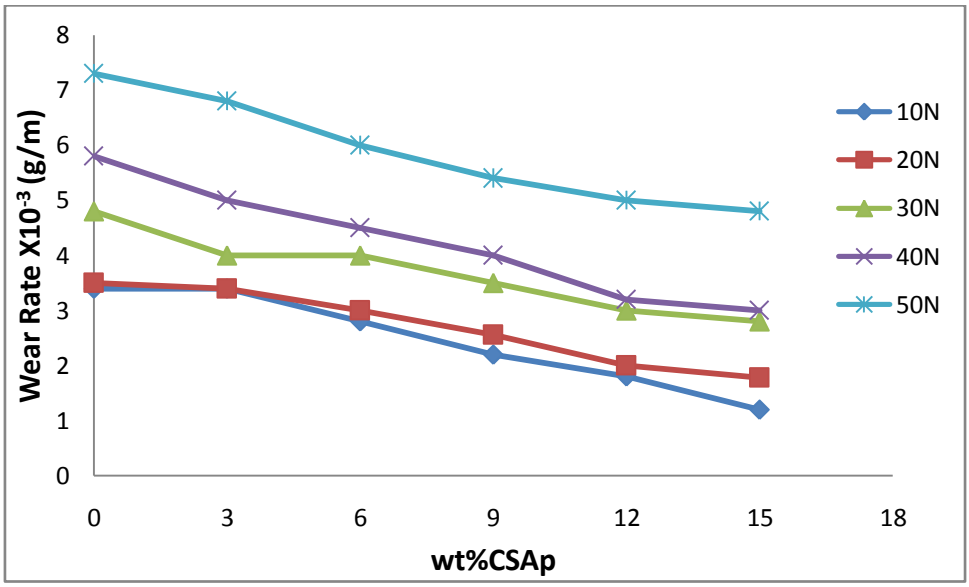
Micrograph 4.10: SEM Micrograph of the Worn surface of the aluminium alloy with 9% by weight CSAp at 50N, 2.0m/s and 4000m of vary applied load.

From Micrographs 4.9 and 4.10, it can be seen that the aluminium alloy with no CSAp reinforcement forms a good thin and uniform transfer film (Micrograph 4.9). In the case of aluminium alloy with CSAp reinforcement (Micrograph 4.10) there appears to be some disruption of the transfer film for CSAp which has affected the wear rate performance. The worn surface of the materials can be described as classical ratcheting wear, as defined by Aigbodion and Hassan (2010), Jasmi (2001) and Basavarajappa *et al*, (2006).

The transition in wear rate observed for many MMCs is faster and is believed to be the result of voiding/cracking between the reinforcement and the matrix, both of which lead to fragmentation and delimitation of the surface (Das *et al*, 1989). Micrograph 4.10 reveals particle cutting and void formations due to chips of the matrix. There is also evidence of Al-Si-Fe alloy removal and deep furrows in the structure.

The propagation of cracks along transverse as well as longitudinal directions is well visualized. Furthermore, crushed and fragmented particles were noticed in Micrograph 4.9. The worn surfaces in some places reveal patches from where the material was removed from the surface of the material. The parallel grooves suggest abrasive wear as characterized by the penetration of the hard coconut shell ash particle into a softer surface, which is an important contributor to the wear behavior of Al-Si-Fe/CSAp composites. It is possible that the scored grooves might have been formed due to the action of the wear- hardened deposits on the disc track. Similar observations were made by Aigbodion and Hassan (2010), and Das *et al*, (1989).

The results of the wear rate and coefficient of friction are shown in Figures 4.13 and 4.14, and Appendix Table A5 and A6.



Figures 4.7: Variation of wear rate with wt% of coconut shell ash particles

From Figure 4.7, it is observed that the wear rate increases with decrease in the weight percentage of coconut shel l ash particles. Also, increase in applied load resulted in increased wear rate of the samples for all composites of coconut shell ash. But at higher applied loads, the samples get well spread with lesser coconut shell

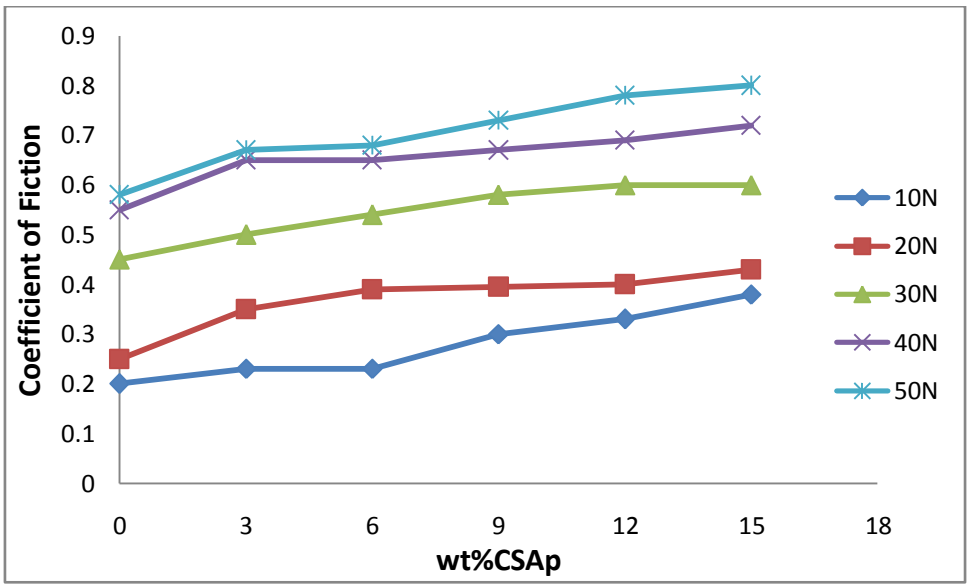
particles getting exposed and breakages of CSAp taking place. This is attributed to the extensive loss of the material due to fragmentation of the CSAp and its detachment from the test material due to the non-availability of a medium to hold them.

The beneficial effect of the reinforcement on the wear resistance of the Al-Si-Fe alloy composites is observed to be best at low loads, and reduces with increase in applied load. With higher loads, contact temperatures become high and plastic deformation occurs with consequences of high wear. Also, when applied loads are increased, seizure is accompanied by sudden increase in wear rate and heavy noise and vibration were also noticed. This type of seizure has been referred to as galling seizure (Mohan *et al,* 2002, Garcia *et al,* 1996). The wear mechanism reported was oxidation at lower loads and adhesion and delimitation at higher loads (Sahin, 2003, and Banerji *et al,* 1982). This observation is in agreement with that of Aigbodion and Hassan (2010) on bagasse ash reinforced aluminium alloy composite. They reported that the beneficial effect of particle reinforcement was gradually reduced with increasing load.

Also with increased load, friction and wear will increase due to the critical surface energy of the MMCs. Furthermore, this is explained as the frictional heat raised the temperature of the friction surfaces. It is well known that the wear process involves fracture, tribochemical effects and plastic flow. Transitions between regions dominated by each of these give rise to changes in wear rate with load. Furthermore, this result is closely related to structural characteristics and chemical effects which occur in frictional processes as well as transfer film formation on the counter face (Micrographs 4.9 and 4.10).

At higher loads, the oxide debris is expected to get better, compacted to form transfer layer, and spread over a larger area of the sliding surface. However, the wear rate under such circumstances takes place also by flaking of the transfer layer during sliding, apart from the processes of adhesion, micro-cutting and abrasion. At higher loads, the wearing process could be more aggravated by the transfer layer flaking off as indicated by the presence of a chunky sheet of oxide agglomerates, in the wear debris as observed in Micrographs 4.9 and 4.10.

Al-Si-Fe alloy and the composites containing CSAp have been examined for their friction behavior, determined by the variation of the coefficient of friction during tests of dry sliding wear under different loads as shown in Figure 4.14.



Figures 4.8: Variation of Coefficient of Friction with wt% of Coconut shell ash particles

The friction force rises in the initial period and then fluctuates around a mean during dry sliding. The mean has been determined from the individual values of coefficients of friction excluding the initial rising part, and it has been observed that the mean coefficient of friction increases with increasing load for the Al-Si-Fe alloy and the composites containing CSAp as shown in Figure 4.8. At a higher load, the

frictional force increases with greater dissipation of energy leading to a higher temperature at contact which results in a higher of coefficient of friction with increasing load. But a higher coefficient of friction with increasing CSAp content in the composite is surprising as these particles are supposed to create weak junctions with the asperities of the counter face because of low oxide-metal interfacial energy and also, contribute in the formation of a greater cover of transfer layer which should make relatively weak junctions. Therefore, the only inescapable conclusion is that ploughing of the sliding surface and micro-cutting during the wear test contributes to higher frictional forces in composites containing more hard oxide particles.

The coconut shell ash particle composite exhibited high wear resistance under different applied loads. This behaviour can be attributed to the presence of CSAp on the counter surface, which acts as a transfer layer and effective barrier to prevent large-scale fragmentation of the Al-Si-Fe matrix. This is also evident from the small size of the wear debris particles as determined by SEM analysis (Micrograph 4.10). The wear resistance of the composite is improved by preventing direct contact that induces subsurface deformation. The addition of hard ceramic particles improves the resistance to seizure. Coconut shell ash particulate allows considerable thermal softening effects without having adverse effects on wear behavior. The reinforcement also causes higher hardness and lower coefficient of thermal expansion of the Al-Si-Fe alloy matrix (Figure 4.14). The presence of the ceramic particles provides higher thermal stability, increased abrasion and sliding wear resistance at high loads and delays the transition from mild to severe wear (Natarajan, *et al*, 2007, and Basavarajappa, *et al* 2006).

The wear rate increased with increasing applied load while it decreased with increasing volume fraction of the CSAp material. This may be due to the reason that

addition of ceramic content resulted in a pronounced drop in ductility accompanied by an increase in hardness which may further increase the wear resistance of the composites. At any load, wear rate decreases with increase in addition of CSAp and improves the load bearing properties of Al-Si-Fe alloy matrix during sliding. The addition of CSAp restricts the flow or deformation of the matrix material with respect to load. It is observed that, as the applied load increases, the wear rate also increases. This is because, whenever applied load increases, the friction at the contact surface of the material and rotating disc obviously increase.

4.9 THERMAL BEHAVIOUR

The thermal stability of metal composite plays a crucial role in determining the limit of their working temperature and the environmental conditions for their uses, which are related to their thermal decomposition temperature and decomposition rate. Figures 4.15 and 4.16 contain plots of the DTA/TGA decomposition data of the alloy and it composite at 15% by weight CSAp.

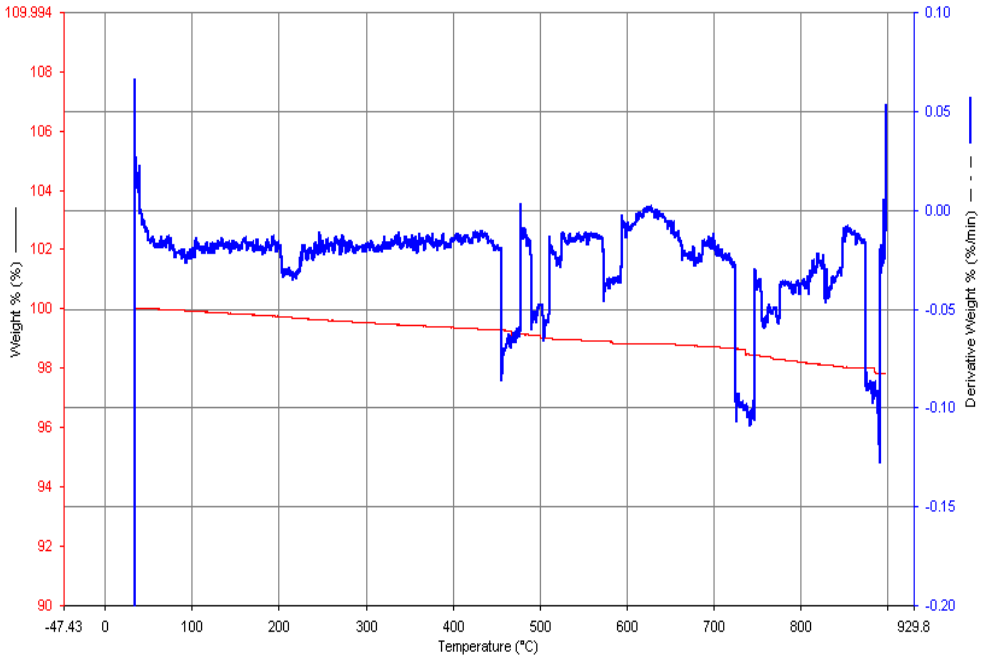


Figure 4.9: DTA/TGA of Al-Si-Fe alloy

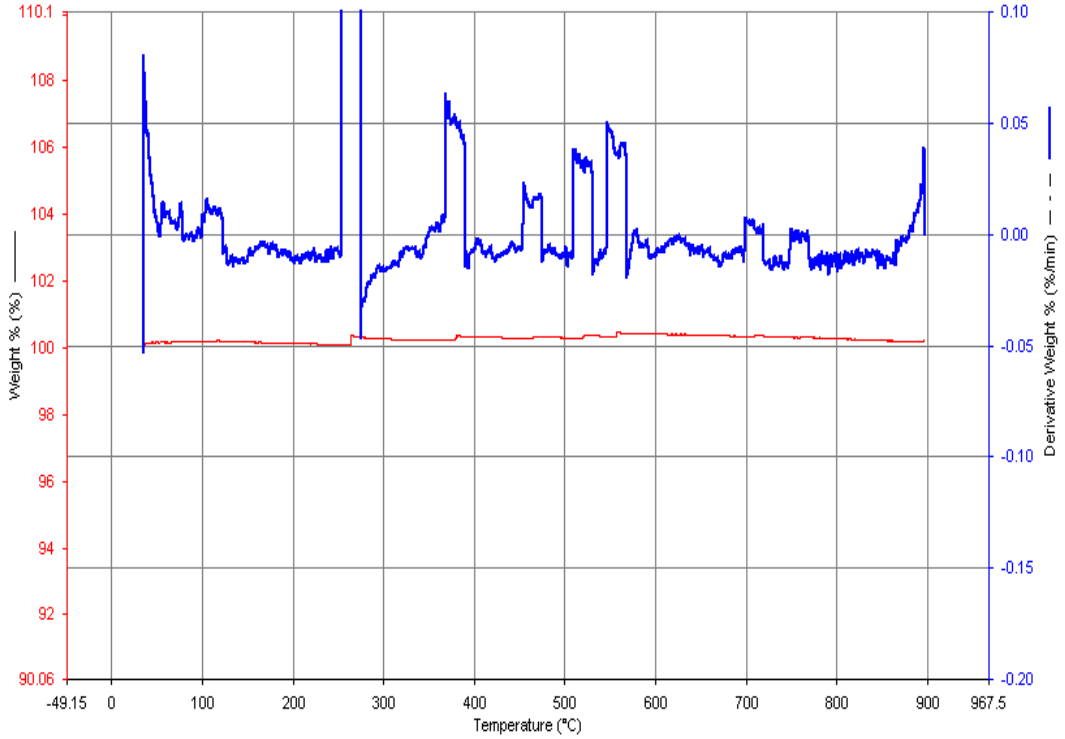


Figure 4.10: DTA/TGA of Al-Si-Fe alloy/15% by weight CSAP

The patterns of TGA curves for the composite are similar to those of the Al-Si-Fe alloy (compare Figure 4.9 with Figure 4.10) implying that the thermal decomposition of Al-Si-Fe/CSAp composites may mostly stem from Al-Si-Fe alloy. From the curves the temperature of maximal decomposition and destruction all fall between 700 – 800^{0}C.

The pronounced single endothermic effects observed in the DTA curves correspond to the oxidative degradation process and the release of violate matters. From the DTA curves, the temperature of maximal decomposition and destruction of the Al-Si-Fe alloy matrix and Al-Si-Fe alloy/CSAp composite fall between 700 to 800^{o}C (Figures 4.9 and 4.10).

The total burning and degradation of the residual Al-Si-Fe alloy took place at the temperature interval of 600-700^{0}C. In the last temperature interval the mass loss was minimal; this last step is due to the degradation of the CSAp material in the composite. The results indicate that the Al-Si-Fe alloy/CSAp composite biomass

show less percentage of decomposition. At temperatures above 700^{o}C, the residual weight stabilized and agrees with the silica and carbon content earlier reported in literature.

As shown in Figures 4.9 and 4.10, incorporation of the CSA particles into Al-Si-Fe alloy matrix increased the thermal decomposition temperatures and the residual yields of Al-Si-Fe alloy/CSAp composite. This result indicates that the presence of CSAp leads to the stabilization of Al-Si-Fe alloy and results in the enhancement of the thermal stability of Al-Si-Fe alloy/CSAp composite. In the Al-Si-Fe alloy/CSAp composite, the CSA particles act as physical barriers to prevent the transport of volatile decomposed products out of the composite during thermal decomposition.

4.10 CORROSION BEHAVIOUR

Figure 4.17 and Appendix Table A8 show the variation of corrosion rate with time for Al-Si-Fe alloy and its composites in neutral 3.5% by weight of salt solution.

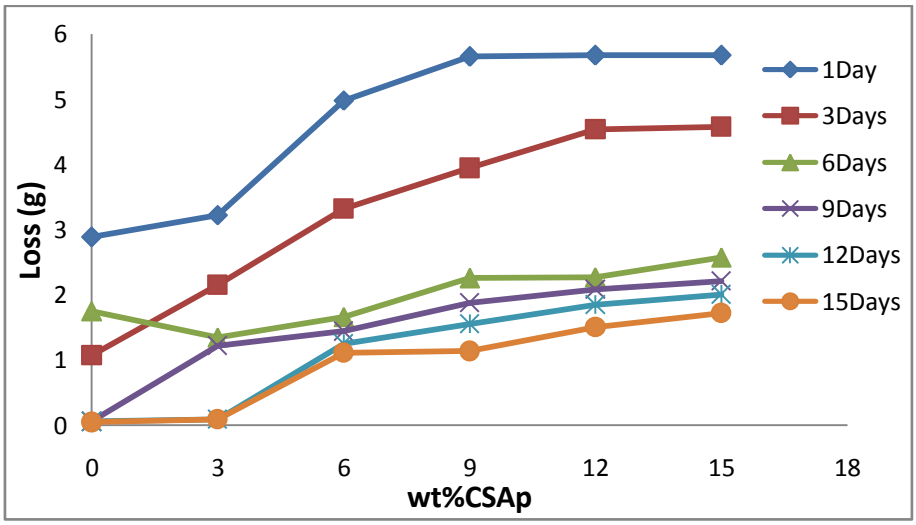


Fig. 4.11: Average corrosion rate Al-Si-Fe/Coconut shell ash (CSAp) composites immersed in 3.5%NaCI Solution.

The corrosion rate of the materials increased slightly as CSAp content increased, with the unreinforced alloy and Al-Si-Fe/15% by weight CSAp losing the least and greatest weights, respectively. It can be seen that the matrix alloy (Al-Si-Fe) and its composites showed similar corrosion behaviour. The corrosion rates of all the tested materials decreased rapidly during the first three days of exposure to the electrolyte but, with further exposure time, the decrease was very gradual.

Passivation of the matrix alloy is believed to be responsible for the monotonic decrease in corrosion rate with increasing exposure time observed in these materials. It is also seen that Al-Si-Fe/15% by weight CSAp showed the highest rate of corrosion. It was also observed that the corrosion of the composites was accompanied by the loosening of CSAp particles. It is believed that the corrosion of the CSAp-matrix interface caused the loosening of CSA particles which were finally dislodged from the specimen during the post-immersion cleaning process. Similar observations were made by Bienias *et al* (2003) who reported that fly ash particles acted as pit initiation sites in fly ash/Al-Si alloy composites and that there was a buildup of corroded fly ash particle debris in corrosion pits. The loss of such particles during post- immersion cleaning contributed to the high weight loss recorded for the composites in the present study.

Engineering materials used for construction and other applications for example automotive connecting rods experience different forms of interactions with different environments. The service life of such an engineering component such as the automotive connecting rod depends on its ability to resist degradation.

Studying the physical properties such as density and porosity of the developed composite therefore is significant because strength, stiffness as well as its low density

are properties that are well suited for weight-sensitive automotive and other industrial sectors.

Since corrosion decreases the load-bearing capacity of parts resulting in catastrophic failures, studying the corrosion properties of the MMC can limit the application of such components in corrosion environments especially in the presence of stresses (Zakari, 2014).

4.11 TESTS OF THE CONNECTING RODS PRODUCED.

The composite with coconut shell particles was used in the production of the connecting rods, using the double stir casting method, which was earlier used in the production of the specimen and selecting the best composition 6 – 9% by weight.

The tests carried out on the MMC connecting rods are:

Tensile and yield strength tests.

Hardness test

Impact energy test.

TABLE 4.5: Result of the Tensile Strength (N/mm^2)

Wt% CSAP	TS (N/mm^2)
0	159.84
3	160.23
6	186.05
9	200.77
12	196.77
15	196.05

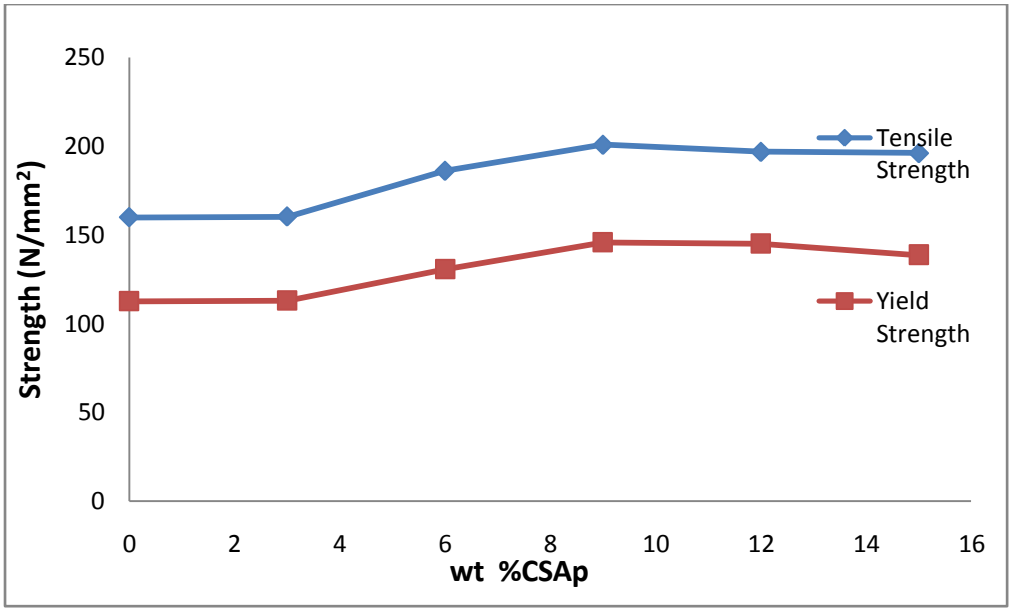


Fig. 4.12. Tensile strength and Yield strength test result.

TABLE 4.6: Result of the Yield Strength at 0.2% Upset

Wt% CSAP	YS (N/MM^2)
0	112.65
3	112.89
6	130.57
9	145.65
12	145.00
15	138.65

The results indicate that the yield and tensile strengths increased 28.38 and 24.86% at 12% by weight CSAp respectively. With increasing volume fraction, more loads are transferred to the reinforcement which also resulted in a higher tensile strength. This behavior is in agreement with the work carried out by Yung *et al* (2004).

TABLE 4.7: Hardness Test Results of the Composite Connecting Rods (Bhn)

wt%CSAp	1st reading	2nd reading	3rd reading	Average(BHN)
0	63.00	64.00	63.50	63.50
3	67.00	68.90	69.00	68.30
6	69.5	68.9	69.00	69.13
9	70.00	69.50	70.50	70.00
12	76.00	75.50	75.20	75.40
15	78.50	78.60	78.70	78.60

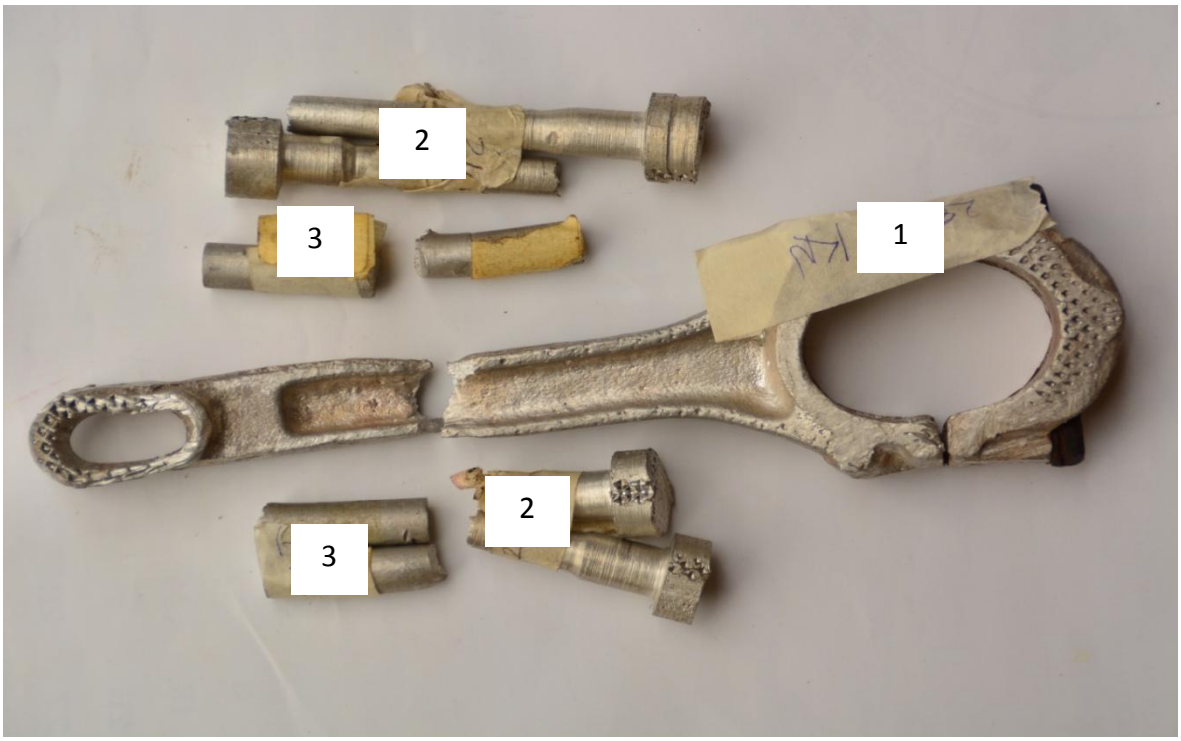


Plate 4.3. Profile of other test results.

1. Tensile test on connecting rod. Breaking load, (26.7 KN).
2. Tensile test on MMC specimen used on the connecting rod. (21.2 KN).
3. Impact e test on MMC specimen used on the connecting rod. 13.65 (J)

Table 4.8: Values of Impact energy test results conducted on composite connecting rods (JOUL)

Wt% CSAP	(J)
0	15.02
3	15.00
6	14.67
9	13.65
12	12.05
15	9.65

The result of the test shows that as the loading of CSAp increases, the ability of the composites to absorb impact energy is supposed to have decreased to a great level since there is a lower ratio of the matrix alloy to reinforcement particles. However the impact energy results obtained at 6-9% by weight CSAp (Fig. 4.12) are within the standard values for impact energy for connecting rod application as shown by the research of Rohatgi and Guo (1997).

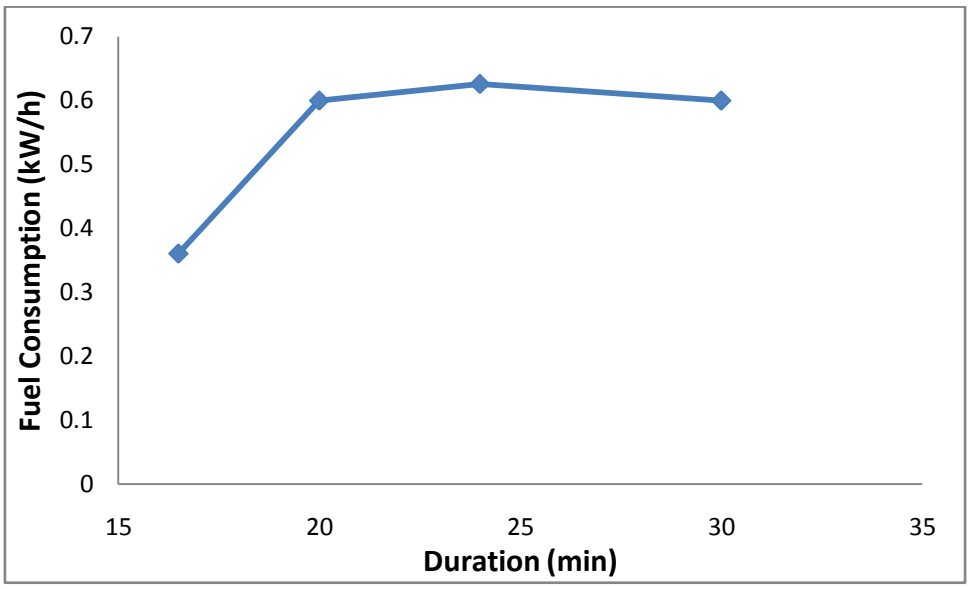


Figure 4.13: Regular connecting rod (Fuel consumption kW/h analysis)

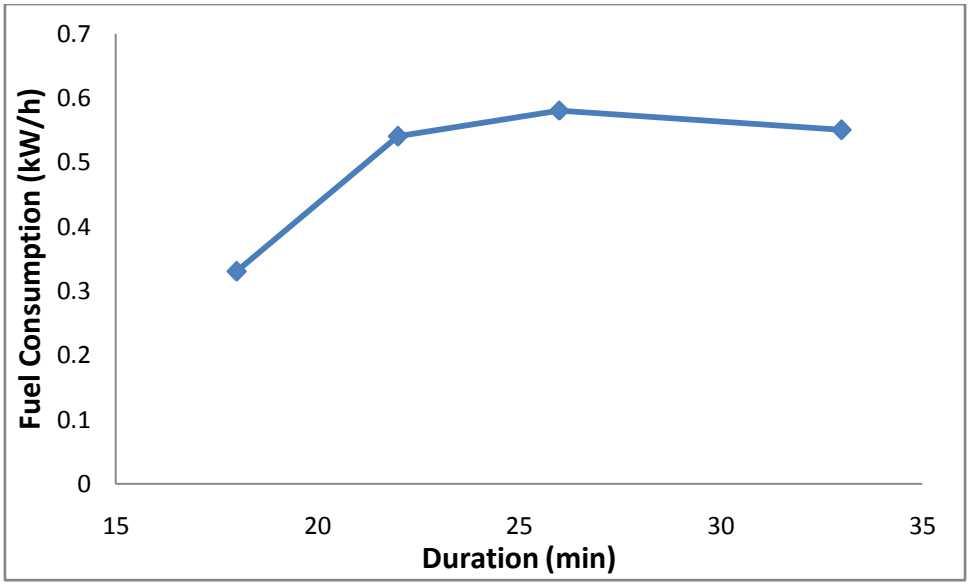


Figure 4.14: MMC Connecting Rod (Fuel Consumption/Kwh analysis)

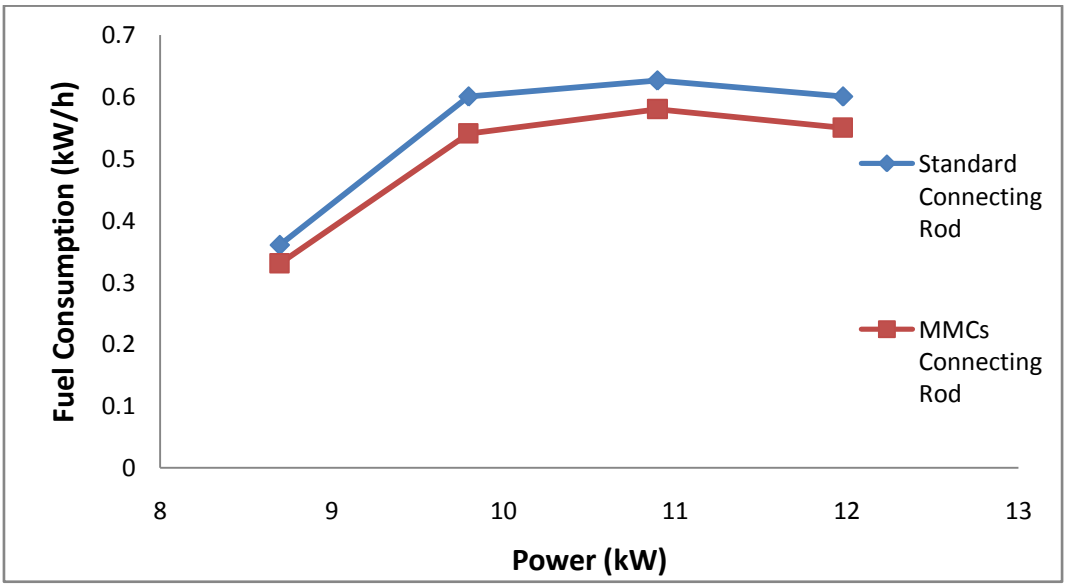


Figure 4.15: Variation of the Fuel Consumption/Kwh with Engine power

From the performance test analysis, it was observed that the duration of fuel consumption for both types of connecting rods are similar Fig.(3.15), e.g. for the regular connecting rod, the rate varied from 0.3 to 0.636kw/h, while that of the developed connecting rod, the rate varied from 0.33 to 0.58kw/h. The developed connecting rod consumed less fuel as the duration of running of the engine increases;

these results are in agreement with the work of Paek *et al*, (1987) and Ishida et al (1985).

Also from the brake force analysis it was observed that the developed composite had lower brake force than the regular connecting rod (Figure 3.16 and Table 3.4). But for both connecting rods as the speed increases the brake horse power also increased. These results are in line with those of elsewhere (Goenka and Oh, 1986).

If the regular connecting rod is replaced with a composite connecting rod it will give improved performance. From results of forces acting on the connecting rod and from comparison of steel and MMCs connecting rods made by Sala (2001), it is clear that stress induced in composite connecting rods is lower than that of the regular connecting rod. Hence the replacement of connecting rod material with MMC, will give improved strength, minimize weight and reduce induced stress in the structure. Fuel saving of 0.0034 liters/min used graduation cylinder and appendix II was achieved with composite connecting rods during performance tests of the connecting rod thereby increasing the strength to weight ratio.

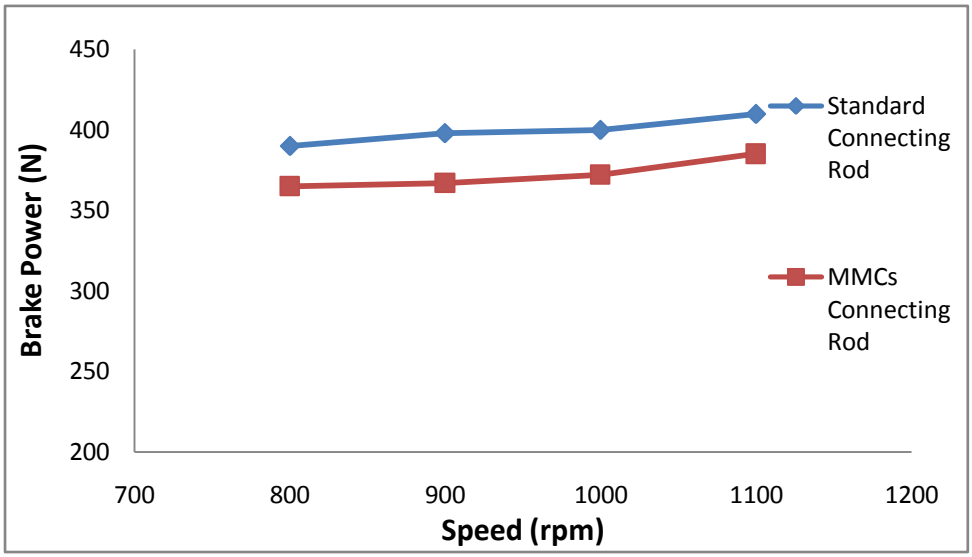


Figure 4.16: Variation of Brake force with Engine speed ratio,

Comments on the performance test results.

A sample of the MMC connecting rod was tested in a 12 valve Toyota automobile engine to determine their performance and effectiveness.

The performance tests showed that the engine fuel consumption when using the MMC connecting rods was lower than that of regular connecting rods, resulting in a 0.34% savings in fuel consumption, leading to lower running costs. From the brake force analysis, it was observed that the developed composite connecting rods had lower brake force than the regular connecting rods.

CHAPTER FIVE

CONCLUSIONS AND RECOMMEDATIONS

5.1 CONCLUSIONS

Aluminium matrix composite (AMC) reinforced with different volume fractions of coconut shell ash particles was fabricated by the double stir-casting method. The microstructures and properties of the composites were characterized and the following conclusions can be drawn:

i. Coconut shell ash particles were successfully incorporated in Al-Si-Fe alloy by using the stir casting technique.

ii. The microstructure analysis of the composites revealed the uniform distribution of the coconut shell ash particles in the matrix. The increase in reinforcement volume fraction resulted in decrease of matrix grain size in the composites.

iii. The addition of coconut shell ash particles reinforcement to Al-Si-Fe alloy increased the tensile strength and the hardness value of composites, but slightly reduced the impact energy.

iv. The increase in strength and hardness was as a result of the increases in the amount of the hard coconut shell ash phase in the ductile metal phase, which led to increase in dislocation density at the matrix-particle inter phase.

v. Fracture mode of composites is particle cracking and matrix ductile tearing.

vi. It is observed that, as the applied load increases, the wear rate also increases. This is because, whenever applied load increases, the friction at the contact surface of the material and rotating disc obviously increases.

vii. The coefficient of friction increases with increasing load for the Al-Si-Fe composite and the composites containing CSAp.

viii. The Al-Si-Fe alloy/CSAp composite, the CSA particles act as physical barriers which prevent the transport of volatile decomposed products out of the composite during thermal decomposition.

ix. The corrosion rate of the composites increased slightly with increasing CSAp, but decreased with exposure time.

x. Incorporation of coconut shell ash particles in aluminium matrix can lead to the production of low cost aluminium composites with improved hardness and strength. These composites can find applications in automotive components where light weight materials are required, with good stiffness and strength that can lead to connecting rod production and testing.

xi. For optimum service performance of this alloy, coconut shell addition should be between 6-9% by weight and not exceed 9% in order to develop better necessary properties. These composites can be used in the production of connecting rods since aluminium composites used in production of these components have similar properties as those of Al-Si-Fe/CSAp composites.

xii. The produced MMCs connecting rod was tested in a 12 valve Toyota automobile engine. The result obtained showed a 3.6% fuel consumption/minute as against 3.26% fuel consumption/min of the same quantity of fuel in the engine of a regular connecting rod, and the MMCs connecting rod respectively, which translates to savings in running costs.

xiii. From the results obtained from MMC connecting rod, as shown in Tables 2.1 and 3.4, and Figures 4.20 and 4.21 respectively, it is clear that the stress induced in the MMCs composite connecting rod is found to be lower than that of the regular connecting rod. Hence, replacement of connecting rod material with the MMC will give good strength, reduced weight and induced stress in

the structure. A fuel saving of 0.34% was achieved, leading to lower running costs.

5.2 RECOMMENDATIONS FOR FURTHER STUDIES

The current study has provided some important information about the development and characterization of the microstructure and properties of Al-Si-Fe alloy, and its composite containing different weight fractions of CSA particles. In the course of the investigation, new areas of research have been identified.

i. Mechanical properties such as fatigue and creep test should be carried out on the material.
ii. The age-hardening behaviour of the developed composite should be investigated.
iii. It is recommended that further matrix-particle interface be investigated, using high-resolution transmission electron microscope
iv. Finally, the National Automotive Council is hereby called upon to support further development of this novel material into commercial preposition.

REFERENCES

Altinkok, N. and C. Aslan (2012). The Tensile Behaviour and Microstructure of Al_2O_3/SiCp Reinforced Aluminium Based MMCs produced by the stir casting method. *International Journal of Science and Advanced Technology* (ISSN2221-8386) Vol. 2 No. 5 pp.221 – 8386.

American Society for Testing and Materials (ASTM) (2000) ASTM D 638-99-2000 and 790-99-2000. ASTM Committee on Standards.

Aigbodion, V.S., and Hassan, S.B. (2007). Effects of Silicon Carbide Reinforcement on Microstructure and Properties of Cast AI - Si - Fe /SiC Particulate Composites. *Journal of Materials Science and Engineering* A 447. (ELSEVIER) pp. 355-370.

Aigbodion, V. S., and Hassan, S. B. (2010). Experimental Correlations between Wear Rate and Wear Particulate1e of AI-Cu-Mg/Bagasse Ash Particulate Composite. *Journal of Materials and Design*. 31. (ELSEIER) pp. 2177-2180.

Aigbodion,V.S. (2007). Particulate-strengthened of AI-Si Alloy/alumino Silicate Composite. *Materials Science and Engineering* A 460-461 pp. 574-578.

Aigbodion V .S. and Hassan, S.B. (2009).Effect of Thermal Ageing Characteristics of Al-Si-Fe/Sic Particulate Composite Synthesized by Double Stir Casting. *Journal of Engineering Research*. Vol.7. pp.53-61.

Annual Books of ASTM Standards (1990). Section I. Iron and Steel Products. Vol. 261 01.04: pp.13-63.

Aylor, D. M., and Moran, P. J. (1985). Effect of Reinforcement on the Pitting Behaviour of Aluminium-Base Metal Matrix Composites. *Journal of the Electrochemical Society*, Vol. 321, No. 6.pp.1277-1281.

Asthana, R. (1998). Solidification Processing of Reinforced Metals. (*Trans. Tech Publication*). Pp. 67-80.

Bamgboye, A. Isaac., and Jekayinfa, S. O. (2006). Energy Consumption Pattern in Coconut Processing Operations. Agricultural Engineering International: The CIGR Journal *Manuscript* EE 05 013. Vol. VIII.

Banerji, A. Prasad, S.Y., Surappa, M.K., and Rohatgi, P.K. (1982). Abrasive Wears of Cast Aluminium Alloy-zircon Particle Composites Wear 82 pp.141-151.

Basavarajappa, S. and Chandrsekar, A. (2006). Dry Sliding Wear Behavior of Al2219/SiC Metal Matrix Composites. *Materials Science* Poland 24, No2/1 pp.357-366.

Basavarajappa ,S. Mukund, K. K., Ashwin, M., and Prabu, M. (2006).Dry Sliding Wear Behavior of Al2219/Sic Hybrid Metal Matrix Composites. *Journal of Materials Engineering and Performance* Vol.15, Issue.6.pp.668-674.

Bienia, J., Walczak, M., Surowska, B., and Sobezaka,J.(2003). Microstructure and Corrosion Behaviour of Aluminium Fly Ash composites. *Journal of Optoelectronics and Advanced Material.* Vol. 5. No.2.pp.93-502.

Bienia, J., Walczak, M., Surowska, B., and Sobezaka,J.(2003). Mechanical Properties and Corrosion Behaviour of Fly ash Particles Reinforced AA2024 Composites. *Journal of Composite Materials* (2012). 46 Source: 2012 *Journal Citations Reports*.pp.1393-1404.

Butler, R.A. (2006). Why is Coconut Replacing Tropical Rainforests? Why are Biofuels fueling Deforestation? http://news.mongabay.com/2006/0425-ai) palm.html (Retrieved 18 Feb 2007).

Candan, S. and Bilgi, E. (2004). Corrosion Behaviour of Al-60 Vol. % SiC Composites in NaCl Solution. *Materials Letters*, Vol. 58, pp.2787- 2790.

Canakci, A., Varol, T., and Ozsahin, S. (2012). Prediction of Effect of Volume Fraction Compact Pressure and Milling Time on Properties of Al-Al_2O_3 MMCs using Neural Networks. Metals and Materials. *International (Springer Link)* Vol. 19 Issue 3. Pp,519-526.

Clyne, T. W (ed.). (2000). Comprehensive Composite Materials Vol. 3. Metal Matrix Composites (ser. eds) Pp. 26-38.

Champion, R. C., and Arnold, E.C. (1978. Motor Vehicle Calculation and Science. Edward Arnold (Publishers) Ltd. London pp.187-197.

Clyne, T.W. (2001). Metal Matrix Composites. Matrices and Processing an *Encyclopedia of Materials Science and Technology* (ed.): A Mortensen (Elsevier) pp. 1-20.

Das, S.V., Prasad, S.V., and Ramachandran, T.R. (1989). *Microstructure and Wear of Cast (Al-Si) - Graphite Composite*, Wear. Vol. 133, No. 1, pp. 173-185.

Demidov, V., and Kolchin, A. (1984).Design of Automotive Engines. Hamburg: Mir Publishers pp.579.

Devaraju A., and Kamar, (2011). Dry Sliding and Static Immersion Corrosion Resistance of Aluminium Alloy 6061-T6/SiCp Metal Matrix Composite Prepared Via Friction Processing. *International Journal of Applied Research in Mechanical Engineering.* (IJARME) ISSN: Vol. 1 issue 2 pp.2231 – 5950.

Dolan, A.J. (1980). Motor Vehicle Technology and Practical Work. London. Heiman Educational Books Ltd. pp. 655-657.

Donne, S., Krishnadey, M.R., and Bouchard, R. (1990). Metal and Ceramic Matrix Mechanical Behavior. *The Minerals, Metals, and Materials Society.* Pp. 243-25I.

Ejiofor, J.U., and Reddy, R.G. (1997). Developments in the Processing and Properties of Particulate Al-Si Composites. *JOM Publication of Minerals, Metals and Materials Society*. 49(11).pp. 31-37.

Guo, R.Q., Rohatgi, P.K., and Nath,D. (1996a). Compacting Characteristics of Aluminium-Fly Ash Powder Mixtures. *Journal of Materials Science*, Vol. 31. Pp.821-1024.

Guo, R.Q., Rohatgi, P.K., and Ray, S. (1996b). Casting Characteristics of Aluminium Alloy. Fly Ash Composites, *Transactions of The American Foundrymen's Society*, Vol. 104 pp. 1097-1102.

García-Cordovilla.C., Narciso, J., and Louis, E. (1996). Abrasive Wear Resistance of Aluminum Alloy/Ceramic Particulate Composites, *pp*. 192.

Giri, N.K. (2010). Automobile Technology, First Edition. Delhi: Hanna Publishers, pp. 137-139.

Harun, M.B., Shamsudin, S. R., Yazid, H., Salamatu .Z., Sattar, .M. S., and Jalil, M. (2006). Effect of Fly Ash Particulate Reinforcement, Porosity and Hardness in Al-(Si-Mg) Cast Composites. Selangor Malaysia. *AJSTD* Vol. 23 Issues 1and 2.pp.113-122.

Hillier, W.A., and Pittuck, F. (1982).Fundamentals of Motor Vehicle Technology Third Edition. London: Anchor Press Ltd pp.31-32.

Ikechukwuka, N., and A, Oguocha .(1997). *Characterization of Aluminium Alloy 261 X and its Composites containing Alumina Particles*. (Unpublished PhD thesis). Department of Mechanical Engineering. University of Saskatoon. Pp. 1-2000.

Itskos, G., Rohatgi, P. K., Moutsatsou, A., Roven, H. J.,Schultz, B. F., Koukouzas,N., and Vasilatos,C.(2011). Incorporation of High Ca Fly Ash Particles into A356Al by Stir Casting Technique and Characterization of the Fabricated Composites. World of CoalAsh(WOCA) Conference,in Denver Co, USA.

Jasim, (2001). The Production of Cast Metal Composite by Modified Stir Casting Method. *Journal Technolog.* 35(A). Pp. 9-20.

Jayaseelan, V., Kalaichelvan, K., Kannan, M., and Vijay, Ananth.S. (2010). Extrusion Characterizes of Al/Sic by Different Manufacturing Process. *Internal Journal of Applied Engineering Research*. Vol.1, No.2.pp.503-585.

Jayalakshmi, S., Seshan, S., Kailas, .S.V., and Srivatsan, S. (2004). Influence Processing and Reinforcement on Microstructure and Impact Behaviour of Magnesium Alloy. AM100 S-adhan-a Vol. 29. Part 5. October 2004. ©Printed in India Pp. 509-523.

Jayaseelan, V., Kalaichelvan, K., Kannan, M. Vijay., and Ananth, .S. (2010). Extrusion Characterizes of Al/Sic by Different Manufacturing Process. *Internal Journal of Applied Engineering Research*. Vol.1, No.2.pp.560-522.

Jit, Nrip., Tyagi, A.K., Singh, Nirmal., and Singh, Amarpal. (2011). Comparison of Porosity and Density for (A384.1)1-x [(Reinforcement)p] x MMC. *Advances in Applied Science Research* 2 (4) pp.240-250.

Jokinen, A., and Rauta, V. (1992). Manufacturing and Properties of Aluminium Alloy Matrix Composites. Final Report. Espoo: *Technical Research Centre of Finland*. Metallurgy Laboratory. Pp. 23.

Kainer, K.U. (2003). Metal Matrix Composites Custome Made Materials for Automotive and Aerospace Engineering Wily-VCH Verlag Gmbh & Co, KGaA Weinheim, Pp. 203-209.

Keneth, K., A, Moyosore T.A., and Olubambi, A.P. (2014). Corrosion and Wear Behaviour of Al-Mg-Si Alloy Matrix hybrid Composites Reinforced with rice husk ash and Silicon Carbide. *Journal of Materials Research and Technology* Vol. 03 No.1 pp.9-16.

Kiourtsidis, S., and Skolianos, S. M. (1998). Corrosion Behaviour of Squeeze-Cast Silicon Carbide-2024 Composites in Aerated 3.5 wt. % Sodium Chloride. Materials Science and Engineering. Vol. A 248, 1998, pp. 165-172.

Korkut, M.H. (2004). Effect of Particulate Reinforcement on Wear Behavior of Aluminium Matrix Composites. *Materials Science and Technology* Vol. 20, PP. 73-81.

Khurmi, R.S., and Gupta, J.K. (2010). A Textbook of Machine Design" India: Rajendra Ravindra Printers Pvt. Ltd. Pp.614-621.

Kumar, G.B.Va., Swamy, A.R.K. bc., and Ramesha Ad. (2012). Studies on properties of as-cast Al6061-WC-Gr hybrid MMCs. *Journal of Composite Materials.* Vol. 46 No.17 pp. 211-2122.

Lloyd, D.J. (1999). Particle Reinforced Aluminium and Magnesium Matrix Composites. *Int. Material* Pp. 39:1-23.

Lokesh, G. N, Ramachandra; M, Mahandra. K.V. and Sreenith, T. (2013). Effect of Hardness, Tensile and Bear Behaviour of Al 4.5wt% CU Alloy/fly ash/SiC Metal Matrix Composites. *International Journal of Modern Engineering Research* (IJMER) Vol.3 (sse) pp.381-385.

Mahamoud, T.S. (2008). Tribological Behavior of A390/Grp Metal-Matrix Composites Fabricated Using A Combination of Rheocasting And Squeeze Casting Techniques. *Journal of Mechanical Engineering Science*. 222(2).

Mahmoud, T. S, El-Kady, Y.E., and Al-Shihiri, M.S. (2012). Corrosion Behaviour of Al/SiC and Al/Al_2O_3 Nano Composites. *Materials Research* 15(6) vol.10 pp.903-910.

Maruyama, B. (1998). Progress and Promise in Aluminium Metal Matrix Composites. The AMPTIAC Newsletter Pp. 23.

Mohan, S., Prakash, V., and Pathak, .J. (2002). Wear Characteristics of HSLA-steel Wear 252.

Mohan, S., and Srivastava .(2006).Surface Behavior as-Cast Al-Fe Intermetallic Composite. Tribology Letters, Vol.22, N0.1.

Mubeen A. (2007), Machine Design (W.S.I UNITS Pp 119 - 620)

Nath, D., and Namboodhiri, T .K .G. (1989). Some Corrosion Characteristics of Aluminium-Mica Particulate Composites. *Corrosion Science* Vol. 29, No. 10.

Naresh, P. (2006). Development and Characterization of Metal Matrix Composite using Red Mud, an Industrial Waste for Wear Resistant Applications. (Ph.D Thesis) Department of Mechanical Engineering, National Institute of Technology Rourkcla -769 008 (India) January, 006 Pp. 23-34.

Natarajan,N., Vijayarangan,S., Rajendran, .I. (2007). Fabrication, Testing and Thermal Analysis of Metal Matrix Composite Brake Drum. *International Journal of Vehicle Design.* Vol.44, pp.3-4.

Prasad, D., and Krishna, A. (2010). Fabrication and Characterization of A356.2-Rice Husk Ash Composite using Stir Casting Technique. *International Journal of Science Engineering and Technology* vol. 2(12).pp.7603-7608.

Prakash, U., Raghan, T., Kamat, S.V., and Gokhale, A. (1998). The Effect of Mg-addition on Microstructure and Tensile and Stress Rupture Properties of a P/M Al-Fe-Ce Alloy. Scripta Met 39.

Prasad, S.V., and Asthana, R. (2004).Aluminium-Metal Matrix Composites for Automotive Applications Tribological Consideration. *Tribology*. Vol.17, N03, pp. 445-453.

Prasertsan, S., and Sajjakulnukit, B. (2006). Biomass and Biogas Energy in Thailand. Potential Opportunity and Barriers. In Renewable Energy. Pp. 599-610.

Rajput, R .K. (2008). Automobile Engineering Maintenance and Troubleshooting of Automobile. Laxmi Publications (P) Ltd. Pp. 697-701.

Rittnes, M. *et al Matrix Composites* in the 21st Century, Market and opportunities. BCC Inc. Norwalk CT.

Rohatgi, P.K., F.M. Yarandi., and Y. Liu. (1988). Proc. of Inter. Symposium on Advances in Cast Reinforced rv1ctal Composites. (S.G. Fishman and A.K. Dhingra. eds.). Materials Park. 01-1: *ASM International Publication:* PP. 249.

Rohatgi, P.K. (1994). Low-Cost, Fly Ash Containing Aluminium Matrix Composites. *JOM,* Vol. 29, pp. 55-59.

Rohatgi, P.K., and Guo, R.Q. (1997). Low Cost Cast Aluminium – Fly Ash Composites for Ultralight Automotive Application. *TMS Annual Meeting, Automotive Alloys*, pp. 157-168.

Rohatgi, .P.K., Guo, .R.Q., and Keshavaram, B.N. (1995). Cast Aluminium Alloy – Fly Ash Composites. *Key Engineering Materials*. Vols. 104-107, pp.283-292.

Rohatgi, P.K., Guo, R.Q., Iksan, H., Borchelt,E.J.. and Asthana,R. (1998). Pressure Infiltration Technique for Synthesis of Aluminium-Fly Ash Particulate Composite. *Metallurgical and Materials Transaction A*, Vol. A244, pp. 22-30.

Sahin, Y. (2003). Wear Behavior of Aluminium Alloy and its Composites, Reinforced by SiC Particles using Statistical Analysis. *Journal of Material Design* Vol.24, pp. 95-103.

Schveier, L. (1999), Tension and compression in connecting RODS> A FAILURE Analysis Peterson Publishing company London pp 1-12

Siva, P.D. and Rama, K.A. (2011). Production and Mechanical Properties of A356.2/RHA Composites. *International Journal of Advanced Science and Technology* Vol. 33, pp. 51-58.

Skibo, M., Morris, P .L. and Lloyd, 0. (1988). Cast Reinforced Composites S.G Fishman and A.K Dhirngra (eds) *ASM International* Pp. 257-261.

Surappa, M. K., and Rohatgi, P. K. (1981). Preparation and Properties of Aluminium Alloy Ceramic Particle Composites. *Journal of Material Science*. Vol. 16 Pp. 983-993.

Wahab, M.N., Daud, A.R., and Ghazali, M.J. (2009). Preparation and Characterization of Stir-Cast Aluminium Nitride Reinforced Aluminium Metal Matrix Composites. *(JME)* vol.4 N0.2.pp.115-117.

Whitehouse, A. F., Shahani, R .A. and Clync, T. W. (1991). Metal Matrix Composites Processing, Microstructure and Properties. 12 *RisO Int. Symp*. Roskilde. N. Hansen et al., eds, Rise National Laboratory, Denmark, Pp. 74 1-748.

Yung, C.K., and Chan, S.L.I. (2004). Tensile Properties of Nanometric Al_2O_3 Particulate Reinforced Aluminium Matrix Composites. *Journal of Materials Chemistry and Physics*, 85, pp.438443.

Zakariya, H.M. (2013). Microstructural and Corrosion Behaviour of Al/SiC Metal Matrix Composites. *Ain Shams Engineering Journal*. Pp.709-718

Zhou, W., and Xu, Z.M. (1997). Casting of SiC Reinforced Metal Matrix. *Journal of Materials Processing Technology* 63: Pp. 358-363.

APPENDIX I

DETAILS OF INTERNATIONAL JOURNAL PUBLISHED

1. S.Y. Aku, D.S. Yawas and A. Apasi:

   Gazi University of Science GUJSci 26(3): 449 – 457 (2013): Evaluation of Al-Si-Fe alloy/coconut shell Ash Particulate composite. (University Journal of Science – Ankara, Turkey (2011)

2. P.B Madakson , D.S. Yawas and A. Apasi

   Characterization of Coconut Shell Ash for Potential Utilization in metal matrix composite for automotive application. International Journal of Engineering Science and Technology (IJEST Banari – Amman, Jordan (2012)

3. A. Apasi, P.B. Madakson, D.S. Yawas, V.S. Aigbodion

   Wear Behaviour of Al – Si – Fe/Coconut Shell Ash Particulate Composites Faculty of Engineering (Journal of Serbian Tribology Society – Kra - Serbian (2012)

4. A. Apasi, A.I. Obi and S.Y. Aku

   Effect of Coconut Shell Ash on the Corrosion Behaviour of Al – Si-Fe/ Coconut Shell Ask Particulate Composites. (2013). Usak University Journal of Material Science.

APPENDIX II

Table A1: The density of the composites

wt%CSAp	Mass(g)	Volume(cm^3)	Density(g/cm^3)
0	5.50	1.93	2.85
3	6.00	2.12	2.83
6	5.00	1.82	2.75
9	5.58	2.07	2.70
12	6.20	2.31	2.68
15	5.89	2.21	2.66

Table A2: Hardness results of the composites

wt%CSAp	1^{st} reading	2^{nd} reading	3^{rd} reading	Average(BHN)
0	63.00	64.00	63.50	63.50
3	67.00	68.90	69.00	68.30
6	69.5	68.9	69.00	69.13
9	70.00	69.50	70.50	70.00
12	76.00	75.50	75.20	75.40
15	78.50	78.60	78.70	78.60

Table A3: Result of the tensile properties

TENSILE STRENGTH

Wt% C SAP	TS (N/MM^2)
0	159.84
3	160.23
6	186.05
9	200.77
12	196.77
15	196.05

Table A4: Result of the yield strength.

YIELD STRENGTH AT 0.2% UPSET

Wt% CSAP	YS (N/MM^2)
0	112.65
3	112.89
6	130.57
9	145.65
12	145.00
15	138.65

Table A5: Result of the Impact Energy

IMPACT ENERGY (J)

Wt% CSAP	(J)
0	15.02
3	15.00
6	14.67
9	13.65
12	12.05
15	9.65

Table A6: Results of Wear rate of the composites

Wt%CSAp	10N	20N	30N	40N	50N
0	3.4	3.5	4.8	5.8	7.3
3	3.4	3.4	4.0	5.0	6.8
6	2.8	3.0	4.0	4.5	6.0
9	2.2	2.56	3.5	4.0	5.4
12	1.8	2.0	3.0	3.2	5.0
15	1.2	1.78	2.8	3.0	4.8

Table A7: Results of Coefficient of friction of the composites

Wt%CSAp	10N	20N	30N	40N	50N
0	0.2	0.25	0.45	0.55	0.58
3	0.23	0.35	0.50	0.65	0.67
6	0.23	0.39	0.54	0.65	0.68
9	0.30	0.395	0.58	0.67	0.73
12	0.33	0.40	0.60	0.69	0.78
15	0.38	0.43	0.60	0.72	0.80

Table A8 - Average values for weight loss (mg) of the composite immersed in 3.5% by weight NaCl solution

Wt % CSAp	1Day	3Days	6Days	9Days	12Days	15Days
0 wt%CASP	2.8816	1.0673	1.7464	0.0534	0.0534	0.0427
3 wt%CASP	3.2244	2.1496	1.3435	1.2181	0.0914	0.086
6 wt%CASP	4.9773	3.3182	1.659	1.4379	1.2443	1.1061
9 wt%CASP	5.6512	3.9429	2.2531	1.8776	1.549	1.13293
12 wt%CASP	5.6713	4.5398	2.27	2.0807	1.8443	1.4981
15 wt%CASP	5.6714	4.5739	2.5728	2.2107	2.001	1.7152

Table A9: Comparison of existing forged steel connecting rod and Metal matrix connecting rod.

Connecting rod	Weight (kg)	Bore (mm)		Length (mm)	Operating temperature (OC)
		Big End	Small End		
Existing forged steel	5	48.12	21.00	22.26	1230
Metal matrix composite	1	47.34	20.40	26.68	929.8

Table: A10 (a) Performance test (Standard connecting rod)

S/No	Description	Time		Duration (min)	Ambient temp (^{O}C)	Fuel consumption duration (lit/min)	Average voltage	% fuel consumption/ min	Average idle speed (rpm)
		Initial	Final						
1.	100ml (0.1litre) of petrol	10.15am	10.31am	16.5	31^{0}C	0.1/16.5= 0.006	13.8	.6	800
2.	200ml (0.2litre) of petrol	10.30am	10.45am	20	31^{0}C	0.2/20 = 0.010	13.8	1	900
3.	250ml (0.25litre) of petrol	10.55am	11.20am	24	31.5^{0}C	0.25/24 = 0.010	13.8	1	1000
4.	300ml (0.3litre) of petrol	10.45am	11.15am	30	32^{0}C	0.3/30 = 0.010	13.8	1	1100
								3.6	

Table: A.10 (b) Performance test (MMCs connecting rod).

S/No	Description	Time		Duration (min)	Ambient temp (^{O}C)	Fuel consumption duration (lit/min)	Average voltage	% fuel consumption/ min	Average idle speed (rpm)
		In0020itial	Final						
1.	100ml (0.1litre) of petrol	10.20am	10.38am	18	31^{0}C	0.1/18= 0.006	13.8	.5	800
2.	200ml (0.2litre) of petrol	10.55am	10.17am	22	31^{0}C	0.2/22 = 0.010	13.8	.9	900
3.	250ml (0.25litre) of petrol	11.05am	11.21am	26	31.5^{0}C	0.25/26 = 0.010	13.8	.96	1000
4.	300ml (0.3litre) of petrol	10.25am	11.58am	33	32^{0}C	0.3/33 = 0.010	13.8	0.9	1100
								3.26	

Table A.11a Experimental results (Regular connecting rod)

Speed (rpm)	Brake load F (N)	Pb (kW)	Fuel consumption (min)	Fuel (kW/h)
800	390	8.7	0.006	0.36
900	398	9.8	0.01	0.6
1000	400	10.9	0.010	0.626
1100	410	11.98	0.010	0.6

Table A. 11 Experimental results (MMCs connecting rod)

Speed (rpm)	Brake load F (N)	Pb (kW)	Fuel consumption (min)	Fuel (kW/h)
800	365	8.7	0.005	0.33
900	367	9.8	0.009	0.54
1000	372	10.9	0.010	0.58
1100	385	11.98	0.009	0.55

APPENDIX III

Regular connecting rod (Fuel consumption kw/h analysis)

$$= \frac{volume\ of\ \ fuel\ in\ litres\ x\ 60\ x\ 60}{Time\ taken\ to\ consume\ \ fuel\ (s)\ x\ kw}$$

$$= \frac{0.1\ x\ 60\ x\ 60}{16.5\ x\ 60} = 0.36$$

$$= = 0.6 \text{ (Giri 2010, Arnold E.C \& Champion RC 1978) } \frac{0.2\ x\ 60\ x\ 60}{20\ x\ 60}$$

$$= \frac{25\ x\ 60\ x\ 60}{24\ x\ 60} = 0.626$$

$$= \frac{0.3\ x\ 60\ x\ 60}{30\ x\ 60} = 0.6$$

MMCs Connecting Rod (Fuel Consumption/Kwh analysis)

$$= \frac{volume\ of\ \ fuel\ in\ litres\ x\ 60\ x\ 60}{Time\ taken\ to\ consume\ \ fuel\ (s)\ x\ kw}$$

$$= \frac{0.1\ x\ 60\ x\ 60}{18\ x\ 60} = 0.33$$

$$= \frac{0.2\ x\ 60\ x\ 60}{22\ x\ 60} = 0.54$$

$$= \frac{0.250\ x\ 60\ x\ 60}{26\ x\ 60} = 0.58$$

$$= \frac{0.250\ x\ 60\ x\ 60}{33\ x\ 60} = 0.55$$

APPENDIX IV

EXPERIMENTAL CALCULATIONS

Torque T = FL

Where F = Brake load/balance readings, N

L = Torque arm length, m

Brake power P = T x Angle (rad)

= T x 2π x N/sec

T = 104Nm

$P_b = 104 \; x \; 2\pi X \; \frac{800}{60}$ = 9.7kw

$P_b = 104 \; x \; 2\pi X \; \frac{900}{60}$ = 9.8kw

$P_b = 104 \; x \; 2\pi X \; \frac{1000}{60}$ = 10.9kw

$P_b = 104 \; x \; 2\pi X \; \frac{1100}{60}$ = 11.98kw

$P_b = 104 \; x \; 2\pi X \; \frac{800}{60}$ = 9.7kw

$P_b = 104 \; x \; 2\pi X \; \frac{900}{60}$ = 9.8kw

$P_b = 104 \; x \; 2\pi X \; \frac{1000}{60}$ = 10.9kw

$P_b = 104 \; x \; 2\pi X \; \frac{1100}{60}$ = 11.98kw

Table A 12- Basic constructional parameters of the (Small end) of the connecting rod.

Description	Ratio	Petrol engine	Diesel engines
Piston pin diameter dp		16mm	
Small end inside Diameter $id_{se:}$ without bushing			
		$Id_{se} \approx$ dp	$Id_{se} \approx$ dp
With bushing id_{se} (b) Small end outside Diameter OD_{se}	$Id_{se}(b)/dp$ Od_{se}/dp	0.95 – 1.03 1.15 – 1.90	0.95 – 1.03 1.20 – 1.95
Length of small end L_{se}	$L_{se}/L_{sec}(max)$	0.66 – 1.07	0.66 – 1.07
Radial thickness of end wall rt_{ew}	Rt_{ew}/dp	0.19 – 0.30	0.19 – 0.30

Table A 13- Basic constructional parameters of the (Big end) of the connecting rod.

Description	Ratio	Variation limits
Crank pin diameter dep	$D_{cp}/L_{sec}(max)$	0.99-1.02
Shell wall thickness t_{sh}: Thin- walled	T_{alt}/dcp	0.10 – 0.17
Thick- walled	t_{sh}/ dcp	0.35
Length of big end L_{be}	L_{be}/dcp	0.82 – 0.99
Distance between connecting rod bolts D_{eb}	D_{cb}/dcp	1.25 – 1.45

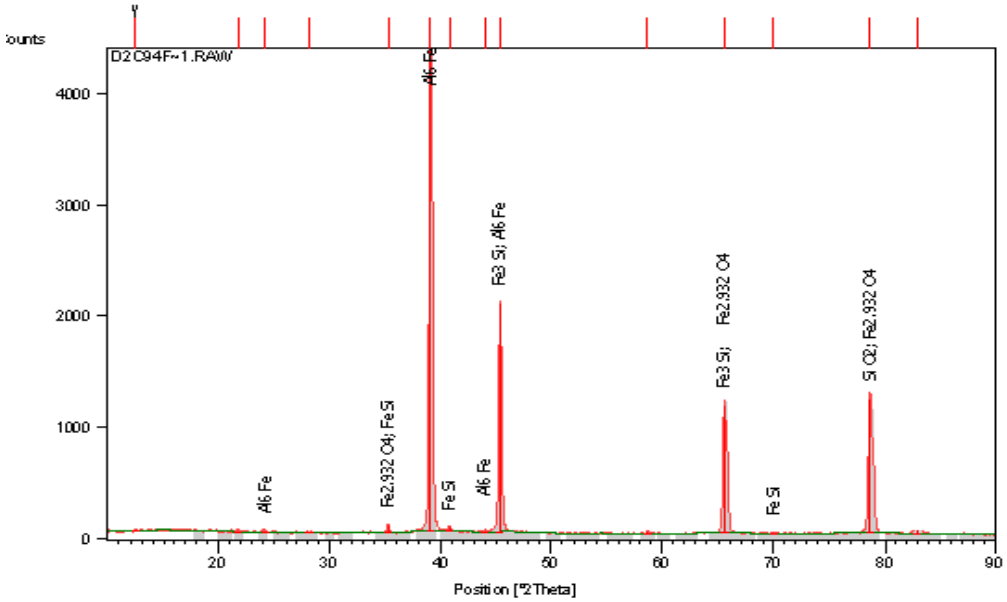
Table A 14 Basic constructional parameters (rod shank) of the connecting rod.

Dimension of section	**Ratio**	**Petrol engine**	**Diesel engine**
L_{sec}	L_{sec}/OD_{se}	0.62 – 1.07	0.62 – 1.07
L_{sec} (max)	L_{sec} (max/L_{sec}	1.01 – 2.03	1.01 – 2.03
b_{sec}	b_{sec}/L_{sec} (max)	0.64 – 0.83	0.69 – 0.98
$t_{sh} \approx t_{fl}$		3.5 – 5.0	5.0 – 9.0

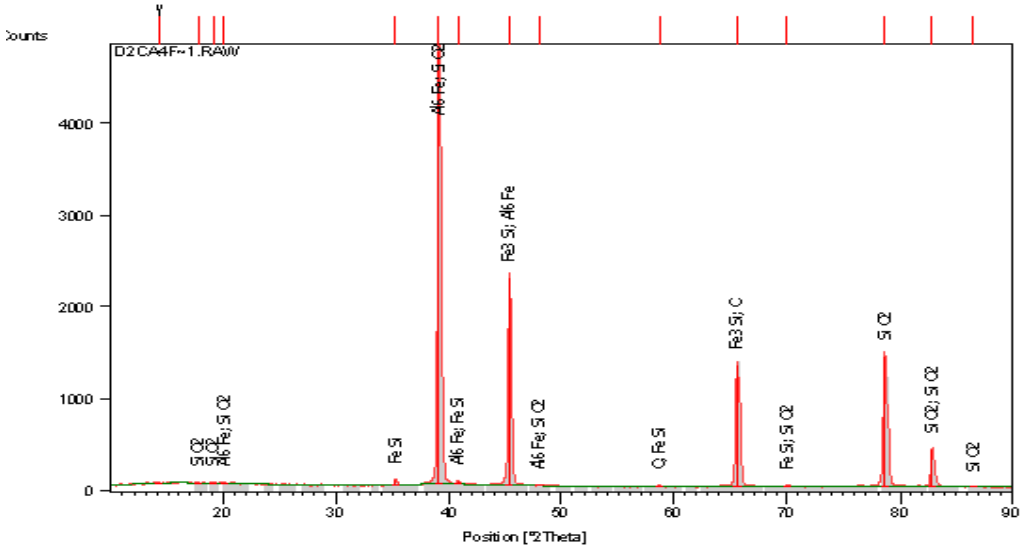
Table: A 15 Summary of result of force acting on connecting rod

S/No	Description	Regular connecting rod	Produced MMCs connecting rod
1.	Maximum force on the piston due to gas pressure F_L	23760N	10464.8N
2.	FC = F_L	23760N	10464.8N
3.	Maximum inertia force of reciprocating parts F_I	12672N	1358.53N
4.	Maximum bending or whipping stress due to inertia bending forces σ_b (max)	3.14 x 10^{-6} N/m^2	2.84 x 10^{-6} N/m^2
5.	Maximum compressive stress in the connecting rod σ_c (max)	84.7 MP_a	81.7 MP_a
6.	Maximum bending moment M_{max}	138.3 N-m	124.76 N-m
7.	Maximum angular speed W_{max}	261.8 rad/s	115.2 rad/s
8.	Ratio of the length of connecting rod to the radius of crank	4.3	3.1

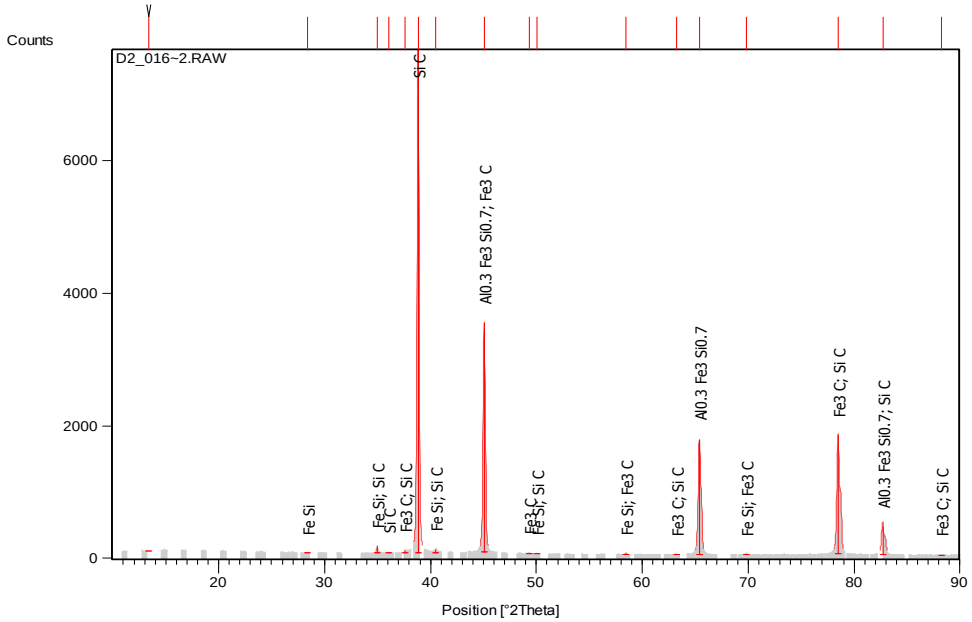
APPENDIX IV
XRD PATTERS OF THE COMPOSITE 0-15 % BY WEIGHT



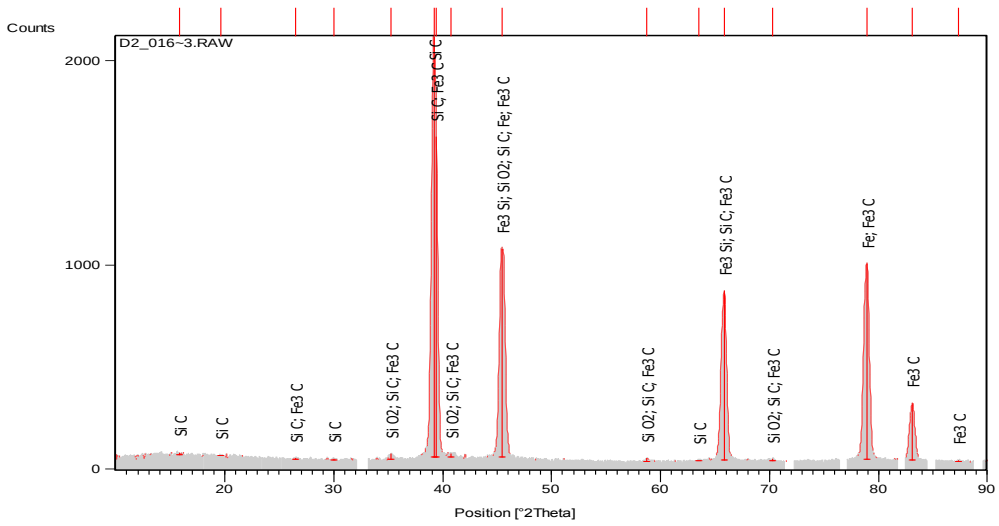
XRD pattern of the Aluminium alloy



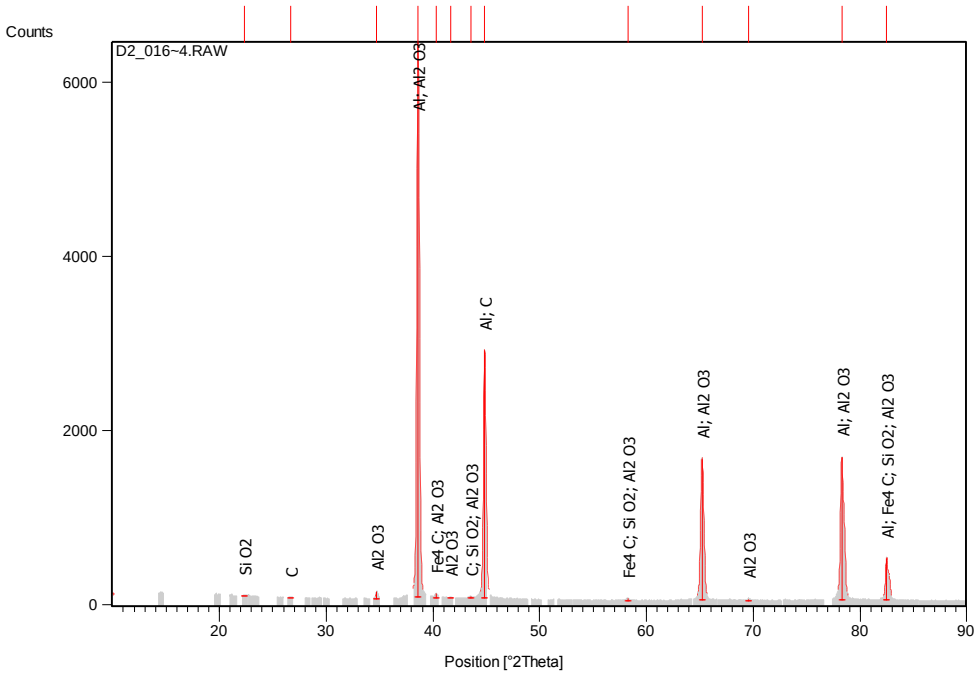
XRD pattern of the composite with 3wt%CSAp



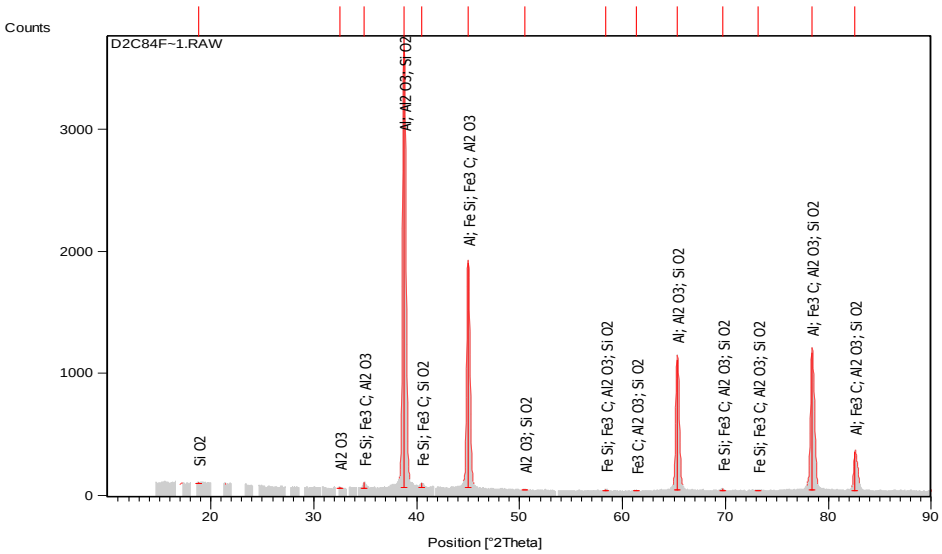
XRD pattern of the composite with 6% by weight CSAp



XRD pattern of the composite with 9% by weight CSAp



XRD pattern of the composite with 12% by weight CSAp



XRD pattern of the composite with 15% by weight CSAp